FIBER REINFORCED PLASTIC OVERLAY RETROFIT OF HOLLOW CLAY TILE MASONRY INFILLED REINFORCED CONCRETE FRAMES

by

Kemal Burak Hanoğlu

B.S. in C.E., Boğaziçi University, 1994

M.S. in C.E., Boğaziçi University, 1996

Submitted to the Institute for Graduate Studies in
Science and Engineering in partial fulfillment of
the requirements for the degree of
Doctor
of
Philosophy

Boğaziçi University

2002

FIBER REINFORCED PLASTIC OVERLAY RETROFIT OF HOLLOW CLAY TILE MASONRY INFILLED REINFORCED CONCRETE FRAMES

APPROVED BY:

Prof. Gülay Altay ....
(Thesis Supervisor)

Prof. Ali Rana Atılgan ....

Prof. M. Cengiz Dökmeci ....

Prof. H. Turan Durgunoğlu ....

Prof. Turan Özturan ....

DATE OF APPROVAL: ....16/12/2002....................................

To my dearest Cumult...

ACKNOWLEDGEMENTS

The author gratefully acknowledges the support and contributions of the Consortium formed by *SBD Weber & Broutin of UK,* and *EKON Yapı Onarım Koruma Tic ve San Ltd. of Turkey*, who awarded a research contract to Boğaziçi University Department of Civil Engineering on undertaking of experimental studies on *"Composite Laminate Application to Masonry Brick Infill Walls of R/C Framed Structures"*. The project was run by a team formed by Prof. Dr. Gülay Altay, Prof. Dr. Turan Özturan and the author acting as the principal investigator. However, results given and opinions expressed in this dissertation are the responsibility of the author and do not necessarily represent the views of the supporting organizations.

Support of the Boğaziçi University Structural Engineering Laboratory staff and the workers seconded by *EKON Yapı Onarım Koruma Tic ve San Ltd*, and efforts of Mr. Kadir Başoğlu of *ASLAN Tuğla San Ltd* in helping with the production of tailor made model scale clay tiles are greatly appreciated.

Most sincere thanks are due to a dear friend and colleague Dr. Orkun Akkol, who shared most of his valuable time with the author at various stages of the experimental work. The help of Dr. Yılmaz Yuva, Mr. Barış Sarı, Mr. Uğur Seymen and Mr. Onur Kantar during the long and difficult period of laboratory testing is gratefully acknowledged. Thanks are also due to Mr. Chai Seng Chiew of *Orient Research Consulting Engineers* for encouraging the research work of the author.

The author wishes to express his sincere gratitude to his thesis supervisor, Dr. Gülay Altay, Professor of Civil Engineering, Boğaziçi University, for her invaluable guidance, encouragement and support throughout the course of the studies. Thanks are also due to the members of the examining committee for their efforts in reviewing the thesis.

ABSTRACT

FIBER REINFORCED PLASTIC OVERLAY RETROFIT OF HOLLOW CLAY TILE MASONRY INFILLED REINFORCED CONCRETE FRAMES

Stiffness and strength contribution of hollow clay tile infills to ductile and non-ductile reinforced concrete frames were evaluated using 1:3 scale specimens tested under quasi-static reversed cyclic seismic loads. Four ductile and four non-ductile framed single-bay-single-story specimens with and without infill panels were tested in tandem specimen configuration simulating the seismic actions on lowest interior spans of typical of low-rise infilled frame structures. During the tests on masonry infill material, the testing procedures originally developed for solid brick masonry were shown unsuitable for the hollow clay tile masonry testing. A new method for tensile strength testing of the hollow clay tile units was proposed and used coupling with finite element models to establish a tile tensile strength estimate. Infilled frames with plain hollow clay tile infill were shown to have failure loads well in excess of the bare frames. Glass fiber woven sheet and carbon fiber reinforced plastic laminates were used to confine and brace the hollow clay tile infill. Addition of glass-fiber overlays and carbon fiber laminates increased the strength of the infilled frames above the conventionally infilled frames. However, the maximum displacement capacity of the new system reduced due to low compressive strength of the tile infill, which confined the failures and deformations to infill corners and column mid-height. A new finite element modeling approach was developed based on the use of plane-framework analysis methods for plane stress analysis. Two different model scales were considered to show the capabilities of the proposed approach and the possibilities of simplification for engineering office use. A standard finite element analysis package with point-wise nonlinear element capability was used to calculate the pushover curve of the tested specimens. The results showed a good agreement with the test results for the detailed model, and the engineering model was regarded amenable for further calibration.

ÖZET

DELİKLİ TUĞLA DOLGU DUVARLI BETONARME ÇERÇEVELERİN FİBER ESASLI KOMPOZİT YAYGILARLA GÜÇLENDİRİLMESİ

Delikli tuğla dolgu duvarlı betonarme çerçevelerin rijitlik ve dayanımlarının incelenmesi ve fiber esaslı malzemeler kullanılarak arttırılması amacıyla 1:3 ölçekli model çerçeveler statik tersinir yanal yükler altında deneye tabi tutulmuştur. Dört düşük ve dört yüksek süneklikli dolgu duvarlı/duvarsız numune ikiz tek-kat-tek-açıklıklı çerçeveler halinde, az katlı betonarme binaların alt katlarındaki bir iç açıklığı temsil eden yüklere tabi tutulmuştur. Deneylerde, dolgu duvarlı çerçevelerin yanal dayanım ve rijitliğinin boş çerçevenin eşdeğer özelliklerinden üstün olduğu gösterilmiştir. Fiber esaslı malzemeler kullanılarak yapısal davranış ve dayanımın iyileştirilmesine çalışılmış, örgülü cam fiber yaygılar ve karbon fiber esaslı şeritler yardımıyla dolgu duvarlar kuşatılmış ve çaprazlanmıştır. Bu uygulamalarla yanal yük altındaki dayanım ve rijitliğin önemli ölçüde arttığı görülürken, sistemin toplam deplasman yeteneğinin kısıtladığı da tespit edilmiştir. Malzeme deneyleri sırasında, dolu tuğlalar için geliştirilmiş olan deney metotlarının delikli tuğlaların malzeme dayanımlarının belirlenmesi için yeterli olmadığı görülmüş, çekme dayanımı tahmini için basit bir deney metodu ortaya atılmış ve sonlu eleman modellerinin de beraberinde kullanılmasıyla çekme dayanımı tahmin edilmiştir. Dolgu duvarlı betonarme çerçevelerin nümerik modellenmesi için, iki boyutlu kafes sistemlerin analizinde kullanılan çubuk modellerin doğrusal olmayan davranışına dayanan bir modelleme yaklaşımı ortaya atılmış ve iki farklı detay seviyesinde ele alınarak, deneyler sırasındaki hasarların takibi için detaylı ve ofis uygulamaları için ise basitleştirilmiş geometrideki birer tekniğin deneylerlerle karşılaştırılması yapılmıştır. Doğrusal olmayan malzeme davranışını modelleyen noktasal mafsal elemanları kullanılarak dolgu duvarlı çerçeve modelleri monoton artan yanal yük altında analize tabi tutulmuştur. Detaylı modelin sonuçlarının deney sonuçlarına yakınlığı ve mühendislik modelinin de kalibrasyona elverecek özellikler taşıdığı kaydedilmiştir.

TABLE OF CONTENTS

LIST OF FIGURES

LIST OF TABLES

LIST OF SYMBOLS / ABBREVIATIONS

a	Height of a Hrennikoff plane stress cell
A_1	Area of a horizontal bar element of a Hrennikoff plane stress cell
A_2	Area of a vertical bar element of a Hrennikoff plane stress cell
A_b	Area of beam section
A_B	Area of bed joint boom
A_c	Area of column section
A_D	Area of a diagonal bar element of a Hrennikoff plane stress cell
A_H	Area of the mortar at head joint
A_M	Area of a mid-height flange boom
A_s	Total steel bar area in a reinforced concrete section
A_{S1}	Sum of boom areas at or adjacent to bed joints
A_{S2}	Sum of boom areas at or adjacent to head joint
A_T	Area of a hollow clay tile flange
A_V	Area of a vertical truss element
b	Frame section width
d_m	Length of masonry diagonal strut
E_c	Modulus of elasticity of concrete
E_m	Modulus of elasticity of masonry
f'_c	Specified concrete compressive strength
f_{ck}	Characteristic concrete compressive strength
f_{ctk}	Characteristic concrete tensile strength
f'_m	Specified masonry strength
f_{yk}	Characteristic yield strength of longitudinal reinforcement
f_{ywk}	Characteristic yield strength of transverse reinforcement
H	Story height
h	Frame section height
h_m	Net infill height
I_b	Beam section moment of inertia
I_c	Column section moment of inertia

k	Aspect ratio of a Hrennikoff plane stress cell
L	Bay or bent length
l_m	Net infill length
M_p	Plastic moment of the section
P	Axial forces on columns
P_1, P_2	Individual column axial loads
P_{min}, P_{max}	Minimum and maximum column loads
P_{DL}	Column axial load under dead load only
P_{couple}	Column axial load change under overturning moment
R_c	Diagonal compressive force under corner crushing
R_s	Diagonal compressive force under bed joint sliding
T	Infill thickness
T_c	Compressive capacity of reinforced concrete column
T_t	Tensile capacity of reinforced concrete column
V	Shear force or strength
V_b	Shear force at sliding initiation
$V_{cr,c}$	Shear resistance of concrete under compression
$V_{cr,t}$	Shear resistance of concrete under tension
V_f	Maximum strut force
V_i	Bed joint sliding resistance including column contribution
V_{max}	Maximum shear strength of the story
V_p	Required shear resistance for member end zone plastification
V_r	Column shear resistance
V_w	Shear strength contribution of web reinforcement
w	Equivalent strut width
z	Vertical contact length at column-infill interface
α_b	Infill contact length with beam
α_b	Infill contact length with column
Δ	Top sway displacement
ϕ	Reinforcement diameter notation
λ	Relative stiffness parameter of an infilled frame

θ	Diagonal strut angle
σ	Normal stress
σ_{max}	Maximum principal stress
σ_{min}	Minimum principal stresses
τ_o	Bed joint nominal shear strength
τ_{xy}	Shear stress

ABYYHY	Afet Bölgelerinde Yapılacak Yapılar Hakkında Yönetmelik
ACI	American Concrete Institute
ASCE	American Society of Civil Engineers
ASD	Allowable Stress Design
ASTM	American Society for Testing and Materials
ATC	Applied Technology Council
BR	Bare frame, infill, prism or coupon
CC	Code-Compliant
CMU	Concrete Masonry Unit
DL	Dead Load
EL	Earthquake load
FE	Finite Element
FEM	Finite Element Method
FEMA	Federal Emergency Management Agency
FRP	Fiber Reinforced Plastic
GL	Glass sheet applied and laminated
GS	Glass sheet applied
HCT	Hollow Clay Tile
HJ	Hydraulic Jack
IN	Infilled frame
LC	Load Cell
LL	Live Load
LVDT	Linear Variable Displacement Transducer
NC	Non-Compliant
NCEER	National Center for Earthquake Engineering Research

NEHRP	National Earthquake Hazards Reduction Program
PB	Bare prism
PG	Glass sheet applied prism
PR	Rendered prism
R/C	Reinforced Concrete
RW	Rendered Wall
TCBIB	Türkiye Cumhuriyeti Bayındırlık ve İskan Bakanlığı
TS	Türk Standardı
TSE	Türk Standardları Enstitüsü
URM	Unreinforced Masonry

1. INTRODUCTION

Hollow clay tile masonry infilled reinforced concrete frame structures form the majority of the existing building stock in Turkey. Most of these structures are designed to codes older than the earthquake resistant design rules currently in force, and thus regarded as a major threat to life safety. Contribution of Hollow Clay Tile (HCT) infills to lateral load resistance has been ignored in past national design practices, and infilled frame structural systems have been treated as-if bare frame structures due to the assumed low strength and rapid stiffness degradation of infills. Although the interference of the infills with the structural behavior of the surrounding framing is known, new designs to the current standards still continue without proper address of the interaction of infill stiffness and strength due to lack of data and unifying theory.

Starting with the basic research on infilled frame behavior in 1950's, it was acknowledged that the infill walls alter the boundary conditions of the framing members and violate the basic design assumptions for both stiffness and strength of the structural system. Substantial stiffness added by the infill due to interaction changes the dynamic response of the structures by shortening the fundamental period, which in turn causes higher seismic demands to develop during seismic events. Independent of infill properties, this stiffening effect bears pronounced significance for older construction where the low lateral loads specified at their design time yielded very slender framing members. Therefore, a critical review and assessment of the existing infilled reinforced concrete construction is in due order to reconcile the state-of-the-practice with the latest research findings.

Aside from proving or disproving the past practices accountable, infills may be regarded as additional sources of stiffness and strength to complement the existing structural resistances to deal with today's seismic design demands. Strength and deformation characteristics of infill panels can be tailored applying a new structural skin to work in parallel or integrally with the existing infill. Fiber Reinforced Plastic (FRP) based strengthening applications are amongst the best candidates for such applications because of the ease of installation, efficient weight to strength balance, and high strength and stiffness able to cope with the high demands imposed.

This dissertation is intended to review and question the past design practice of infilled frames with the objective of defining and quantifying their vulnerabilities and reserve strengths. Amplification of the positive contribution of the infills and suppression of their negative impact on surrounding framing are sought using fiber-reinforced plastic based strengthening overlay and bracing applications. Inherent qualities and weaknesses of the existing infilled frame construction, proposed rehabilitation schemes and reference cases are explored by laboratory testing and analytical / numerical modeling.

1.1. Existing Buildings

Most of the existing structures in Turkey are regarded as vulnerable to seismic events of a magnitude much smaller than that specified for the design of state-of-the-art earthquake resistant structures. This idea is mainly supported by the substantial increase in the code specified design lateral loads over the past few decades.

Material condition and detailing quality found in the existing structures do not favor ductile response and thus presence of major overstrength must be demonstrated to qualify these structures as satisfactory under today's new design codes. This trivially leads to the conclusion that all existing construction poses a life safety hazard. However, the postulated vulnerability is not reflected in the actual seismic performance of the old construction (Hassan and Sozen, 1997; Otani, 1999; Gülkan and Sozen, 1999). Thus, several of the ordinary existing structures must possess substantial additional sources of strength not accounted by the assessment procedures based on design codes for new buildings.

1.1.1. Seismic Design Criteria

Earthquake resistant design in Turkey has been ruled with a series of documents issued by Türkiye Cumhuriyeti Bayındırlık ve İskan Bakanlığı (TCBIB), now entitled Afet Bölgelerinde Yapılacak Yapılar Hakkında Yönetmelik (ABYYHY), starting with the issue of Zelzele Mıntıkaları Muvakkat Yapı Talimatnamesi in 1944 (TCBIB, 1944), followed by several revisions (TCBIB, 1949, 1953, 1962, 1968, 1975, and 1998). In retrospect, these design rules can be split into two distinct groups. First group comprises of the codes earlier than 1975 where strength based ductility criteria were not specified, and the second group includes the most recent two codes enforced in 1975 and 1998.

All codes prior to 1998 were Allowable Stress Design (ASD) codes for both reinforced concrete and steel structures. The 1998 code still allows the use of ASD approach for steel structures but specifies all requirements for reinforced concrete structures in ultimate strength design format.

Codes earlier than the 1975 involved descriptions of generic structural forms by limiting structural geometry and material properties where experience indicated satisfactory performance of such or similar structures during the past earthquakes. Bare basics guidance was provided on load combinations, and order of magnitude of the lateral loads to be used in earthquake resistant design were specified. Several of the codes recommended the use of light infill materials such as HCT explicitly, thereby trying to reduce the total building mass. Distinction for structural framing type in lateral load assignment was first introduced in 1962 version but left out in the 1968 issue. Reinforced concrete detailing requirements were incorporated as late as 1968 and were prescriptive.

With the 1975 version of the earthquake resistant design regulations, the detailing requirements were based on strength criteria to allow member end zone plastification and confinement. Seismic hooks for ductile detailing were specified and joint shear reinforcement requirement introduced. This version also included a limitation on the interstory drift and associated design suggestions for the infill walls. Infill walls forming slit windows and imposing acute ductility demands due to short column effect were required to be considered explicitly in the analysis by using the higher apparent stiffness of the short columns. Such columns were to be reinforced to meet the higher shear forces obtained accordingly. Infill walls were referred to alter the lateral load response and required to be included in the structural analysis or to be constructed isolated form the adjacent framing.

The 1998 issue furthered the code development by including the lateral load modifiers for structural ductility, irregularity and strength continuity, and provided insight into the structural detailing of frame and wall elements relating to overstrength and local ductility demand. As in all contemporary structural design approaches, current ABYYHY assigns a key role to ductility for satisfactory seismic performance, and requires major contribution from the element level reinforcement detailing.

Detailing for ductility dictates closely spaced transverse ties and hoops at the critical zones of the beams, columns, and connections, where the amount of the transverse reinforcement is to be assigned based on calculations accounting overstrength under flexure and aiming the suppression of brittle modes of failure. Such ductile design rules were already enforced in the 1975 version of the ABYYHY, where two separate design load levels for structures with ductile and non-ductile details were specified, and ductile structures were defined as those compliant to the set of detailing rules as given in this document. However, several of the existing structures assessed by local professionals and universities before and after the recent seismic events of the 1999 revealed that the structures designed to the 1975 code were invariably analyzed as-if ductile but built as non-ductile structures. Therefore, amongst existing structures, excluding very recent constructions, fully ductile frames are relatively rare and non-ductile frames are most common. These non-ductile frames are not detailed considering the behavior of the dissipative zones and may have several common deficiencies, such as columns that are weaker than beams, all lap splices placed in column hinge zones, and insufficient detailing and lack of transverse reinforcement use for confinement, shear strength, and longitudinal reinforcement stability (Bracci *et al.*, 1995).

1.1.2. Common Properties of Existing Buildings

Considering that most of the existing buildings in the urban nuclei date earlier than the enforcement of the two latest earthquake resistant design codes, these structures are expected to have little margin to overloading under seismic loads. This is mainly due to the nominal lateral load levels used in their original design, and is also supported by the fact that the overstrength available due to gravity load design can encompass such low lateral loads already (Jain and Navin, 1995; Kunnath *et al.*, 1995; Bracci *et al.*, 1995; El-Attar *et* *al.*, 1997; Balendra *et al.*, 1999). Tied to this fact, the gravity loads on the existing buildings are expected to stress the elements close to the maximum allowable region due to the optimizations made in the calculations, which is motivated by the larger load or safety factors for the gravity design and nominal lateral load levels with lower load factors in contrast. Therefore, the magnitude of the additional margin on top of the strength defined by the gravity load design can only be related to the conservatism of the designer exercised independent of the code requirements and random effects of deterioration or higher quality of materials.

Typical residential construction in Turkey has discontinuous frame lines with 3-5m spans frequently varying upon architectural need, which support a floor height of 2.4-3m. Most of the structures have infill walls that are placed as per the use of space dictated and more often than not non-uniformly distributed. Seen from aseismic design perspective, the orientation and distribution of the frames and walls do not follow an intended pattern. Moreover, due to the land value and size, the buildings are designed to fit a given narrow or irregular oblong space, which ultimately results in structures with low redundancy in one or both orthogonal directions.

Typical floor thickness may be expected to comprise of a structural slab section in the order of 100-150mm that is topped with a generous coat of leveling concrete of 40-70mm, 10-20mm render on the ceilings and the floor tiling material of 20-40mm including the mortar. Therefore, a generic section for the weight calculation may be assumed as of 210mm thick and in equivalent weight of reinforced concrete (adding up to 5.25kPa uniformly distributed load).

Additional floor loads under gravity can be computed allowing 0.75kPa for wall load as-if uniformly distributed and using 2kPa Live Load (LL) generally specified for residential construction. Therefore, it is likely that the factored Dead Load (DL) and live load amount to 11.6kPa under gravity (1.4DL + 1.6LL), which should be discounted to calculate the expected load present on a structure under a rare action such as Earthquake Load (EL), (1.0DL + 0.30LL + 1.0EL). A rough allowance for the weight and mass of the structural framing would add a 10 per cent to the dead load values given above.

In earlier design codes issued by Türk Standardları Enstitüsü (TSE), reinforced concrete columns were allowed to be loaded up to the 60 per cent of the plain concrete cross section capacity calculated by using the characteristic concrete strength, $0.6f_{ck}$, (TSE, 1981; TCBIB, 1998). Therefore, assuming only 30 per cent of the live load present during an earthquake, the axial stress levels may be assumed in the order of 30-35 per cent of the characteristic compressive strength.

Longitudinal reinforcement ratios of the columns are in the range of 0.8-2 per cent and 1-2 per cent in beams. For most of the existing construction, the beam sizes are kept close to minimum dimensions and reinforcement ratios are close to the upper end of the given range. However, no similar generalization for the columns can be made.

Most commonly specified concrete strength values for the older construction in Turkey were between 14-18MPa, and, very frequently, the assessed concrete strength today would be in a range of 8-14MPa. In contrast, current ABYYHY does not allow for concrete strengths below 20MPa for building systems of high ductile framing, nor allows the use of nominal ductility framed systems at high-risk zones 1 and 2.

Detailing of the structural elements of the existing construction are invariably non-ductile due to the site practices, which did not improve along with the developing international experience in aseismic design. Column splices are placed at the bottom end of the columns and all bars are spliced at the same cross-section. This results in a critical stress transfer at a highly stressed and congested region. Moreover, the length of overlap and the confinement of the splice zone are generally inadequate. Beam detailing is also poor due to the discontinued bottom reinforcement at the supports and the extensive use of bent bars and addition of discontinuous bars at supports. Shear reinforcement amount in the columns and the beams are not capable of developing and maintaining element plastic moments, and violate the design assumptions based on response modification relying on dissipative behavior. Moreover, the provision of seismic hooks of 135 degrees at the tie and stirrup ends has hardly ever been practiced due to the claimed installation difficulties.

As discussed above and aside from the strength and condition of the concrete used, the condition and detailing of the reinforcement are invariably poor and not suitable for ductile response, and majority of the existing construction falls, thus, outside the code specified safety limits. Therefore, most of our existing structures may be regarded as constructed and detailed merely for gravity loads, and analyzed for reduced lateral loads without complying to the basic prescriptive requirements, which allow such a reduction.

1.1.3. Observed Seismic Vulnerability

When executing seismic safety surveys according to the current ABYYHY developed for the design of new structures, most of the existing buildings built prior to the last code update end up to be assessed as vulnerable and assigned a qualitative collapse risk of unknown magnitude. However, all structures have some built-in overstrength due to safety and load factors used, the inherent conservatism in design procedures due to the approximations involved, and additional stiffness and strength sources unaccounted for in the structural design phase. The sources of overstrength ignored in case of a new design may significantly contribute to the structural resistances during a seismic event. These reserve capacities may provide extra strength and stiffness to withstand substantially larger demands, and create the discrepancy between the observed and calculated performance levels of the structures. Therefore, recent guidelines developed by Applied Technology Council (ATC) for the assessment of structures include the evaluation of such expected overstrength (ATC, 1997a).

Seismic damage surveys, undertaken after the major seismic events of 1992 Erzincan, 1995 Dinar, 1998 Adana, and 1999 İzmit and Düzce in Turkey, and similar work in other countries, indicate that the assumed vulnerability of the low rise structures under seismic events is not justified (Otani, 1997 and 1999). Studies exploring the overstrength inherent to structures designed to old seismic or non-seismic codes show that to a limited extent the survival of these structures may be attributed to safety margins used in the use of materials, over specified loads, and penalties applied for structural irregularities. However, for major seismic events, overstrength of framing only may not be enough to explain the non-failure for all cases, and other sources such as contribution of non-structural elements to lateral resistance may be of further importance.

Solid clay brick and hollow clay tile infill walls of existing buildings are possible sources of substantial additional strength that was customarily not accounted for in the original structural design, (Hassan and Sozen, 1997; Gülkan and Sozen, 1999). Amongst the recent construction, buildings with hollow clay tile are in majority, and existing literature on the solid brick infills provides reliable and redundant data. Therefore, current research aims to assess the performance of the hollow clay tile infilled frames and retrofit strategies based on application of fiber-reinforced plastic overlays to the infills to enhance their strength, stiffness and ductility characteristics.

1.1.4. Scope of Research

Past research and practice on seismic upgrading of structures suggest that replacement or strengthening of infill walls with reinforced concrete proves to be successful in meeting today's seismic safety demands (ATC, 1997a). However, construction of new R/C walls or a substitute structural skin against an existing infill requires evacuation of the building as a whole or in parts, which cannot be easily achieved for several reasons beyond the design, finance and construction of any retrofit project. Alternatives that can be developed in structural steel are largely limited due to the low concrete strength of existing buildings where quality of anchorages under seismic loads would be questionable. Moreover, such alternative designs also require the replacement of the infill walls, major non-structural alteration and disruption.

Currently, there are no mandatory rehabilitation schemes in force, and assessment and retrofit of the structures are undertaken by the initiative of the landlords or tenants. Apart from construction costs, the building owners are mostly disturbed by the thought of long construction periods, major geometrical changes, and loss of space resulting from member size increase or new structural member addition. Therefore, if ever assessed, safety hazards due to structural failure remain mostly uncured and resolutions postponed until the next seismic sign or its aftermath.

Research presented herein seeks to develop an alternative to R/C and steel upgrading schemes by using high strength fiber reinforced materials applied on infill panels to create strengthened elements that can be used as a structural part of the existing structural system and to contribute to the existing seismic resistance. After the intended retrofit, increase in strength could provide the ability to sustain the loads that would be attracted by the stiffness of existing panels and the "new" structural element thus developed could be an alternative, that is easy to construct, detail and tailor, to meet the earthquake demands of existing structures. Therefore, the current study is aimed to assess the strength and stiffness of existing hollow clay tile infill walls retrofitted with fiber reinforced plastic sheets and laminates. Principal strengthening scheme is defined as the application of glass sheet overlays to the infill surface and fixing Carbon FRP laminates both to infill and to the surrounding frame. Investigations based on laboratory testing of such prepared 1:3 scale one-bay-one-story specimens, under quasi-static loading and analytical / numerical modeling of the tested specimen behavior are reported in what follows.

1.2. Infilled Frame Behavior

Infilled frames are hybrid systems made up of interacting components such as the infill-panel, elements surrounding it, and bare frame and/or shearwall components working in parallel. Classification of these frames is based on material, connectivity and detailing of the infill panel and the frame.

Infill materials may be of diverse origins such as, brick, stone, light and normal weight concrete, reinforced concrete, and modified or layered light materials. For masonry infills, further differences are brought in by the unit size and shape, laying arrangement, reinforcement and bonding agents used. Furthermore, infills constructed with shear connectors between the infill and the frame elements are called integral and otherwise non-integral.

Steel and reinforced concrete frames can be built with any one of the infill materials mentioned above or combinations thereof. Either type of framing is further classified by their ductility potential, and reinforced concrete infilled frames with non-ductile detailing and unreinforced hollow clay tile masonry infills are the most common form of local construction.

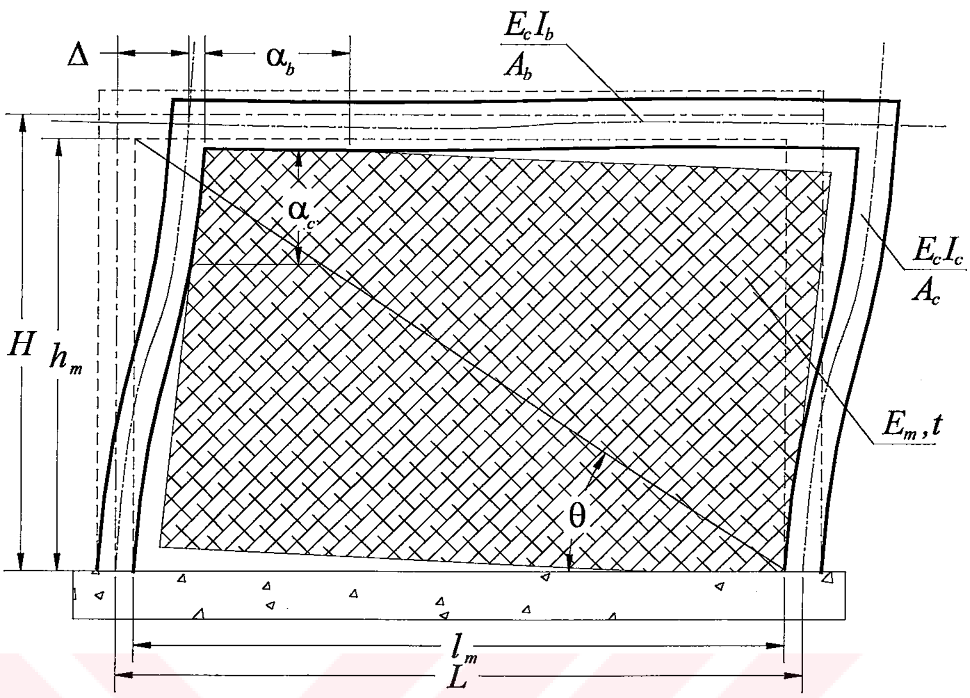

Figure 1.1. Infilled frame geometry and notation

Stiffness and the strength of the infilled frames are governed by their material properties, geometrical configuration and contact at the infill-frame interface. Frame materials modulus of elasticity, E_c, column and beam section areas and inertia, A_c, A_b, I_c and I_b, span length, L, and story height, H, define the stiffness of the bounding frame. Similarly and neglecting the material anisotropies, infill materials modulus of elasticity, E_m, net span length, l_m, clearstory height, h_m, and infill thickness, t, define the stiffness of the contained panel. Infilled frame stiffness is further a function of the contact length between the panel and the columns, α_c, and the beams, α_b, Figure 1.1.

1.2.1. Monotonic Tests

Influence of infill walls on the overall system stiffness and strength has been subject to research starting with the works of Wood (1952 and 1958), Polyakov (1952 and 1956), Benjamin and Williams (1958), Holmes (1961), and Stafford Smith (1962). Early works on infilled frame behavior were motivated by the observed stiffness contribution of the infills and implications of their bracing action on column design (Wood, 1958).

Several of the early test programs were based on small scale (1:10 – 1:6) samples constructed using solid rectangular steel bars to model the steel framing, and micro-concrete or mortar used as infill material. As sketched in Figure 1.2, testing arrangements involved (a) diagonal compression loading, (b) racking loading with overturning restraint, (c) racking loading with axial loads, and (d) tandem or back-to-back test arrangement of infilled frames. On the other hand, large scale or actual size tests such as by Polyakov (1952 and 1956), Benjamin and Williams (1958) and Mainstone (1971) involved mostly simple racking load setups, Figure 1.2 (b).

Polyakov (1952, 1956, 1960, and 1963) investigated various parameters affecting the behavior of infilled steel frames, via large-scale tests of 64 frames with different types of masonry units, mortar, method of loading, and wall openings. An additional test on a three-story, three-bay frame of about one-quarter scale demonstrated that the multi-story, multi-bay infill system behaved as a group of individually braced frames and not as a single monolith.

Investigations on actual size and small-scale infilled walls undertaken in Stanford University from 1951 to 1956 were reported by Benjamin and Williams (1958), where tests on 22 frames infilled with solid brick and two bare wall panels were conducted. Two of the infilled frames were steel and used to check the contribution of infill walls with and without openings. Remaining twenty reinforced concrete frames were infilled with four different types of solid brick of varying model scales as compared to the overall framing scaling. Extensive materials testing of the infilled masonry material was also undertaken for various failure conditions. These included the couplet brick tests with the loads applied at several different angles to the mortar bed joints. The scale effect of using brick with the same dimensional scaling as the surrounding frame or without such uniform scaling was found insignificant, and the confining action of the surrounding frame was regarded as the main reason of the mobilized shear strength of the infill walls.

Reporting on the preliminary test results of Building Research Station of United Kingdom on infilled frames, Wood (1958) observed the composite action between the steel frames and infill panels and the differences between the racking load, displacement patterns and plastic hinge zone locations of the infilled and bare frames.

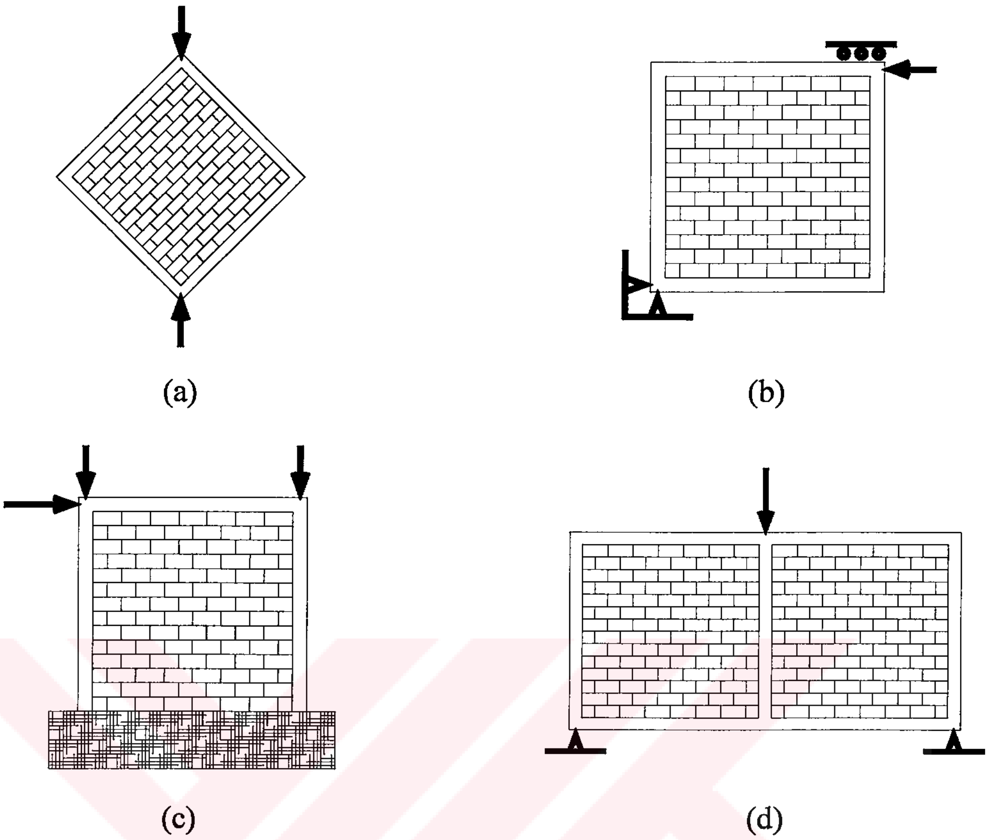

Figure 1.2. Loading arrangements frequently used for infilled frame testing

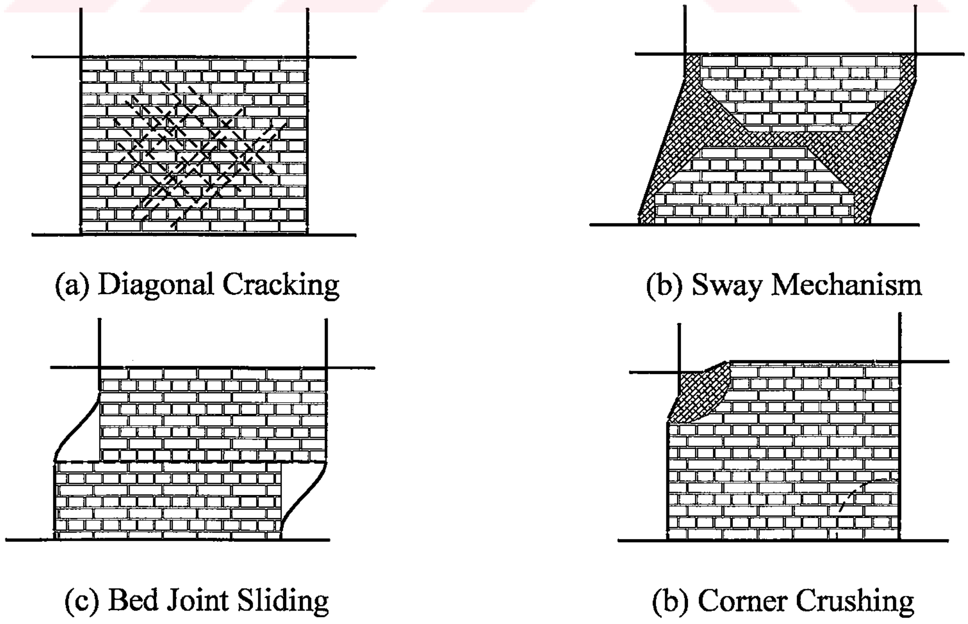

Figure 1.3. Failure mechanisms commonly observed for one story infilled frames

Motivated by the comments of Wood (1958) and works of Benjamin and Williams (1958), Holmes (1961) conducted four tests using 1:8 scale square steel frames with plain concrete infill. Two different framing profiles with relative flexural stiffness of 1:3 were used and two infilled frames of either type tested. The infills were observed to separate from the surrounding frame near the ultimate load. Failures of the infilled frames were due to the corner crushing of the infill panel. Additional tests that were not fully reported were undertaken on infilled frame specimens with openings. Openings were suggested to cause a 30-40 per cent drop in the peak load. Later, Holmes (1963) performed tests to explore the capacity of infills under combined lateral and vertical loading.

Devising the diagonal compression load setup, Stafford-Smith (1962 and 1966) investigated the behavior of small mortar-filled steel frames subjected to diagonal and racking loads. The frames were of solid cross section and fully welded at the corners. To simulate the racking behavior, back-to-back loading arrangement was introduced and the tested specimens included one- and two-story mortar infilled frames with varying aspect ratio, mortar infill thickness and frame section. Observed contact lengths during testing were noted and diagonal cracking and corner crushing loads were given.

Using three demonstration tests on infilled frames formed by mortar panel and steel rectangular bars, Mallick and Severn (1967) explored the effect of slip at frame-infill interface. One of the three frames included shear connectors to prevent slip and the other two were without such connectors. Both the load-deformation response and the strain gauge readings made on one of the non-integral samples indicated that the interface slip significantly influenced the lateral load response. The integral infilled frame showed stiffer lateral load response for the loads past the cracking load and the load drop at the ultimate load was abrupt. After proposing a Finite Element Method (FEM) based analysis procedure, seven more tests on single panel infilled frames were executed to verify the proposed theory.

Mallick and Severn (1968) conducted eight tests on integral and non-integral frames to determine their hysteretic response characteristics. Four specimens of each type were tested where each had a counterpart with same dimensions within the other test set. Damping in the infilled frame response was attributed to solid friction at the frame-infill interface and viscous damping was assigned a role of same order of magnitude. For non-integral infilled frames, the observed damping was solely due to viscous damping.

Summarizing and unifying the much-quoted tests undertaken at the Building Research Station of United Kingdom starting from 1950's, Mainstone (1971) presented the results of nine small-scale model brickwork infilled frames, eleven small-scale micro concrete infilled frames, and three actual size brickwork infilled frames. Test confirmed that the range of possible behavior of infilled frames was broader than as modeled by simplified approaches presented in earlier studies and wide variations were observed between nominally identical specimens.

Mallick and Garg (1971) investigated the effect of openings on infilled frame behavior using sixteen mortar filled steel model frames with square openings at various locations. Eight of these specimens were with shear connectors at the frame-infill interface. Integral frames, with shear connectors, were observed to be stiffer than non-integral frames, cracked under diagonal tension before corner crushing, and reduced the probability of lack of fit. Openings were recommended to be placed close to the center of the span and lower than the diagonal line.

Exploring the effect of the openings on multistory infilled frame behavior, Liauw and Lee (1977) performed a test series on four-story micro-concrete infilled steel frames with and without shear connectors. Span to height ratios of 2:1, 2.5:1 and 3:1 were tested. Fifteen of the specimens had a central opening of 20, 25 and 30 per cent of the infill width. For the eight frames without shear connectors, separation of the frame was observed after a slip at the frame-infill interface in early loading stages. This separation was more obvious for infills with openings. Peak load was reached after diagonal tensile cracking and with the compression failure of the lowest panel corners for solid infills, and due to shear failure of the infill portion above the opening. For integral frames, the interface separation was not present and the failure loads were reached after extensive cracking of the infill.

Liauw and Kwan (1983b) performed a series of tests comprised of six four-story small-scale model micro-concrete infilled integral steel frames with finite interface strength. Four failure modes were identified for integral frames: corner crushing with failure in the columns, corner crushing with failure in the beams, diagonal crushing with failure in beam connections, and diagonal crushing with failure in column connections.

Influence of initial gaps on infilled frame behavior was explored by Riddington (1984) where significantly lower stiffness and slightly lower ultimate capacities were observed for the frames with initial gaps. As in previous research, diagonal cracking and corner crushing failure modes were found.

Dhanasekar and Page (1986) tested steel framing with grouted brick infills to verify a biaxial masonry constitutive model. The specimens were tested under increasing monotonic racking load. After initial failure of the infill, the composite stiffness approached that of a corresponding bare frame, yet it continued to resist a proportion of lateral load by frictional shear on the planes of failure.

Behavior of the multibay frames was explored by Liauw and Lo (1988) with tests on twelve small-scale micro-concrete infilled steel frames where equal numbers of integral, non-integral, single- and two-bay frames were included. Load deflection diagrams, principal panel stress plots, and interface stress diagrams of selected tests were given. The strengthening effect of the connectors was regarded as significant for both of the frame geometries. The ultimate loads of the non-integral two-bay infilled frames were significantly (55 to 61 per cent) higher than the single-bay specimens, but only in one case the load was close to the double (85 per cent). Interaction of the middle column common to both of the bays in the two-bay frame was regarded as important to model the correct behavior.

Dawe and Seah (1989) investigated the behavior of concrete masonry infilled steel frames by testing 28 large-scale specimens with monotonic racking loads. Their intention was to study a broad spectrum of characteristics that might affect infill stiffness and strength. They observed that tightly packed mortar between the infill and column flanges increased initial stiffness but did not affect panel cracking load or capacity, that panel-to-column ties increased the initial stiffness but did not affect panel cracking load or capacity, and that a 20mm gap between the panel and top beam significantly reduced the infill stiffness and strength.

Kwan *et al.* (1990) constructed six large-scale lightly reinforced concrete infilled steel frames where equal numbers of integral and non-integral frames were included. Two single-bay-two-story and four two-bay-two-story infilled frames were tested. Although the cracking patterns and failure loads were different, the collapse modes of the frames were found to be the same.

Mehrabi *et al.* (1996) performed in-plane testing of reinforced concrete moment resisting frames infilled with hollow or solid concrete masonry units. Observations were that stronger infills exhibited higher load resistance and better energy dissipation capability. However, the post-peak strength of stronger infills dropped more rapidly than weaker infills as the displacement increased. Stronger infills were also recognized to be more likely to cause brittle shear failure in the concrete columns.

Al-Chaar (1998 and 2002) tested five single story multibay reinforced concrete frames under lateral loads. Three of the frames were of single span. One of these single bay frames was tested bare and the other two had Concrete Masonry Unit (CMU) and clay brick infills. The two and three span specimens were with masonry infills of concrete masonry unit and clay brick, respectively. All of the specimens exhibited large deformation capacity after the peak load and had significant amount of dilation in the later stages of loading. At large deformations the failure of the column upper ends under shear loading was observed.

1.2.2. Cyclic Tests

Klingner and Bertero (1978) simulated the three lower stories of a one-third-scale sub-assemblage of an 11-story infilled frame building. This three-story prototype consisted of reinforced concrete framing with fully grouted and doubly reinforced concrete masonry infills. It was suggested that the increase in strength provided by the infill exceeded the potentially detrimental effects of increased inertial forces arising from the added stiffness of the infill. The lateral load resistance beyond the peak load was observed to decay like an exponential function with negative power proportional to the experienced displacement.

Kahn and Hanson (1979) tested reinforced concrete frames with post-installed reinforced concrete infill panels. Two of their specimens were constructed using precast infill panels with interface connectors and a gap adjacent to the column. Their observation was that the post-infilled frame behavior was different from the monolithic shearwall behavior with the characteristics such as infill shear strength deterioration and shear failure modes of the columns forced due to the interface separation.

Irwin and Afshar (1979) undertook the in-plane cyclic load tests on six reinforced concrete frames with various types of infills. Specimens included one bare and four plain lightweight concrete masonry infills with different render coats, and one with polystyrene filler material coated with glass fiber reinforced cement. All infilled specimens had initial diagonal cracking, corner crushing and shear failure in the columns. Infills were observed to contribute to the strength between 5-14 times of the bare frame, whereas the initial stiffness was increased by 3-9 fold.

Bertero and Brokken (1983) tested subassemblages simulating the three lower stories of a one-third-scale sub-assemblage of an 11-story infilled frame building. Different types of infilled frames were tested. Amongst the eighteen specimens, two were bare and another two had unreinforced masonry infills. It was concluded that the increase in strength and energy dissipation afforded by the infill exceeded the potentially detrimental effects of increased inertial forces arising from the added stiffness of the infill. However, the limits imposed for the suggested improvement were up to 0.26g seismic design lateral loads for the ductile and 0.12g for the non-ductile frames infilled with unreinforced solid brick masonry.

Govindan *et al.* (1986) tested two-quarter scale seven-story reinforced concrete frames, one as bare frame and another with unreinforced masonry infill. The bare frame was observed to provide 3.29 times the ductility of the infilled frame. Initial stiffness of the infilled frame was observed to be five times of the bare frame, whereas the cumulative energy dissipation capacity was only 1.5 times.

Exploring the influence of the order of frame and wall construction, Achyutha *et al.* (1986) tested nineteen half scale reinforced concrete frames infilled with brick masonry panels with and without openings. Using the first set of eleven specimens the influence of the method of construction on the infilled frame behavior was evaluated. Four different construction procedures were considered, where constructing the frame and infilling later (Type I), building a panel wall and casting the frame around it (Type II), a case similar to the second but including shear connectors (Type III), and an additional case similar to the third but oiling at the interface to remove friction (Type IV). Under lateral load, the infill separated from the frame for the Type I and Type IV, whereas no separation occurred for the other two cases. Additional eight specimens were also tested to investigate the influence of the stiffeners near the openings.

Mander *et al.* (1993) studied the effect of brick infill on steel framing. A three-story, one-bay frame sub-assemblage was tested with only the center bay infilled in each story. Lowest and the top bays of the frame were braced with diagonals of similar stiffness to the infill walls tested. Primary diagonal strut action was observed in the infill and secondary struts developed as the loading continued. In-plane shear strength relationships for the infill based on the square root of the prism compressive strength were provided.

Mosalam *et al.* (1997) tested gravity load designed infilled frames using quasi-static cyclic reversing lateral loads. Solid infills were observed to cause the behavior of infilled frames to be brittle. The infills with openings were observed to reduce the initial stiffness by 40 per cent for loads below the infill panel cracking, and induced a more ductile behavior. Based on the observed behavior, a hysteresis model formed using physically meaningful parameters was proposed.

Flanagan and Bennett (1997) tested hollow clay tile infilled steel frames under in-plane and out-of-plane loads applied using airbags. They observed that the infills maintained their out-of-plane stability even under substantially damaged conditions and the out-of-plane loading mainly masked the diagonal cracking behavior but did not alter the in-plane peak load capacity.

In an attempt to investigate the dynamic characteristics of actual size infilled frames, Chaker and Cherifati (1999) undertook site testing of two identical reinforced concrete frames under construction. One of the frames had infill masonry in place and the other was bare. Vibration measurements executed under a high wind loading indicated that the infill wall contributed a significant amount to the stiffness of the composite structure and the infill wall could not be considered as non-structural. The small strain behavior of the infill panels were observed to be closer to plane stress rather than to a diagonal strut.

Buonopane and White (1999) applied pseudo-dynamic tests to a half scale two-story-two-bay masonry infilled reinforced concrete frame with openings in the second story. The specimen was loaded under Taft earthquake record scaled to four different peak ground acceleration levels. Several equivalent strut models were used to compare with the test results. All strut formula were found to provide an order of magnitude estimate but failed to model the behavior entirely. Friction based strut strength formulae were found to underestimate the strut strength and to heavily depend on the assumed friction coefficient.

Flanagan and Bennett (1999a) tested eight large-scale hollow clay tile infilled steel frames. Significant pinching was observed and attributed to the boundary zone deterioration, plastic deformation of the infill material and the make-break contact under cyclic loading. Most of the frames showed a major drop after the peak load was attained. Three strength levels were observed to be significant to define the infilled frame characteristics, diagonal cracking, tile failure and corner crushing.

Hakam (2000) investigated the feasibility and effectiveness of a retrofit method for hollow concrete masonry infilled steel frames using glass fiber reinforced plastic laminates. The investigations comprised of materials and model frame testing at 1:3 scale subjected to in-plane loads. In materials testing phase, 64 masonry block prisms were tested under loading introduced inclined to their bed joints at 0, 30, 45, 60, and 90 degrees, where half of these samples were coated with glass fibers. Diagonal tensile testing and tripled shear bond testing of the infill panel material were also undertaken. Second phase involved the testing of five steel frames with two different steel frame profile sizes. One of the frames was tested bare, other four were infilled, where two of these were retrofitted with glass fiber. Tests indicated that the shear strength and ultimate strength of the infills were increased, no change in the pure compression failure modes was observed, effect of the glass fiber on the stiffness was marginal, laminates reduced the variability and anisotropy of the infills, and all retrofitted infills failed by corner crushing.

Zarnic *et al.* (2001) tested two quarter-scale masonry infilled reinforced concrete frame buildings on shaking tables. One of the structures was a single-span-single-story structure in both orthogonal directions and the second was a single-bay-two-story structure on one elevation and had two bays on the perpendicular direction. Structures designed to Eurocode were demonstrated to have adequate overstrength to resist large lateral loads.

1.3. Infilled Frame Modeling

Attempts of modeling the infilled frame behavior followed most of the tests reviewed above. These included phenomenological models, analytical models, and finite element modeling approaches. Modeling efforts, initiated with the stiffness and strength representation of a single panel, advanced to multibay and multistory frames and to general approaches as non-linear finite element models with various material, geometrical, and contact properties.

1.3.1. Phenomenological Models

Early models for infilled frame analysis were on phenomenological basis, where a dominant feature of the problem as observed during testing was weighed to be the cause of the distinct behavior of these structural configurations. Some of such models were based on assumed shear and normal stress distribution (Benjamin and Williams, 1958), or a diagonal strut element with assumed contact length with the bounding frame (Holmes, 1961).

Benjamin and Williams (1958) assumed a nominal level of shear and normal stresses acting on the infill as deduced from a large pool of test data. Proposed formulae included the explicit material model of the tested solid brick and the mortar based on their strength characteristics. Since deformations past the peak strength were regarded as of no design interest, the predictions were provided only for the elastic regime.

Based on infill tests by Wood (1958), Benjamin and Williams (1958) and four additional tests, Holmes (1961) proposed a linear equivalent strut equal to one-third of the panel diagonal length for computing ultimate stiffness and strength. The diagonal strut was assumed to form at a load close to failure where the infill wall was observed to separate from the bounding frame. Assumed infill-to-wall contact stress distribution was triangular with maximum stress at the loaded corners and zero at the unloaded corners. Ultimate load of the infilled panel was estimated based on the diagonal deformation of the composite structure due to the shortening of the equivalent strut and deformations of the frame. Limiting strut strength was based on an assumed maximum allowable strain of 0.002, and a width of one-third of the panel diagonal.

Holmes' work (1961) received much attention and criticism due to the large frame-to-infill contact surface allowed, the choice of the failure strain for the infill material, and the use of a single (corner crushing) failure mode (Smith *et al.*, 1962). However, maintaining the same assumptions Holmes furthered this model to include an empirical combination of lateral and vertical loads acting on single- and two-story single bay steel frames with concrete infill, (Holmes, 1963). It was observed that the presence of vertical load increased the diagonal cracking load but decreased the ultimate crushing load.

1.3.2. Analytical Models

Due to the discrepancies between the proposed phenomenological models and test results other than these models were calibrated for, attention was shifted to models based on theory of elasticity. In these works Airy's stress function for plane stress was evaluated numerically using observed boundary conditions with separation (Stafford Smith, 1962 and 1966; Stafford Smith and Carter, 1969), or for fully integral behavior (Liauw, 1970).

Stafford Smith (1962) modeled the lateral stiffness of the infilled frames based on the tested stiffness of the mortar panels and matching these to numerically solved plane stress problem to derive the equivalent diagonal strut width. Initially three infilled frame specimens were tested to get an estimate of the contact at the frame- infill interface. Based on the observations made and assuming a conservatively small contact length, stand-alone mortar panels of 1:1, 1:2 and 1:3 aspect ratio were tested and the strains along the diagonal were compared with the numerical results. The diagonal shortening of the mortar panels were matched with an equivalent diagonal strut to define the strut width. This width was used in the analytical prediction of the stiffness of a braced frame model replacing the infilled frame. Two separate models one with and the other without the flexural stiffness of the surrounding frame elements were proposed. These formulations were checked with additional tests on mortar infilled one- and two-story single bay steel frames. Test results correlated well with the proposed method of calculation. Having established the braced frame analogy with an assumed mortar panel contact length, the relaxation of this assumption was a key issue in the overall applicability of the developed analytical tools. Furthering his analytical and numerical studies on mortar filled steel frames, Stafford Smith (1966) derived an index stiffness parameter, λ, and contact length, α_c, of the infill on the surrounding frame using a tiered analytical approach based on two different infill contact stress distributions assumed. Both the triangular and parabolic distributions yielded close results. As the parameters of the derived model were investigated, an empirical equivalence to the behavior of beams on elastic foundation was demonstrated and the formulations thus simplified.

$$\lambda H = H\sqrt[4]{\frac{E_m t}{4E_c I_c L}} \tag{1.1}$$

$$\frac{\alpha_c}{H} = \frac{\pi}{2\lambda H} \tag{1.2}$$

Relevance of the above formulation was verified using mortar panels simulating infill panel loaded with known contact lengths and mortar infilled steel frames. Corner crushing and diagonal tensile failure loads obtained from these tests were compared with the predictions of the proposed method on a non-dimensionalized plot.

Mallick and Severn (1968) proposed two simplified models for dynamic analysis of infilled frames based on shear beam and bending response. Results of forced vibration tests were used for comparison and showed good correlation with one- and two-story model tests. However, in the case of the three- and four-story models the simplified models overestimated the frequencies of vibration indicating stiffer behavior.

A design method based on equivalent strut concept for the multistory infilled frames was proposed by Stafford-Smith and Carter (1969). Design charts plotting the tensile and compressive failure envelopes of the infill material were provided and a design example that is further compared with a tested model structure was reported.

Liauw (1970) numerically evaluated Airy's stress function for an infilled frame, where the frame was modeled as a boundary constraint and assumed to be in full contact with the infill panel. Using a photo-elastic material as infill material a specimen was constructed and the stress pattern and magnitude were estimated. Results compared well with the stress distributions found in the numerical analysis for the linearly elastic region of the infill behavior that was modeled.

Mainstone (1971) commented on the limitations of the equivalent strut based methods, however, granting their usefulness and simplicity, chose to cast his results still into this format. He proposed a set of empirical equations for equivalent strut stiffness calibrated using the analytical work of Stafford-Smith (1966), which were to be used to define the stiffness at initial linear elastic part, and to predict the diagonal tensile cracking and the ultimate load.

Smolira (1973) proposed an approximate numerical method based on the force method of analysis for infilled frames with gaps at frame-infill interface.

Liauw and Lee (1977) developed two methods for the elastic analysis of integral and non-integral infilled frames with openings. In the first approach, the equivalent diagonal strut width was estimated using a replacement sub-frame configuration modeling the infill sections as pseudo columns and beams connected by rigid elements. In the second method, the frames were analyzed employing hypothetical composite section stiffnesses accounting for the stiffness of adjacent tributary infill portions. Comparison with the test results indicated that using the proposed modeling approaches an order of magnitude displacement estimate could be made.

Wood (1978) observed a shear or shear rotation mechanism in tests presented by Mainstone (1971) which involved strong frame members. This failure mode included panel cracking followed by plastic hinges forming at the frame joints, rigid body rotation of restrained panel corners, and diagonal tension failure in the panel. For weaker frames, compression bands in the brickwork were observed as the infill developed significant diagonal cracks, diagonal compression or corner crushing failure modes followed. He used the plastic analysis methods to define the failure modes and loads of the infilled frames, and the method was demonstrated to capture the failure mechanisms of infilled walls and the failure loads agreed with the test results reasonably well. Introducing an empirical coefficient to account for the discrepancies between the experimental results, he incorporated a factor to account for the suggested incomplete plastification of the infill panel. To demonstrate the relevance of the proposed method, failure modes and loads of the earlier tests on the in-plane lateral load tests of concrete encased steel frames with brick and clinker-block filler walls were used. Later, May (1981) extended this work to cover the failure modes of infills with openings.

Liauw and Kwan (1983a and 1983b) developed a plastic collapse theory for infilled frames. Their method used interface forces as assumed or obtained from finite element analyses, and argued that the overestimation of the earlier methods, that were based on partly or fully plastic methods, was due to excessively high contact forces used. The modes of failure observed in the non-integral and integral infilled frame tests were modeled and the conditions for transition from one mode to another defined. Later, they have recast the findings and the formulations proposed into a graphical design procedure (Liauw and Kwan, 1984b), and unified all previously discussed aspects of their research (Liauw and Kwan, 1985). This theory was later extended to the analysis of multibay multistory frames with the assumption that the contact stresses in these frames were the same as in single bay frames, (Kwan *et al.*, 1990).

Saneinejad and Hobbs (1995) developed an alternative inelastic analysis and design method for infilled steel frames subjected to in-plane forces. They discussed the reasoning behind the penalty factors used in Wood's work to change the infill diagonal strut parameters and proposed an alternative where the modification was in the framing due to the imperfect plastification.

Flanagan and Bennett (1999a) proposed simplified formulae for corner crushing loads and initial stiffness of hollow clay tile infilled steel frames motivated by the failure of available methods based on plastic theories or equivalent strut approaches for this type of infill. Later, they proposed a calibration to Federal Emergency Management Agency (FEMA) Document No 273 (ATC, 1997a) out-of-plane stability formulae based on their earlier tests and a large pool of data available in the literature, (Flanagan and Bennett, 1999b).

1.3.3. Finite Element Models

Mallick and Severn (1967) proposed a finite element method analysis procedure for infilled frames and incorporated the interface slip into their modeling which was shown to be of significance in their demonstration tests. Contact was modeled using constraints between the infill panel and frame elements. These constraints were relaxed using an iterative procedure to model the no-tension condition at the interface. Slip was incorporated using the contact forces and applying additional shear forces at the corresponding infill boundary nodes that are of magnitude of friction coefficient times the contact force. Using the described procedure the tested seven single panel infilled frames and five two-story single bay frames tested earlier by Stafford Smith (1966) were modeled and good agreement observed.

Mallick and Garg (1971) used the FEM modeling technique of Mallick and Severn (1967) to model the initial stiffness of infilled frames with openings. The stiffnesses assigned followed the general pattern of the experimental results but were less sensitive to the location of the opening.

To model the effect of boundary friction on multistory and multibay frame behavior, Riddington and Stafford Smith (1977) developed a finite element procedure and executed a parametric analysis. They have varied the relative stiffness parameter, the infill aspect ratio, and considered cases with and without boundary friction. Listing the stress level at the center of the infill and at the loaded corners in tables and contour plots; they have demonstrated that the relative stiffness parameter could only control the effective width of the equivalent strut and the stresses at the loaded corners. However, the stress level at the center of the infill was governed by the aspect ratio. Later, Stafford Smith and Riddington (1978) proposed a design method for infilled frames based on these FEM results.

King and Pandey (1978) introduced an element for the frame-infill interface where the shear strength was modeled explicitly. It was observed that the exact value of the friction forces influenced the overall behavior only at the early stages of loading and had no impact once a stable contact condition was reached. The use of equivalent diagonal strut was demonstrated to fail to model the contact configurations other than those in the diagonally tested cases. Therefore, the use of FEM to model multistory structures under gravity loads was proposed. May and Naji (1991) extended this modeling approach to include the nonlinear material properties of the framing material.

Liauw and Kwan (1982 and 1984a) developed a FEM modeling and analysis procedure using unidirectional material nonlinearity, make/break contact checks with iterative friction force control, and residual slip at frame-infill interface. Their models allowed the analysis of non-integral and integral frames and showed good correlation with the earlier test results up to the peak load (Liauw and Lee, 1997), (Liauw and Kwan, 1983b). This finite element modeling procedure was later applied to multibay frames as well (Liauw and Lo, 1988).

Achyutha *et al.* (1986) simulated the elastic behavior of the infilled frames with openings where they have accounted for the contact nonlinearity at the frame-infill boundaries.

Liauw and Lo (1988) furthered the research into the plastic theory of infilled frames using non-linear finite element models. They used multibay multistory FEM models to check the applicability of the theories developed for single story single bay frames. Panel and interface stress distributions were found close to the single bent framing but an additional interaction was observed in behavior of columns common to adjacent bays.

El-Haddad (1991) developed a finite element for the frame elements, which incorporates the compliance due to the crack formation and propagation and used in a parametric study of infilled frame analysis. Magnitude and location of the infill maximum stresses were found to depend on the frame cracking level.

Madan *et al.* (1997) developed an infill macro model for global analysis of masonry infilled frames. The model was shown to replicate a wide range of stiffness characteristics of infill panel behavior.

Singh *et al.* (1998) developed an inelastic finite element model to simulate the behavior of masonry infilled reinforced concrete frames under static and dynamic lateral loads. Nonlinear behavior of the infill material, surrounding frame and interface were accounted for in the element formulations. Proposed method showed good agreement with the previous tests from literature, and modeled the time-history of loading closely.

Seah (1998) developed a set of interface elements, which can simulate tensile failure, shear failure, slip and friction, but assumed to be rigid under compression. Masonry elements were modeled as quadrilateral shell elements with non-linear material properties whereas the frame elements were modeled as non-linear beam-column finite elements. Modeling several of the infilled frame tests, the adequacy of the proposed technique to model the infilled frames was shown. Upon justification, a parametric study on generic frame configurations was conducted to form a pool of standardized data. These data were used to derive simplified equivalent strut material and geometrical properties for the simplified analysis of the large infilled frame structures. The method was applied to model a multistory structures test results and suggested to be efficient and accurate.

Al-Chaar (1998) conducted extensive FEM analyses to decide upon the locations of the measurement and loading instrumentation. Solid elements were used to model both the reinforced concrete frame and the masonry infill inside. Reinforcing bars were explicitly modeled as truss elements.

Chiou *et al.* (1999) presented a discontinuous deformation analysis application to infilled frame analysis and compared with experiments with reinforced concrete infilled frames. Three actual size reinforced concrete frames, bare, fully infilled and with a half height infill, were tested to demonstrate the applicability of the developed analysis method. Analysis results were observed to closely model the lateral load deformation behavior under monotonic loading.

Hakam (2000) employed nonlinear finite element modeling to model the behavior of the infilled frames in addition to his laboratory tested specimens, and used the materials test results to define the FEM material properties. The modeling involved a diagonally braced frame with a single compression only strut with non-linear material properties calibrated to reflect overall deformation behavior of the masonry infilled frame. To define the strut width two analytical methods were employed, (Stafford Smith and Carter, 1969; Saneinejad and Hobbs, 1995). The first method was favored for its simplicity and the marginal differences found between the results of the two.

Ghosh and Amde (2002) formulated an interface element to model the frame-infill and mortar bed behavior of brick infilled steel frames. Analyses based on the material and geometry of previously reported infill frame tests found in the literature indicated a good agreement between the model and the experiments. Moreover, the simplified methods based on plastic theories were regarded as to provide reliable results.

2. TESTING SCHEME

Within the scope defined, tests on individual brick units, masonry prisms, small wall sections (wallette) under diagonal compression, and infilled frames under quasi-static cyclic reversing lateral loading were conducted. The tests were executed in increasing order of complexity and results of earlier tests were incorporated to the prediction calculations of the following. Twenty-four wallette, forty wall coupon and prism, nine triplet shear, three masonry elastic modulus and eight infilled frame tests were undertaken. Several material tests on steel tensile strength, concrete compressive and split tensile strength, and mortar compressive strength followed the corresponding specimen tests.

2.1. Hollow Clay Tile Masonry

Hollow clay tile is the most frequently used infill material in our national residential construction. However, only the nominal strength and density characteristics of the hollow clay tile units are ruled in regulations and the material properties of the final infill masonry constructed is not inspected or tested (TSE, 1985). Therefore, the workmanship, strength and durability characteristics of infill walls are uncontrolled and expected to show a large scatter.

Hollow clay tiles are produced using a die extrusion process applied to naturally available clays, modified or improved natural clays or artificially produced / purified plastic mixes of clay minerals and oxides to be fired to ceramic masses. During the extrusion process, the highly plastic clay material is pressed against a nozzle that holds up several rigid pieces that are held together by metallic bridges for blocking the flow of the clay mass and producing the desired cored shape. After the material leaves the die, the trimmed edges reconnect and webs / shells of the cored mass “heal” and form an intact hollow extrusion. After cutting, drying, firing and cooling the hollow clay mass becomes a perforated ceramic tile (Illston, 1998).

Production process of the hollow clay tiles starts with selected materials that are ground and mixed with water to achieve a uniform material mass for production. However, the forming, drying and firing steps introduce non-uniformities into the final product.

During extrusion, the moisture content of the mix is of highest importance to provide the proper healing of the bridge cuts, and frequently some of the webs or face shells may be left slit due to variations in moisture content. Drying shrinkage introduces shrinkage cracks along the web and face shell boundaries. Firing accentuates any defects mentioned before by accelerating the shrinkage at low temperatures and contraction of material during sintering. Therefore, hollow clay tiles have many sources of defects that could impose considerable scatter to their stiffness and strength.

2.1.1. Model Hollow Clay Tiles

Commonly used hollow clay tiles have large perforations with thin web and face shells and a large percentage of coring. The shell thickness of the current typical HCT products is in the order of 4-8mm, whereas the products of 1960's and earlier had thicker shells of 6-15mm. Therefore, two types of hollow clay tile were used in the pilot studies. One type of the tiles was already available in the laboratory storage (Type I) and the other one was custom produced (Type II), Figures 2.1 and 2.2.

Scaling of the hollow clay tile size and thickness lower than 1:2 reduces the shells and unit sizes to a range where existing extrusion, handling and firing equipment cannot be used. Therefore, the Type II clay tiles were custom built only to one-half scale and produced using a standard industrial process. Resulting bricks indicated common flaws to their actual size counterparts when inspected. The similitude of the flaws was needed to reproduce a realistic model of the original material, and if the scale would be made smaller, could be masked by other effect such as extensive slitting, cracking and splitting during drying, and over-sintering during firing due to higher exposed surface to volume ratio.

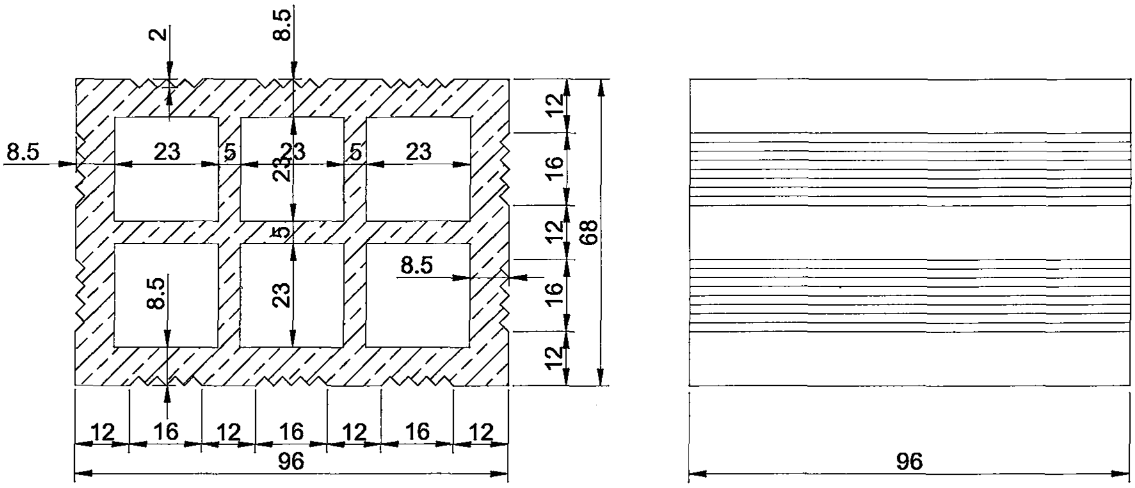

units are in millimeters

Figure 2.1. HCT Type I – Heavy hollow clay tile unit with thick shells

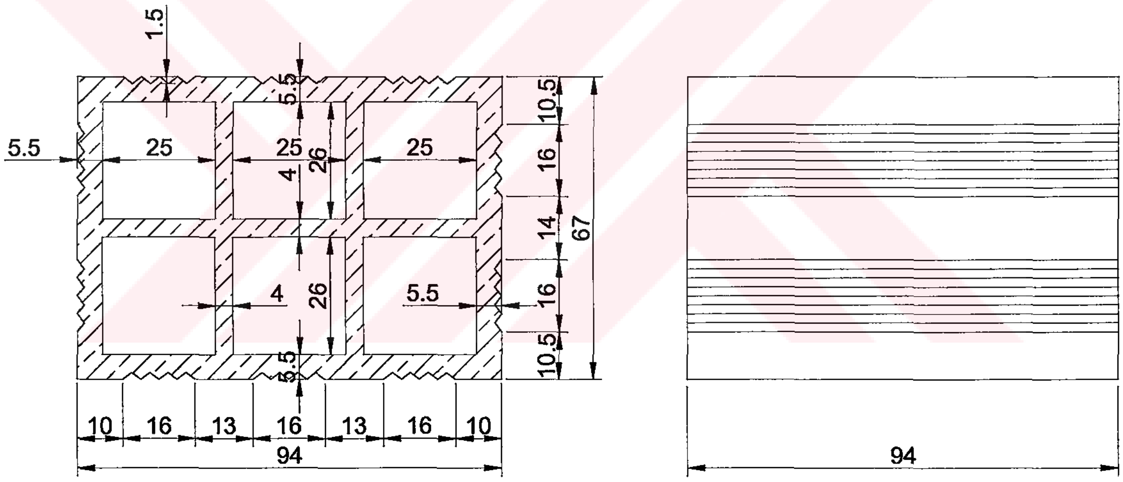

units are in millimeters

Figure 2.2. HCT Type II – Light hollow clay tile unit with thinner shells

2.1.2. Mortar and Render

Mortar and render preparation are generally regarded as simple site practices rather than designed and controlled construction step for infill walls. Since these walls are not regarded as load bearing, no inspection or quality control is exercised. Therefore, the production is not standardized and left to the masons care, ability and experience.

Two different mortar mixes were prepared by two different masons during the laboratory works and their recipe recorded measuring the amounts per volume and / or per weight and uniformity was assured by using materials out of the same batch. The stronger mix was proportioned using five parts of coarse river sand, one part of fine quartz sand, three parts cement and one part lime. The weaker mortar used eight parts of river sand, two parts of cement and one part lime. During each preparation, all ingredients were thoroughly mixed in air-dry condition and the measured water as required by the mason for the workability added. For neither of the mixes the water content was strictly fixed and the mason was allowed to improve the workability if required. However, the batches were prepared enough for a panel to reduce the need for tempering. Mortar and render used in specimen construction for laboratory testing were tested using the relevant American Society for Testing Materials (ASTM) specifications (ASTM, 1981a).

2.1.3. Prism Compressive Strength Tests

Strength characteristics of the masonry are generally defined by compression testing along the orthogonal directions. These tests yield the compressive strength and modulus of elasticity of the masonry for the tested orientation. Compression tests for masonry are standardized under (ASTM, 1981b), and require testing of prisms constructed from the specified masonry units and the mortar in a calibrated testing machine under compression. During the laboratory works, several prism specimens were tested and the results presented in the following sections.

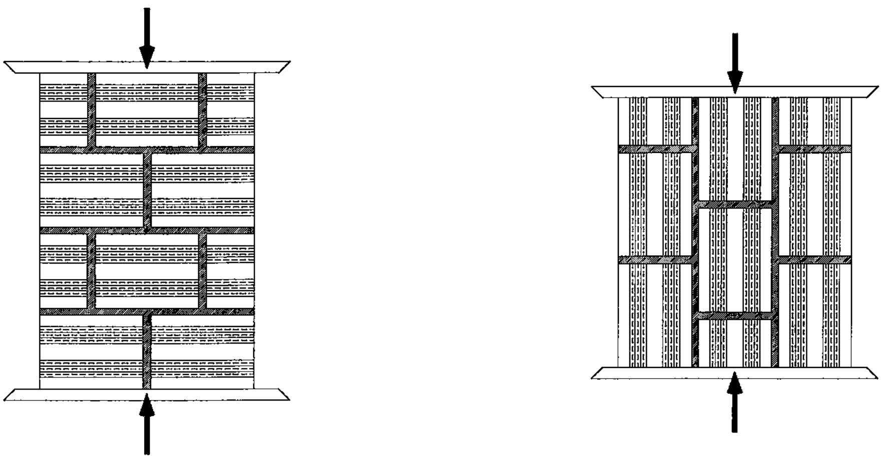

(a) (b)

Figure 2.3. Standardized tests on brick prisms

2.1.4. Shear and Diagonal Tensile Strength Tests

Shear strength testing of masonry has not been standardized thoroughly and there are still attempts to find simplified ways of testing this strength parameter. One of the available standards (ASTM, 1981c), is based on testing of a large square panel wall under diagonal compression to force diagonal tensile splitting. The size of the panel, specified as a 1200x1200mm small wall (wallette) specimen, is intended to include a representative number of masonry blocks and head and bed joints in the specimen. However, working with scaled masonry units, this requirement can be met with a smaller wallette size as well. Therefore, the diagonal tensile test specimens used for testing were kept to a size that is easy to handle for testing and for instrumentation, Figure 2.4.

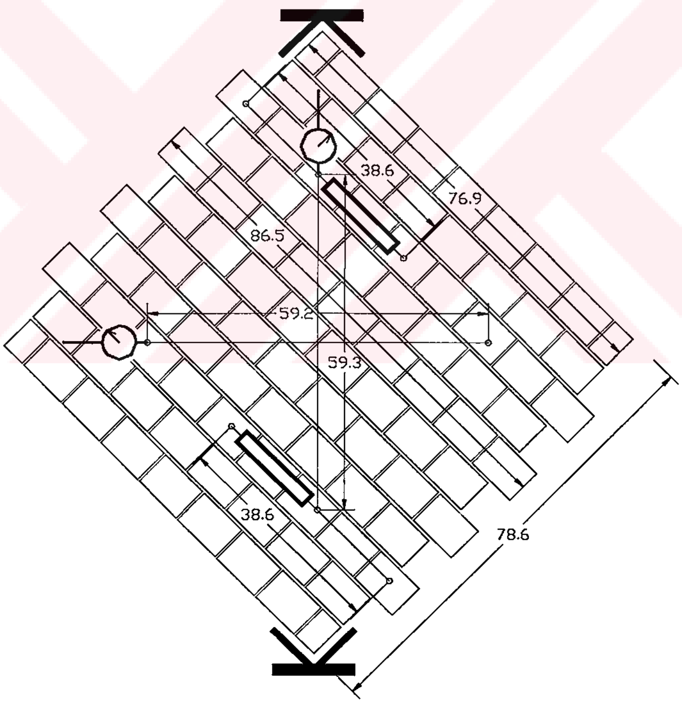

units are in centimeters

Figure 2.4. Small wall specimen (wallette) diagonal compression test arrangement

2.1.5. Non-standard Masonry Tests

All standards for masonry testing were originally intended for solid clay brick and hollow concrete masonry, where the applied stresses are distributed to comparably larger net area and the errors in load introduction can be accommodated by local yielding or minor crushing which does not impair the load transfer appreciably. However, the imperfections inherent to hollow clay tile and its brittle thin cellular structure accentuate the errors in load introduction, irregularities in specimen construction or material flaws in general. Moreover, a very large wallette size cannot produce the desired failure mode due to the load for compressive failure under loading shoe being comparable or less than the load to impose diagonal tensile failure. Therefore, a smaller scale coupon tests such as in Figure 2.5 (a) may be better suited to induce the desired mode of failure and to collect the required index strength values. On the other hand, the diagonal tensile failure of HCT involves face shell and web cracking in contrast to the bed joint failure common to their solid brick counterparts. Therefore, the resistance provided by the web cracking and mortar bed joints remain unidentified. However, the triplet tests as shown in Figure 2.5 (c) and a test devised during the current research for the specific definition of the web and face shell shear strength under double shear, Figure 2.5 (d), may provide the missing information and enable better structural and material modeling.

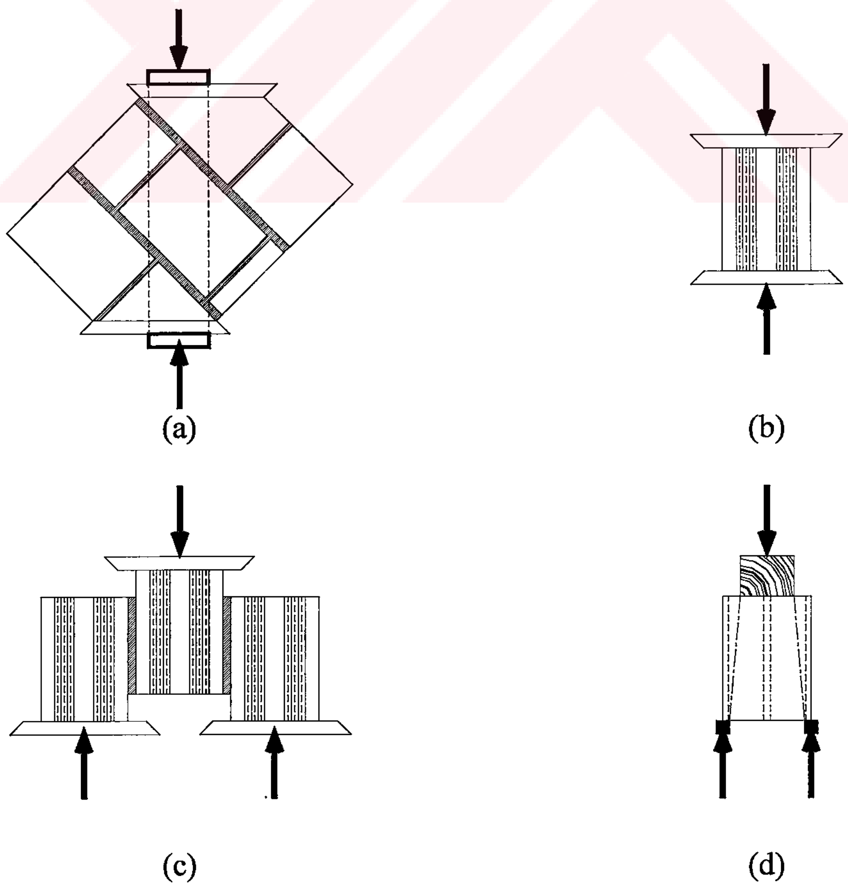

Figure 2.5. Non-standard hollow clay tile masonry tests

2.2. Infilled Frame Specimen

The infilled frame test program was planned to encompass common material and detailing flaws of existing construction and to contrast these with reference cases constructed as recommended in the latest codes. Therefore, the concrete strength was specified as 14MPa, and the reinforcing steel as low yield (220MPa). However, major strength loss and defects due to gross errors such as placing less amount of longitudinal reinforcement than specified, lack of proper and sound cover, and improper spacing and corrosion of reinforcement were not considered.

Two bare frame and six infilled frame specimens were designed based on an overall model scale of 1:3 of the actual size. The reinforcement arrangement of the specimens were based on preliminary design calculations of a five story regular structure with reference to building design standards (TSE, 1972; TSE, 1984; TCBIB, 1975), executed using a 2D simplified model. The spans of this prototype structure were taken 4.5m along both of the orthogonal directions and the standard dead and live loads referred in the paragraphs above were used. The structure was assumed to have three spans in the analyzed direction and modeled to repeat the same arrangement every 4.5m using symmetry constraints. Section sizes for columns were taken close to one tenth of the span length such as 450, 400, 400, 300, and 300mm staring from the lowest to highest floor. The lateral load coefficient was specified as 0.10, and the best soil conditions allowed were used. It was observed that a longitudinal reinforcement ratio of 1.5 per cent of the gross concrete section area was required for the first story columns, and 0.75 per cent beam top steel were adequate to meet the seismic demand requirements.

Detailing of the members was chosen to reflect the site malpractices on one end and the recommended and codified good practice on the other. Therefore, two sets of specimens denoted as Non-Compliant (NC) and Code Compliant (CC) were detailed. Non-compliant details involved 90-degree hooks for column ties and poor spacing arrangements. The spacing of the ties was so chosen as to fail member end-zone plastification criteria calculated using nominal material overstrength. Code compliant details included 135-degree seismic hooks on all ties and the tie spacing was defined to provide the required shear strength to maintain the plastic moments at member ends.

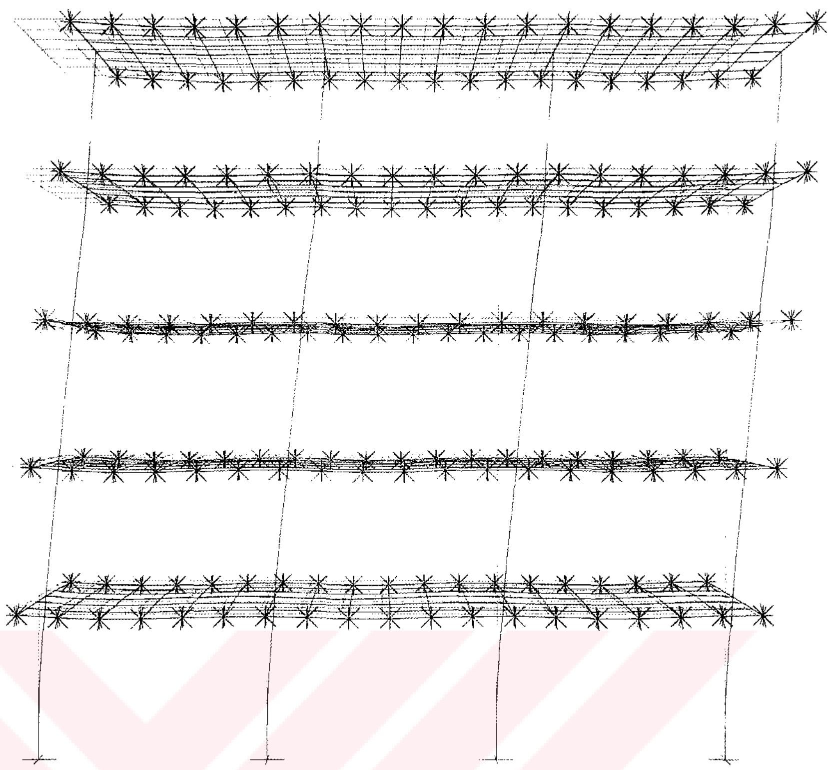

Figure 2.6. Plane frame building model with symmetry boundary conditions

Dimensions and reinforcement detailing discussed in the paragraphs above were scaled to a third using an overall scale and the final dimensions and detailing of the frame specimens defined. The reinforcement details and the corresponding bar arrangements are shown in Figures 2.7, 2.8 and 2.9. Final design of the specimens yielded 150mm square columns with four 10mm diameter low yield mild steel rebars with 6mm nominal diameter ties at 40, 80 or 100mm center-to-center spacing depending on the detailing requirements. Beam detailing allowed for the discontinuous bottom reinforcement at the support both to demonstrate the slip behavior and to reduce the developed bar strength with the short curtailment, which allowed the use of 10mm bars for all longitudinal reinforcing purposes. Stirrups were used as hooked U-bars with crossties for both CC and NC detailing to account for the support and splicing provided by the flanged construction and slab reinforcement. Axial loading on the columns were defined such that there would be no tension on the columns and thus the longitudinal bar splices at columns ends were not considered as a parameter.

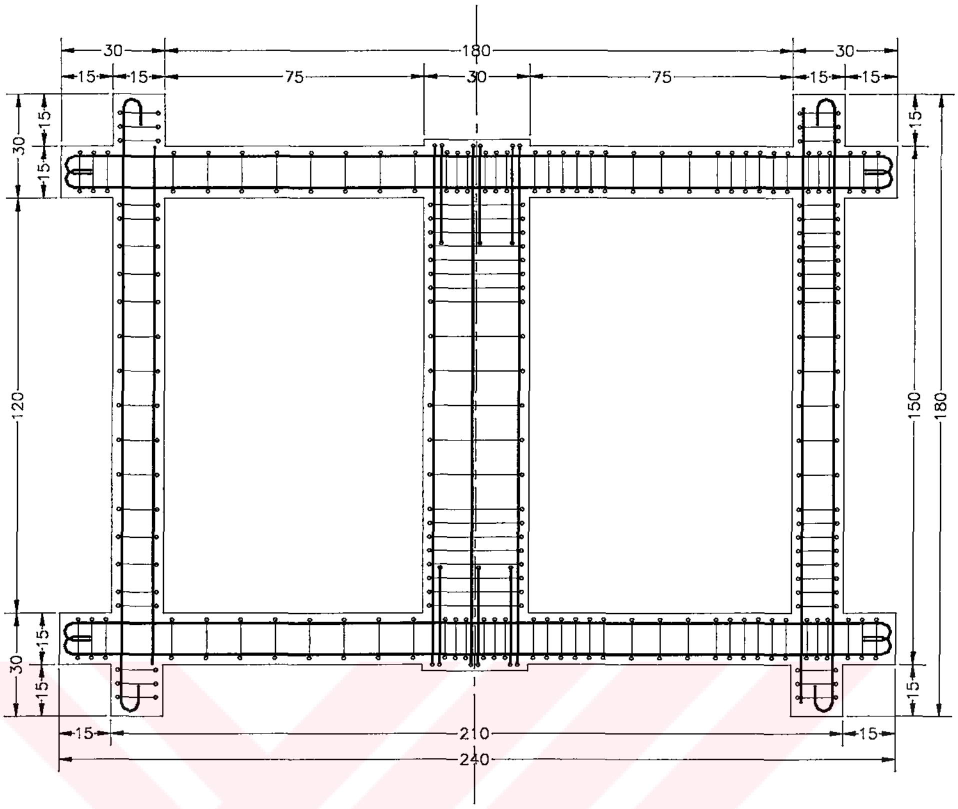

Figure 2.7. Frame specimen overall dimensions

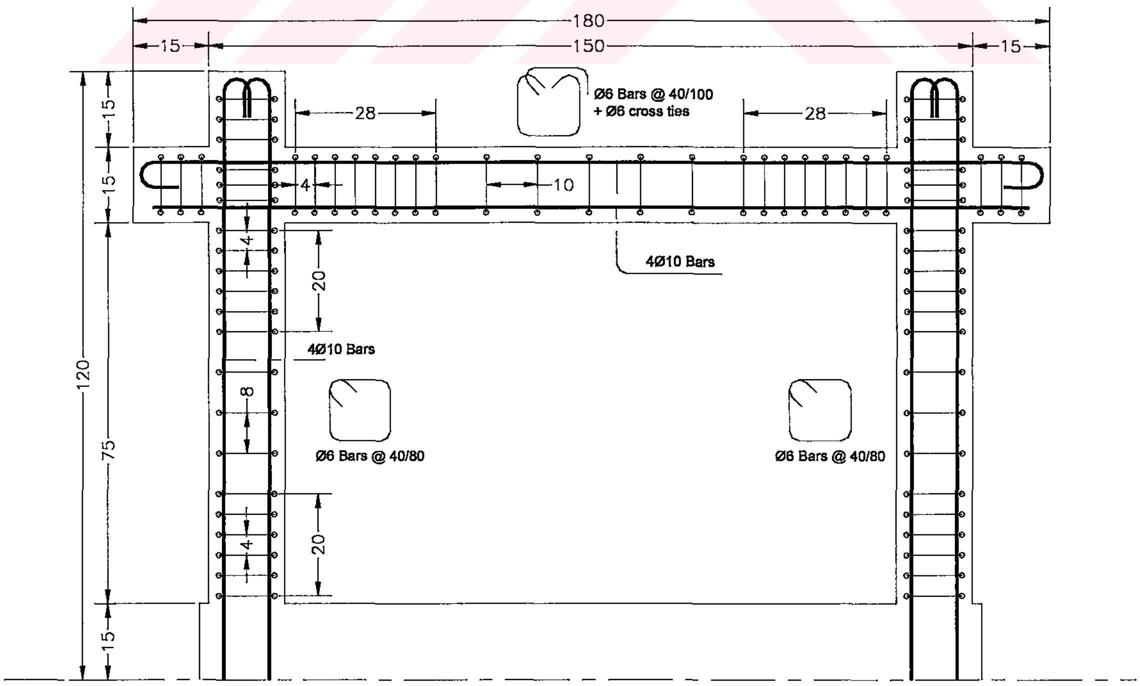

Figure 2.8. Code-compliant ductile frame detailing

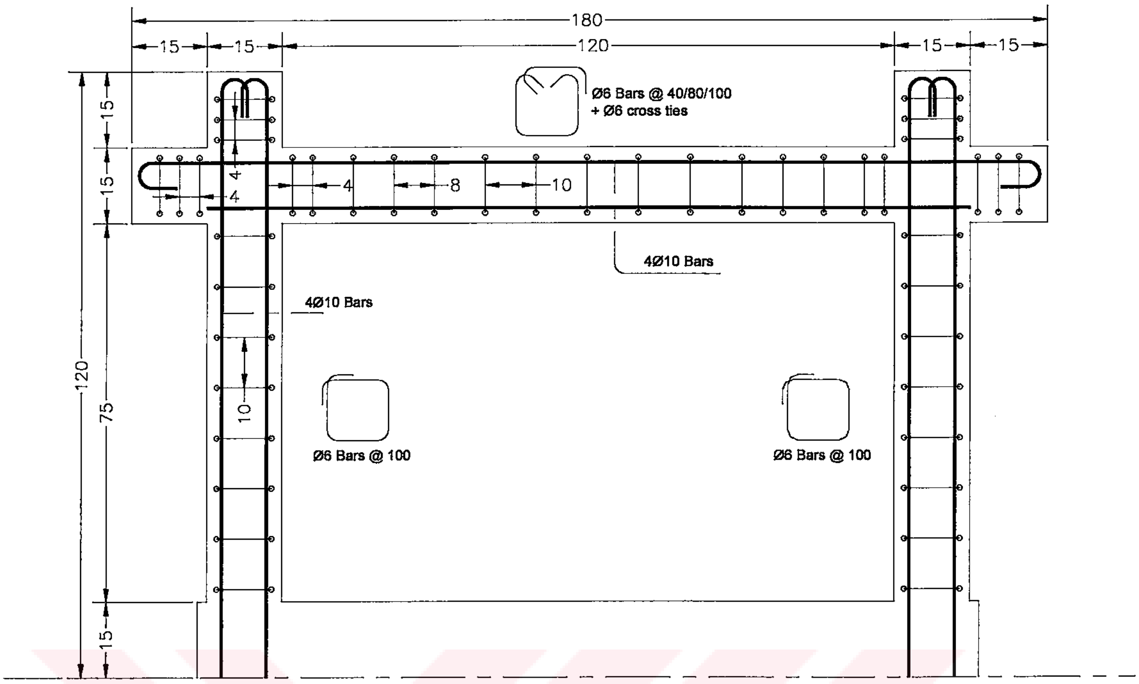

Figure 2.9. Non-compliant non-ductile frame detailing

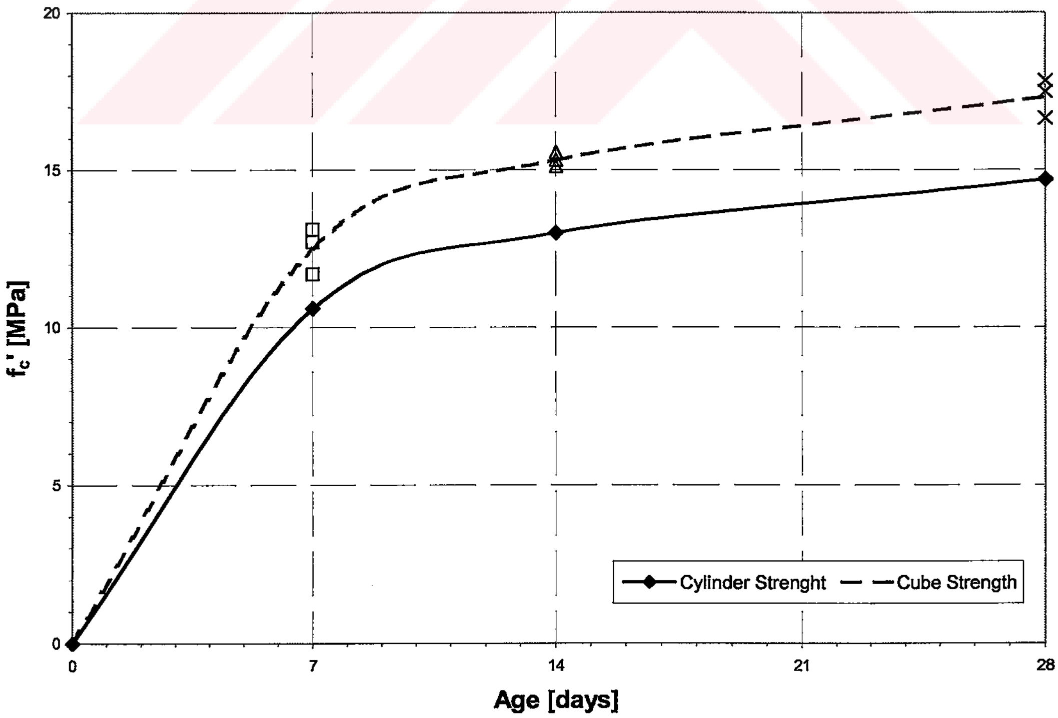

Figure 2.10. Strength development of the concrete used

Steel tensile strength and rupture load were tested by the laboratory of İnşaat Mühendisleri Odası, and found to be appreciably higher than the specified nominal value of 220 MPa. The yield strength of these six tests averaged to 367MPa. Tensile behavior of the steel was demonstrated to be mild with a distinct yield plateau and initial yield peak in five of the six tests. The sixth test did not demonstrate such properties but had the similar ultimate resistance. Inspecting the stress strain curve, the sixth specimen was observed to have uniformly slipped from jaws of the loading mouthpieces until the yield load was reached. Therefore, this specimen was considered an outlier and neglected in evaluations.

Infilled frame specimen column and beam axial force-moment interaction strength envelopes calculated using the tested concrete and steel strengths are given in Figure 2.11.

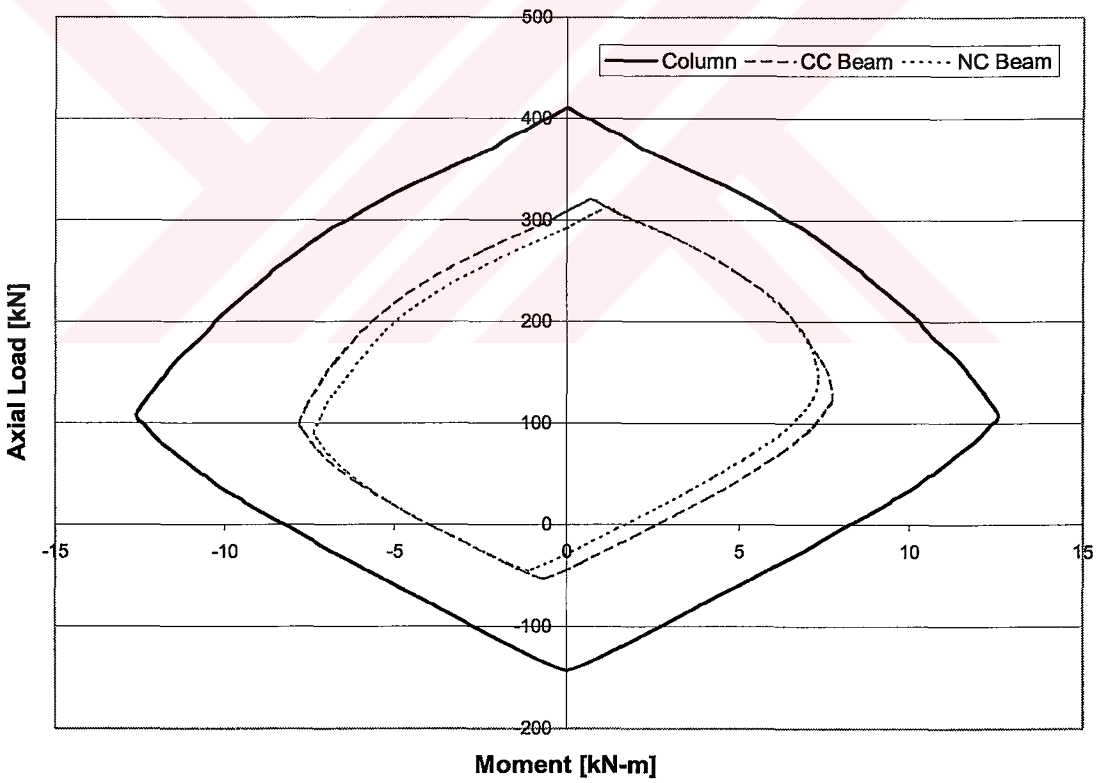

Figure 2.11. Axial force – moment interaction diagrams for columns and beams

2.2.1. Fiber Reinforced Plastic Material

Strengthening existing masonry and reinforced concrete structures with fiber-reinforced plastics is a new and developing field in seismic retrofit of existing structures

(Saadatmanesh, 1994). FRP materials have been in extensive use by automotive and aerospace industries due to their chemical resistance, high strength and stiffness, and comparably low weight.

Fiber reinforced plastics are composite materials formed using aligned, woven or dispersed fibers embedded into an epoxy or polyester resin matrix. This combination allows the use of the highly brittle fibers with little or limited environmental resistance in more flexible geometries and aggressive environments. Epoxy bonded glass fiber overlays were shown to improve the shear strength (Ehsani *et al.*, 1997), and ductility (Schwegler-Koller, 1994) of load bearing masonry structures.

Although the carbon fiber laminates and sheets have been used for extensively to increase the service load capacity of bridges and slabs, and axial load and ductility of columns, a similar frequency for the glass fiber sheets could not be observed due to their lack of alkali resistance. With the development of production processes to include alkali resistant sizes, glass fiber sheet are being used more often and chosen for their lower cost for the HCT retrofit schemes presented herein. The sheets used in the tests presented herein were woven sheets of 0.135mm nominal thickness with equal fiber amount aligned in two orthogonal directions, which had ultimate tensile strength in excess of 1700MPa, modulus of elasticity at 65GPa. For the bracing application, carbon fiber laminates of 1.2mm thickness, 50mm width, with an ultimate tensile strength in excess of 2500MPa, modulus of elasticity at 150GPa were used.

3. TESTS ON MASONRY UNITS AND ASSEMBLAGES

Masonry wall and prism tests were done on two types of hollow clay tiles where the difference was in amount of voids per masonry gross area. Type I brick was of 68x96x96mm dimensions, with (2x3) six square holes leaving 5mm internal and 8.5mm external clay shell thickness. External surfaces were grooved to form a rough surface, where the maximum groove depth was approximately 2 mm. Type II brick had similar overall dimensions with thinner face and web shells of 5.5mm and 4mm thickness, respectively. For both of the brick types following tests were undertaken:

- Prism compressive strength for both of the principal directions, Figure 2.1 (a) and (b).
- Compressive strength test on gypsum capped and uncapped hollow clay tile units both along and across the holes, Figure 2.2 (b).
- Diagonal tensile testing of small wall sections (wallettes), Figure 2.3.
- Mortar cube strength testing.

Masonry material tests are reported in the following sections. Most of the test results are followed by associated plane-stress finite element models with linear elastic material properties. These models were analyzed under the nominal failure loads observed during testing, and used to substantiate better our understanding of the failure modes and the reasons of multiplicity of the modes with fairly close failure loads. Interpretations assume that a Mohr-Coulomb failure envelope applies to HCT.

3.1. Type I Brick and Assembly Tests

To determine the strength of the Type I brick units, compressive strength tests using gypsum capped and uncapped samples were undertaken. Since the units were to be laid their square face down and their holes aligned within the plane of the wall specimen, the tests were conducted for two orthogonal direction of the clay tile unit. These two directions were parallel, Figure 2.2 (b), and perpendicular to the coring of the units. The average of the compressive strength results were found to be 105kN and 74kN for a single brick unit capped with gypsum and with no capping, respectively. Across-the-core-testing of the masonry units were also undertaken and the uncapped strength was found to be 26kN.

3.1.1. Wallette Construction

Twelve hollow brick masonry walls of 580x560mm were built by an experienced mason, who was briefed on the required uniformity of work by instructing the construction of few small wall sections and indicating the possible non-uniformities that could be picked-up during testing and would cause scatter of strength results. He was asked to prepare his typical mortar mix without any intervention or intention to provide guidance on the amount of ingredients. This resulted in the preparation of the strong mortar recipe. Workability of the mix was adjusted by adding extra water measuring the amount and the final proportions recorded. Using this mortar mix proportions 12 small wall specimens (wallettes) were built within 3 consecutive days and numbered from 01-12. Only nominal curing was applied to the specimens since the construction practices for actual structures do not cater for proper curing of the infill walls. Therefore, the walls were swept three times with a moist brush for within the first week of their construction to represent some nominal degree of curing.

3.1.2. Mortar and Render Testing

Mortar sampling was done using the standard procedures (ASTM, 1981a), where three 50x50x50mm cube samples were taken and tested under compressive load. During the construction of the wallettes, mortar samples were taken half the way into construction. This was aimed to provide better correlation with the tested strengths, since the sampled mortar layer would be on the failure path of the wall specimen with a higher probability and represent the average water content of the mortar layers with a better approximation. Mortar samples were not taken from each specimen, since the mix was controlled by weight rather than volume and the batches were prepared enough for only one specimen. Later, these samples were tested within ±2 days of the testing of masonry specimens. The control by weight has resulted in an average compressive strength of 16.7MPa and a coefficient of variation of 16%.

Four of the wall specimens were rendered 10mm thick on both faces using a standard site mix recipe. From three of the walls render samples were taken and tested. Although the mix proportions were controlled by weight, the last render mix indicated a large deviation form the other samples. This is attributed to a deviation in the mix proportions, where this mix was not prepared under inspection. Therefore, in the following discussions no corrections due to the measured render strengths are done.

3.1.3. Wall Specimen Tests under Diagonal Compression

Square wall specimens prepared as described above were tested as per standard procedures (ASTM, 1981c). Specimens were placed in the testing frame and loaded in compression along a diagonal, thus a diagonal tension failure was produced with the specimen splitting along the loaded diagonal. In Table 3.1, tested diagonal tensile strengths and predictions on the specimen strengths based on the failure path observed are given. Mortar shear strength is assumed to be governed by the direct tensile strength of mortar, $0.35(f_m')^{1/2}$, and no size correction for the mortar specimens (50x50x50mm cube) are incorporated. Since the render test results indicated considerable scatter, the rendered walls are assigned additional mortar amounting to the thickness of the present render and the render test data are not used.

Table 3.1. HCT Type I wallette reference notation and failure loads

Specimen Notation	***Wall No(1)***	***Calculated Load [kN] (2)***	***Failure Load [kN]***	***Failure / Calculated Load***	**σ [MPa]**
BR *Bare Wall*	**01**	74.16	70.75	0.95	0.94
	09	43.26	36.58	0.85	0.49
	11		46.56	1.08	0.62
	07		45.95	1.06	0.61
GS *With Glass Sheet*	**04**	*74.16 (3)*	88.59	*1.19*	1.00
	08		93.42	*1.26*	0.96
	10		80.42	*1.08*	1.00
	02		83.45	*1.13*	1.13
RW *With Render*	**06**	89.78	75.28	0.84	1.18
	03		72.56	0.81	1.24
	12		75.28	0.84	1.07
	05		84.96	0.95	1.11

(1) Specimens are listed in the testing order.
(2) Based on 16.7MPa average mortar strength and observed tensile failure path along bed-joints on the diagonal.
(3) Provided for reference only. Actual failure was corner crushing.

3.1.4. Wall Specimen Behavior

During the testing of the bare-wall specimens, a variety of failure modes such as, masonry bed joint failure, crushing of individual masonry units in and near the loading shoes, and breaking of corners of the masonry units on the diagonal line were observed. Failure surfaces mostly followed the individual mortar bed joints crossing the head joints from one layer of brick to another. Specimens 07, 09 and 11 failed in similar modes and comparable loads. However, the specimen number 01 failed in a markedly different mode and failure load. This was attributed to the comparably large amount of mortar used at this specimens head joints. Failure load of the specimens were approximated using the longest path for the failure surface from tests. Based on the observed failure surfaces, it was suggested that the effect of the head joints have been minimal for the bare masonry specimens, except for the specimen No 01. The major influence of the head joints was regarded as to provide interlocking keys (mortar bulbs) and uniform distribution within the bricklayer from one unit to another. Figures 3.1, 3.2 and 3.3 show the force-displacement behavior of the wallettes under diagonal compression. These figures are plotted after truncating the initial slip deformation region, which took place under very low loads and was due to gap closure within the loading shoes.

Failure modes of the rendered specimens included compressive failures at or near the loading shoes and splitting along the diagonal. The failure loads of individual specimens were not correlated with the mortar strength as opposed to the bare masonry case. The failure pattern of the glass sheet applied specimens was substantially different since the global splitting failure was converted to a local crushing mode. This mode was similar to the corner crushing failure of the infill panels.

Load-deformation plots of all specimens indicated a slip-like deformation jump of varying degree at the load interval 20-30kN. This observation implied that for lower mortar strengths, more pronounced slip deformations should be expected and a more extensive and spread mortar bed slip deformation observed.

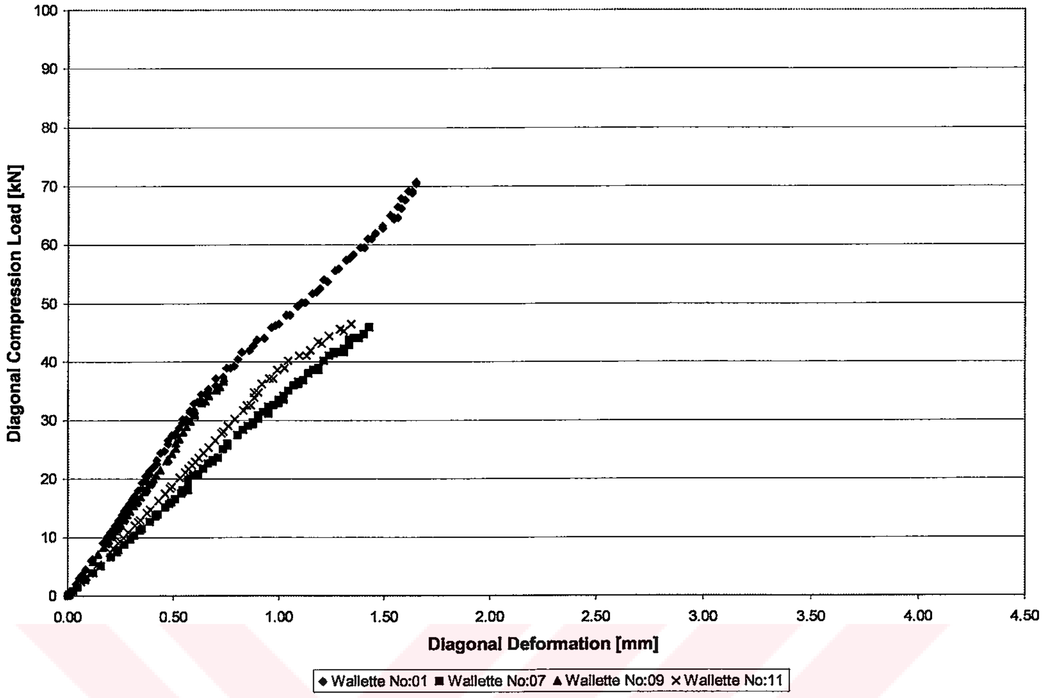

Figure 3.1. Bare Type I brick wall under diagonal compression

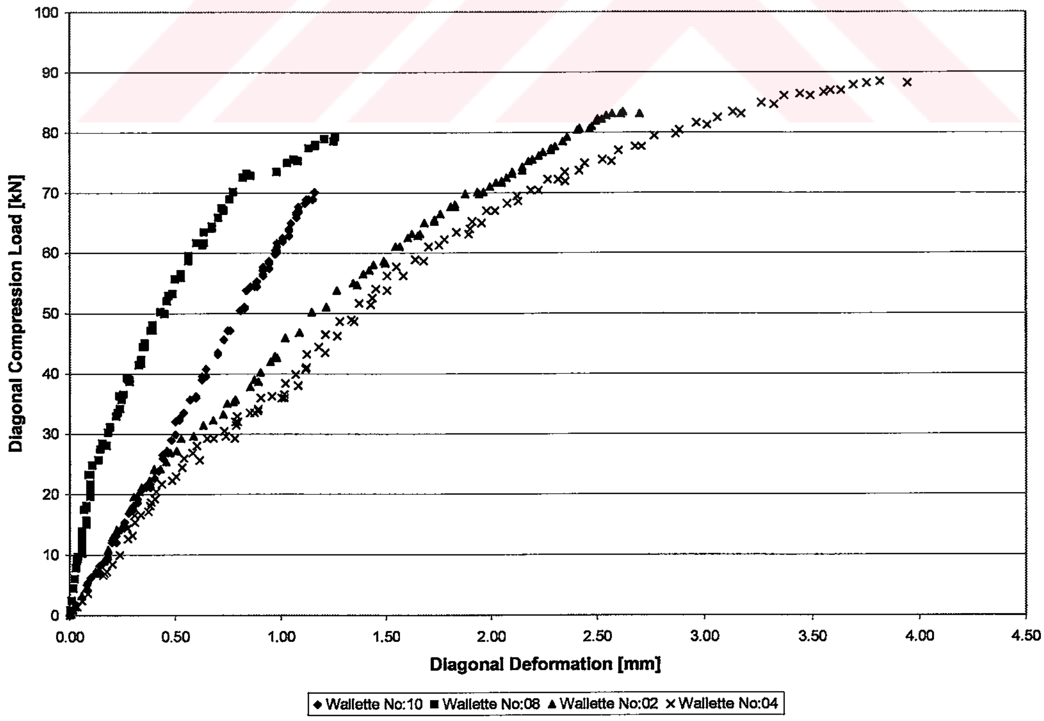

Figure 3.2. Glass-sheeted Type I brick wall under diagonal compression

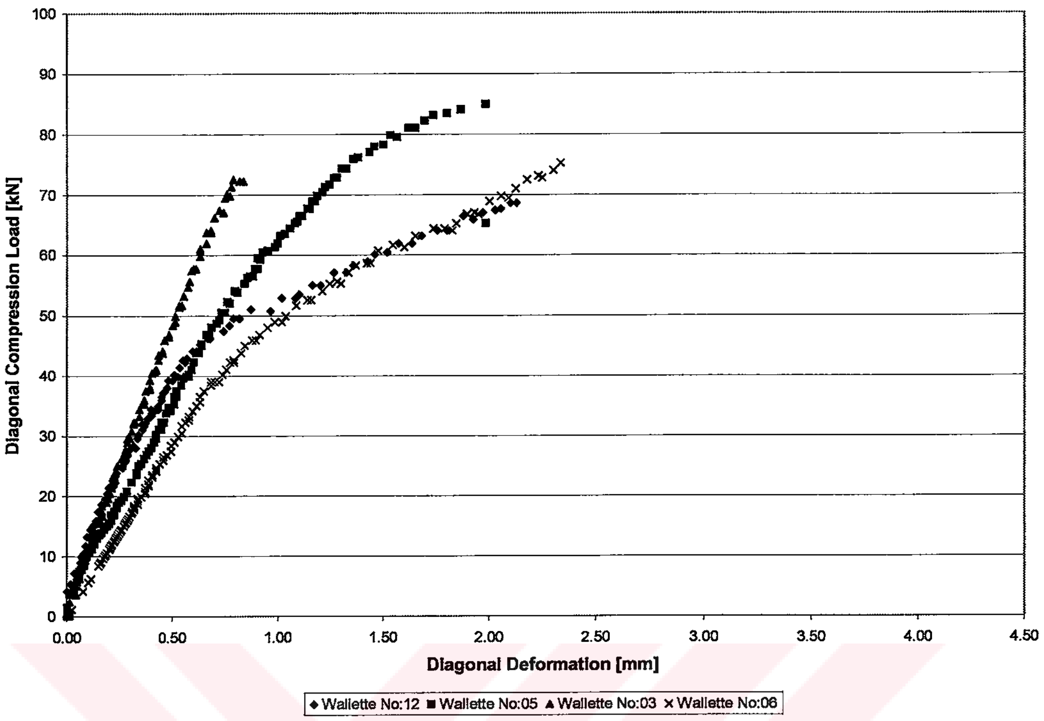

Figure 3.3. Rendered Type I brick wall under diagonal compression

Based on the results of the wallette tests, it was concluded that a properly executed render significantly increased the diagonal compressive strength, however, the failure mode remained global and brittle. A similar strength increase was observed for the case where the specimens were coated with glass sheet on both sides. The glass sheet applied specimens localized acute demands and prevented/delayed the global failure mode, and thus changed the failure pattern under diagonal compressive load from global to local.

3.2. Type II Brick and Assembly Tests

Second hollow clay tile masonry test series was based on the Type II model brick designed anew based on the pilot wallette test results. The hollow masonry units were modified to have 67x94x94mm overall dimensions, with (2x3) six square holes leaving 4mm – 5.5mm clay shell thickness, with external grooved surfaces forming a rough surface, with a maximum groove depth of approximately 1.5mm. With this geometry, scaled hollow clay tile units modeled the infill construction practice of the recent decades more closely.

To determine the strength of the Type II brick units, compressive strength tests of gypsum capped and un-capped samples were undertaken. The tests were conducted for two orthogonal directions of the clay tile unit, parallel and perpendicular to the coring. The average of the compressive strength results were 17kN and 41kN for a single brick capped with gypsum and uncapped, respectively.

Across-the-core-testing of the masonry units were also undertaken and the uncapped strength was found to be 27kN. The failure of the individual bricks was observed and noted. The compressive loads determined with gypsum capping were far less than strength given by the uncapped tests for along-the-core testing. This conflict was a result of the interaction between the cap and the tile where the narrow edges of the tile pierced into the capping and cut gypsum wedges that were pushed into the core of the clay tile and pop the face shells prematurely.

Contrary to the case for Type I bricks, the failure loads of the Type II bricks showed a large scatter due to the various imperfections introduced by their thinner shells and imperfections introduced during manufacturing process. Several of the brick units had unhealed die lines splitting face and/or web shells, and cracks at the joints of merging web shells that run all along the perforations. Since such imperfections are also common in the bricks used in regular construction, no additional measures were taken to better the model brick production and the material was accepted for construction.

3.2.1. Modulus of Elasticity

Modulus of elasticity tests were undertaken for across-the-core direction only. Out of three geometrically identical samples, average values of 2.24GPa based on gross and 13.2GPa for net section area were obtained. Since the web shells were significantly more slender than the mortar bed section, the shells of the HCT defined the systems stiffness, thus the modulus of elasticity. The net section based value recorded under low axial compression as given above was regarded as the uniaxial modulus of elasticity for the fired clay material and used as a reference value.

3.2.2. Wallette Tests

Nine hollow brick masonry walls of 870x790mm were built by an external mason. The different geometry and size of the second set of wallettes were chosen to simplify instrumentation installation, and was mainly required because of the large sizes of the Linear Variable Displacement Transducer's (LVDT's) used. After the bare wall construction, groups of three specimens were kept bare, rendered and glass-sheeted (single side).

For the Type II brick walls and prisms, the mortar mix proportions were controlled using materials by volume rather than by weight and thus all mortar mixes were sampled and tested. Since the mortar strength in the earlier test series was higher than the standard site practice, the mortar quality was reduced and the mix re-designed. The mix proportions by volume were eight parts of sand, two parts cement and one part lime, and the water content was adjusted to get a workable mix. New mix proportions lead to lower mortar strength that revealed itself in the out-of-plane flexural failures of some walls during construction, handling and testing. Two out of three bare masonry specimens and one of the rendered specimens had to be cut into coupons because of these failures.

In instrumenting the specimens, the LVDT's crossing over the diagonal were aimed to measure the sliding component of the diagonal crack to form on the vertically positioned diagonal, and the dial gauges were used to measure vertical diagonal shortening under load and the spread along the horizontally aligned diagonal. In contrast to the Type I brick testing results, all specimens, whether bare, rendered or glass sheet applied, failed under corner crushing mode with the failure of the few bricks at the compressed diagonals. Failures were induced at very low diagonal compressive loads and the LVDT's and the dial gauge along the horizontal did not measure significant deformations as compared to the accuracy of the devices. Therefore, only the failure loads are reported. The reason behind such a response was evident in the low compressive capacity of the new model bricks. In the earlier test series, the compressive strength of the brick units was high enough to develop the mortar bed-joint strength, whereas the new bricks were unable to provide such resistance. Due to the local nature of the failures, each wallette was loaded twice changing the loaded diagonal and the results were close to one another except the considerable drop in load for the bare walls, Table 3.2.

3.2.3. Finite Element Models of the Wallette Tests

Observed behavior in the Type II wallette tests were contradictory to the post-earthquake site records, where stepped bed-joint sliding was associated with a lower lateral load than the corner crushing failure mode. The reason for the test findings was attributed to the method of loading. The standard masonry tests, such as diagonal compression test, were originally intended for the solid brick masonry and/or grouted concrete masonry with high compressive strength in contrast to the weak mortar. Therefore, the loaded area could be confined to a small contact surface. With the HCT, the same loading arrangement was seen to produce corner crushing because of the low compressive strength of these units.

According to the reviewed material on the infilled frame behavior, actual contact area that imposed the diagonal cracking in an existing buildings infill could be expected in the order of one-tenth to one-third of the beam or column length. Therefore, an HCT wall failing in corner crushing under a diagonal compression test may produce higher loads and different modes of failure under loads applied through a larger contact area. To investigate whether this could be the case for the lighter HCT of the second wallette test series, finite element model of the wallettes were developed and the resulting stress distributions under a load close to the experimentally found failure load inspected.

Overall dimensions of the Finite Element (FE) models were taken as the Type II wallette specimen to enable a direct comparison between the two HCT types tested. Plane stress membrane elements available in SAP2000 finite element analysis program (Wilson, 1995) were used to model the face and web shells of the units within the wall plane and frame elements were used to lump the flanges of the units and mortar bed between the units. The four parallel face shells of the tiles were assumed to act as-if a single material sheet and thus the FE thickness was taken as the four fold of the individual webs and face shells. Frame elements that act as the booms of material perpendicular to the webs were assigned flexural releases at their ends and acted as truss elements. Mortar was assumed to act like an added thickness to the tile shells and modeled as an increased thickness of the booms. The head joint was assumed to act like a separate boom of 25mm width based on the observations from the coupons cut from the wall specimens.

Finite element analyses clearly indicated a stress concentration near the loading shoes, which could be negligible in the strong masonry unit – weak mortar combination but was of the governing factor in the HCT case. According to the stress plots of the FE analyses, the sections of the diagonal compressive test arrangement under the highest compressive stress are in the immediate vicinity of the loading shoes. The spread of the stress bulb is approximately two bricks wide and is less in magnitude for the Type I clay tiles due to their thicker shells. Average across-the-core compressive strength of Type I tiles is 105kN, whereas it is 27kN for the Type II tiles. Therefore, the failure modes as observed during testing and indicated by FEM analysis are mortar bed shear failure for heavier hollow clay tile and corner crushing for the lighter Type II tile. Correlation of the diagonal compression test results with the nominal compressive strength of two-unit wide prisms of the Type II material, reported in the following section, also supports these observations.

Table 3.2. HCT Type II wallette reference notation and failure loads

Specimen Notation	***Wall No***[(1)]	***Calculated Load [kN]***[(2)]	***Failure Load [kN]***	***Failure / Calculated Load***	**σ [MPa]**
BR *Bare Wall*	***02a***	80.0	42.9	0.54	0.42
	02b		32.2	0.40	0.31
GS *With Glass Sheet*	***03a***	80.0	55.2	0.69	0.54
	03b		49.6	0.62	0.49
	08a		63.4	0.79	0.62
	08b		61.6	0.77	0.60
	10a		60.6	0.76	0.59
	10b		60.0	0.75	0.59
RW *With Render*	***04a***	97.0	125.7	1.30	1.01
	04b		120.7	1.24	0.97
	07a		90.3	0.93	0.73
	07b		88.3	0.91	0.71

(1) Specimens are tested twice due to corner crushing failure.
(2) Based on 10.4MPa average mortar strength and assumed tensile failure path along bed-joints on the diagonal. Actual failure mode was corner crushing.

3.2.4. Masonry Prism Tests

Prism tests were aimed to provide data for the prediction of the wallette and infilled frame behavior modes and failure loads. These tests employed stacks of masonry units that were constructed from the same batch of materials as infill panels or wallette specimens but as smaller samples. Two types of prisms were prepared for across-the-core testing, running bond masonry samples of two units width and four units height, and stack bond prisms of one unit width and four units height.

The results indicated that the HCT masonry compressive strength had a large coefficient of variation due to the imperfect web and shell (with longitudinal slits) due to the bridge die extrusion involved in the manufacturing process. Based on these observations, the masonry tests were confined to modulus of elasticity tests performed on brick prism specimens, compressive strength tests on coupons, and triplet tests.

Table 3.3. Bare masonry prism test results

Loading	***Code***	***Length* [mm]**	***Width* [mm]**	***Load* [kN]**	**σ [MPa]**
Across	*PB/10C*	215	195	53.1	2.8
	PB/10D	206	192	65.2	4.0
	PB/10F	211	190	14.3*	-
				Average	**3.4**
Along	*PB/10A*	195	212	139.2	6.6
	PB/10B	194	213	189.3	9.6
	PB/10E	198	210	127.8	6.5
**Side faces not orthogonal*				**Average**	**7.6**

Table 3.4. Glass-sheeted masonry prism test results

Loading	***Code***	***Length* [mm]**	***Width* [mm]**	***Load* [kN]**	**σ [MPa]**
Across	*PG/08A*	212	192	72.5	3.8
	PG/08B	210	187	69.6	3.7
	PG/08E	210	192	68.7	3.7
				Average	**3.8**
Along	*PG/08C*	192	215	157.9	7.9
	PG/08D	210	194	146.9	6.9
	PG/08F	196	210	151.3	7.5
				Average	**7.4**

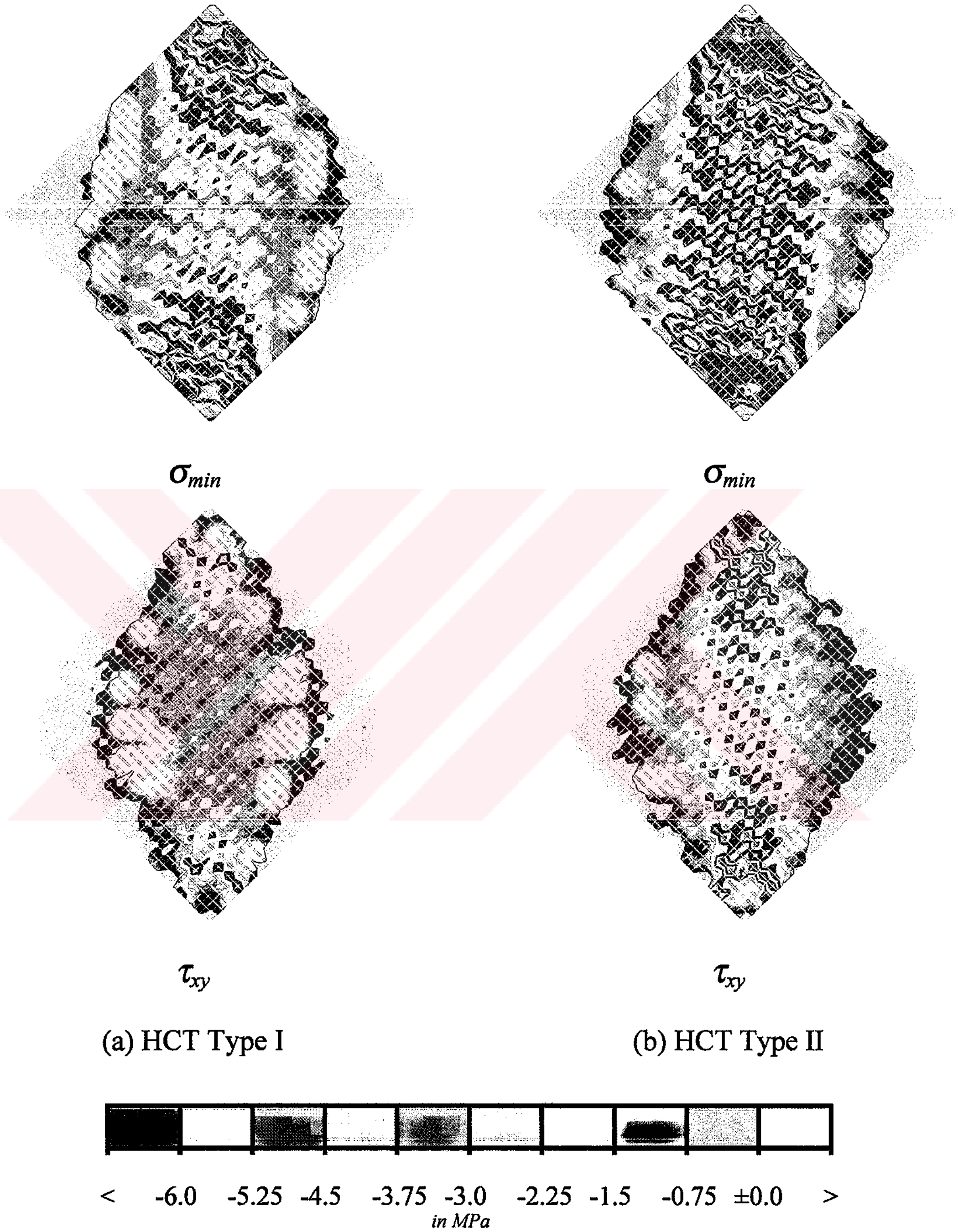

Figure 3.4. Minimum principal and shear stresses in diagonally loaded HCT panels

3.2.5. Coupon Tests

Coupon tests were aimed to provide additional data for the prediction of the wallette and infilled frame behavior modes and failure loads. These tests employed sections cut from the wallette specimens that failed due to out-of-plane flexure during the diagonal compressive test preparations, Tables 3.5, 3.6 and 3.7.

Repetition of the diagonal compression tests on the coupons cut from the not tested wallettes (with out-of-plane failures due to weak mortar) showed that there is a size effect that is governed by the ratio of shear tested area versus the loaded wall portion. Tests on the coupons were more in line with the needs of material property definition for the masonry as infill material, Table 3.7.

Table 3.5. Coupon test results for across-the-core testing

Type	*Code*	*Length* [mm]	*Width* [mm]	*Load* [kN]	σ [MPa]
Bare	*PB/01E*	210	250	49.2	2.0
	PB/05E	282	235	36.6	1.6
	PB/09F	284	240	34.3	1.5
				Average	**1.7**
Render Applied	*PR/06B*	285	243	103,0	3.2
	PR/06E	250	233	44.3	-
	PR/06F	280	280	105.5	3.1
				Average	**3.1**

Table 3.6. Coupon test results for along-the-core testing

Type	*Code*	*Length* [mm]	*Width* [mm]	*Load* [kN]	σ [MPa]
Bare	*PB/01C*	229	208	166.9	8.1
	PB/01D	242	210	78.2	-
	PB/05C	235	210	103.4	5.2
	PB/05D	238	206	108.2	5.2
	PB/09C	235	212	121.5	5.6
				Average	**6.0**
Render Applied	*PR/06C*	245	200	108.6	4.1
	PR/06D	240	210	101.5	4.0
				Average	**4.1**

Table 3.7. Coupon test results under modified diagonal compression

Specimen	*Code*	*Length* [mm]	*Width* [mm]	*Load* [kN]	σ [MPa]
Bare	*PB/01A*	253	365	26.6	1.01
	PB/01B	245	370	27.1	1.03
	PB/05A	250	370	25.0	0.96
	PB/05B	242	360	29.6	1.12
	PB/09A	253	370	22.0	0.82
	PB/09D	250	360	18.7	0.70
				Average	**0.94**
Render Applied	*PR/06A*	237	370	47.4	1.79
	PR/06B	235	370	39.1	1.46
				Average	**1.62**

Coupon tests on the specimens cut from the wallette sections had lower across-the-core compressive strength due to less uniform workmanship, Table 3.5. The prisms were constructed with extra caution and the mortar bed joints were completely filled. However, the coupons had non-uniform and incomplete mortar beds that introduced additional stress concentrations near the joining line of the face shells and the webs, and the stress concentrations caused a drop in the maximum load.

3.2.6. Triplet Tests

Triplet specimens were formed using three bricks with the central brick off-set by a small distance (~20mm) from the outside bricks within the wall plane, like a very short running bond interlock. The triplets were tested imposing "double shear" thereby inducing known nominal shear stresses on the mortar joints. Test results indicated, that there would be stress concentrations on the face and web shells, which would lead to masonry unit governed failure modes.

Triplet tests on the glass-sheet applied samples indicated that if a bed joint sliding failure mode was initiated, the deformation capacity of the walls could be expected to increase and a residual strength based on the glass-sheet plying off would be added to the dry bed-joint friction of the ordinary HCT. Figure 3.5 and 3.6 show the glass-sheet applied triplets after testing where the face shells of the bricks were sheared off due to the forces being carried principally by the glass fibers after the bed-joint shear failure. Table 3.8 summarizes the triplet shear strength results.

Similar to wallette specimens FE models of the triplet test were also developed. Modeling features for HCT were kept the same but for these models the mortar was also modeled using shell elements and the contact boundary established by iterative solution for no-tension support forces.

FEM results help explain the observed failure patterns during testing, Figure 3.7. Several of the tested specimens had tensile cracking along the central vertical axis at the middle web of the central brick, on the interior edges of the face shells of the exterior bricks on the side adjacent to the mortar bed, and along the diagonal of the coring.

Under 30kN, the shear stress on the mortar joint is in the order of 3MPa, whereas the tensile stresses at the bottom edge of the central brick were in excess of 12MPa. Therefore, out of the two dominant modes in tests, mortar bed joint failure and tensile cracking of the clay tile, only the bed joint sliding may be associated with loads in the order of 30kN and the tensile cracking should have preceded this mode. These deductions coincide with the test observations where several tensile cracks had formed before the final failure was reached.

Table 3.8. Triplet test results for 10.4MPa average mortar strength

Specimen	***Glass Sheet Orientation***	***Code***	***Loading in kN***	***# of Failed Joints***	τ_o **[MPa]**
BR *Bare Triplet*	**N/A**	*TP/B01*	30.4	0	2.1
		TP/B02	41.2	2	2.9
		TP/B03	26.6	1	1.9
GS *With Glass Sheet*	**0 / 90**	*TP/G01/90*	47.4	2	3.3
		TP/G02/90	48.0	2	3.4
		TP/G03/90	37.5	2	2.6
	45 / 135	*TP/G01/45*	31.2	1	2.2
		TP/G02/45	42.6	2	3.0
		TP/G03/45	33.8	1	2.4

Figure 3.5. Glass-sheeted triplet after testing

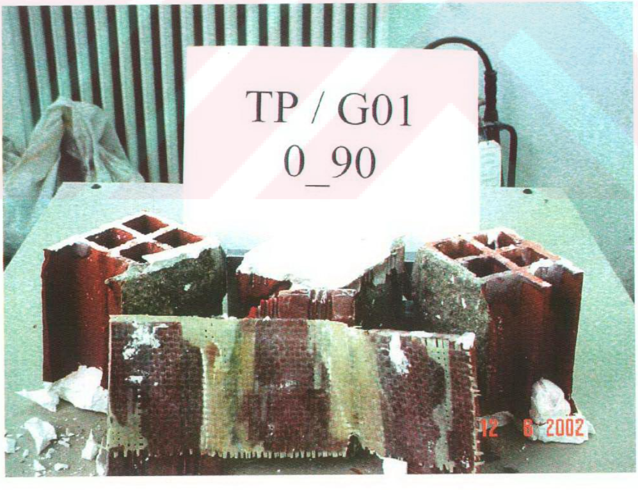

Figure 3.6. Triplet pieces after testing

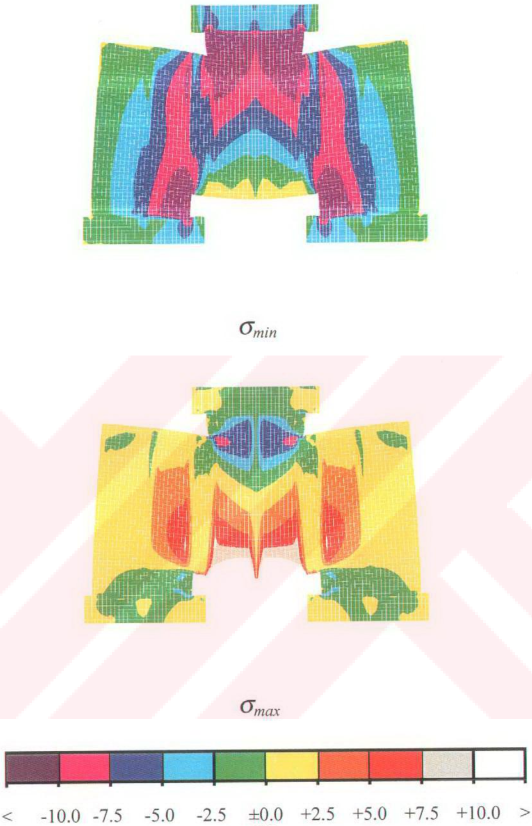

Figure 3.7. Plane-stress analysis results of HCT triplet under 30kN

3.2.7. Hollow Clay Tile Web Shear Tests

To obtain the strength contribution of the sheared webs and shells of the HCT, individual tiles were tested on two steel supports placed under the long side face shells and by introducing the load on the opposite end using a wooden block with a width of half the unit thickness, Figure 2.5 (d). Thus, the load was introduced largely by the middle web and to a lesser extent by the shells perpendicular to this web. Out of the tested twelve bricks, a resistance in average of 10.5kN and with 2.3kN standard deviation was recorded. Converting to shear stress on the total nominal web shell area, a shear resistance of 3.5MPa under single shear was assessed.

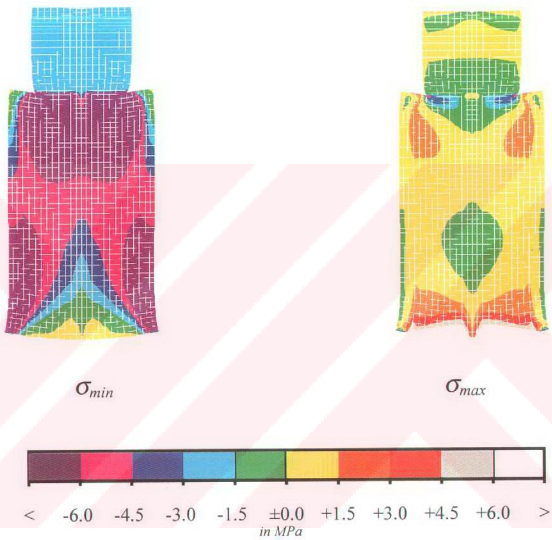

Figure 3.8. Plane-stress analysis results of HCT web shear test under 10kN

Failure modes observed during tests involved several cracking paths on the webs and face shells, splitting at the abutting points of these shells, compressive failure initiation at the lower supports and tensile cracking at the bottom edges of the face shells.

A finite element model of the tested hollow clay tile samples constructed using nominal dimensions indicates the stress concentrations and the maximum principal stress as greater than 6MPa which is a tensile stress largely parallel to the horizontal. Another similar stress level is the shear stress on the web shells. This suggests that the strength values obtained from tests would be governed by two failure regimes such as the tensile failure or shear failure of the web. Referring to the maximum stresses horizontal (σ_{max}) at the bottom of the clay tile, one can argue that the tensile strength of the fired clay used should be in the order of 10MPa, which is expected to be limited by the presence of impurities and shrinkage cracks contained that would act as stress raisers. The FEM analysis can be replaced by a simple beam analysis using the vertical face and web shells to calculate the equivalent inertia, which yields a conservative estimate of 6.9MPa for tensile strength.

3.2.8. HCT Strength Parameters

Failure of HCT masonry prisms loaded across-the-core in compression initiated by the splitting cracking of the flanges connecting the vertical face and web shells of the units at web-flange junctions. These cracks split particularly the face shells from the interior flanges along the coring and pose a higher slenderness ratio for these sections. Under increasing load the face shells fail under stability triggered explosive failure where the complete face shell or parts thereof spall. Similar observations were made by researcher working with larger size HCT units (Johnson and Matthys, 1973; Bennett *et al.*, 1997). Failure under along-the-core loads is less sudden and starts with the crushing and spalling of head joint mortar.

Compressive strength calculated from HCT unit compressive testing for the net section area was found for Type II units as 17.9 and 22.9MPa for along- and across-the-core testing, respectively. Similar relative strength differences were observed by Bennett *et al.* (1997) and by the researches they refer and whose results they recite. The observed difference supports the idea that the across-the-core failures are of instability origin.

For further modeling studies, the use of a modulus of elasticity of 13155MPa, compressive strength of 17.9MPa and a tensile strength half as much as the compressive strength was proposed based on the findings summarized above.

4. TESTS ON INFILLED FRAMES

Amongst the reviewed test methods, testing of the back-to-back specimens in a horizontal bed was chosen in the absence of a reaction wall or frame. Similar tests were already done in the laboratory for reinforced concrete frames with reinforced concrete infills (Türk, 1998). The existing setup comprised of two R/C reaction beams with two steel tie beams for restraining their outward movement capable to support a 60kN load acted at the center of the reaction beam, Figure 4.1. Therefore, the eight reinforced concrete frames were constructed in a back-to-back arrangement.

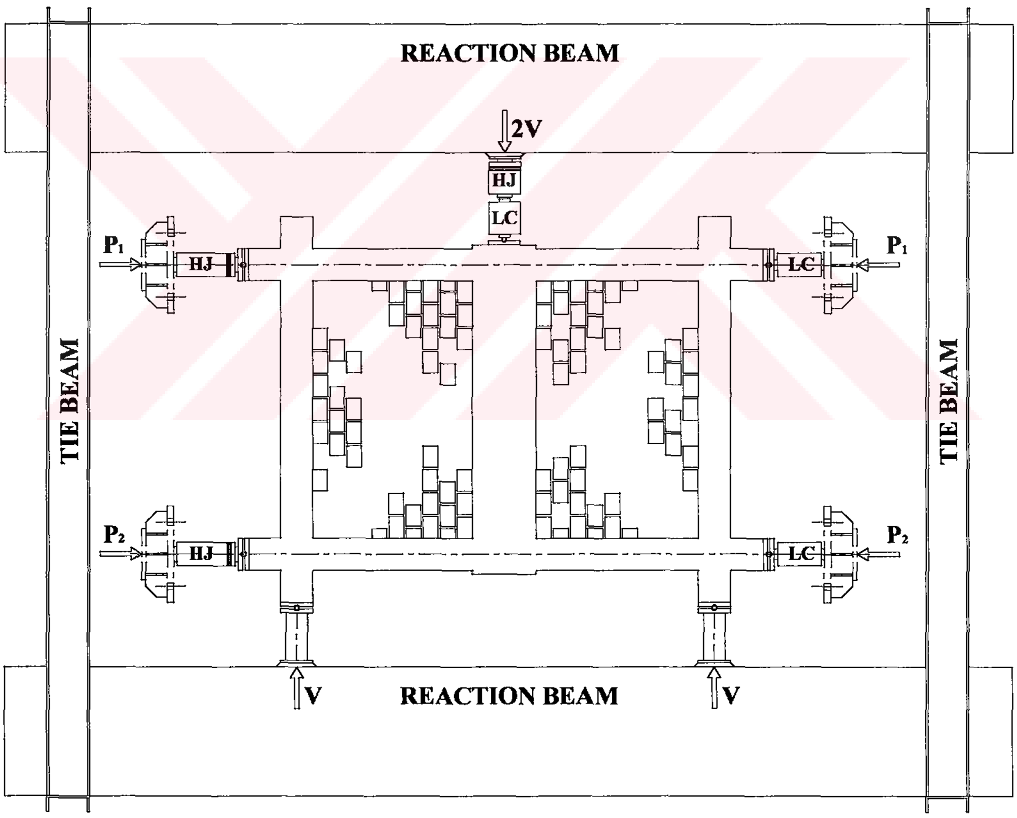

Figure 4.1. Setup for horizontal back-to-back testing of infilled frames

The reinforcing cages of the specimens were prepared by professional construction workers and all pieces were hand tied. Strain gauges were glued on one side of the specimens at six stations. The instrumented locations were one end of the beam, and both ends of the two columns on one side of the specimen. All gauge wires were color coded and extended. After all work with the cages was completed, these were placed into the prepared formwork and all were cast at the same time using a low-strength ready-mix concrete. Several cube and cylinder samples were taken and stored at similar conditions to the infilled frame samples. No curing was undertaken except on the two days following the concrete casting, which was aimed to stop excessive shrinkage cracking only. On the third day of concrete cast, the sides of the formwork was removed.

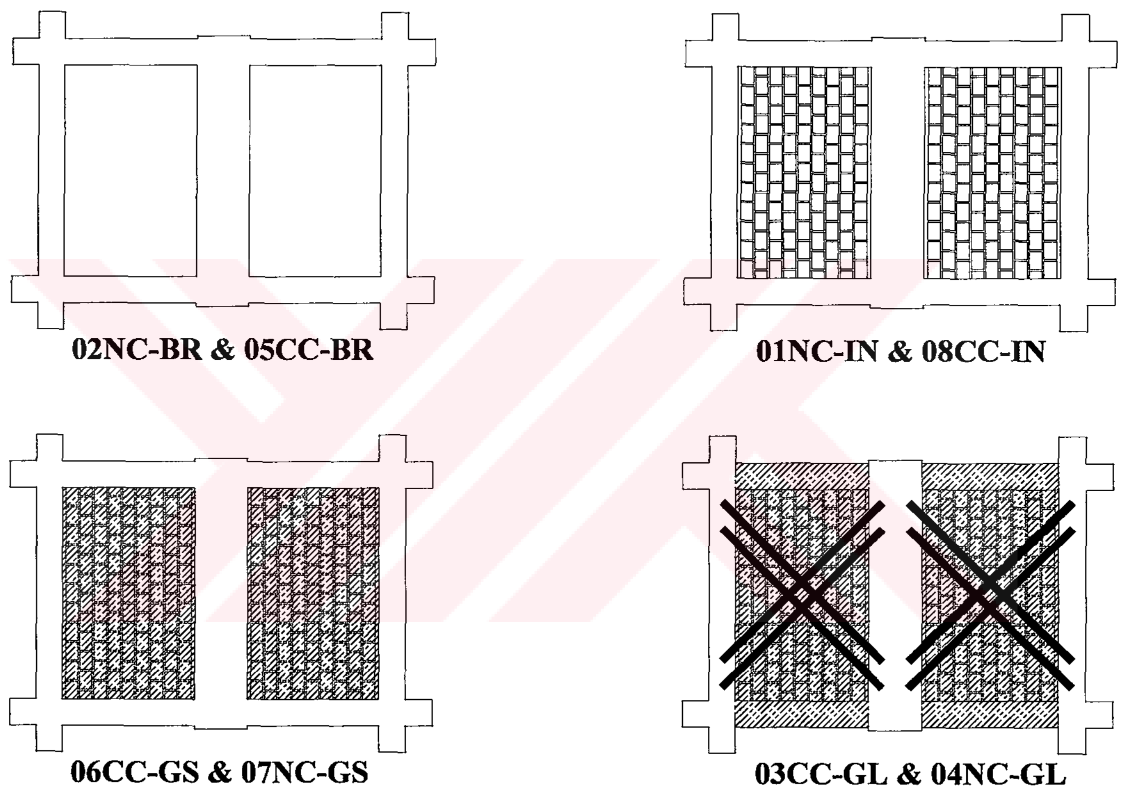

Figure 4.2. Tested specimen types and their code numbers

After the testing of the cube samples in the second week following the concrete cast, six of the frames were infilled with hollow clay tile masonry. Infill walls were constructed while the frames were lying flat on the laboratory floor, thus, flush to one side of the frame columns as common in residential construction. Mortar used in the infill construction was sampled and cubes stored under the same environmental conditions as the infilled frames. In the following weeks the moisture of the infill elements were checked and upon the agreement of the FRP applicators engineer the glass-sheet and the laminates installed.

4.1. Test Setup

4.1.1. Loading and Support Devices

All specimens were tested in the same loading configuration. However, some of the measurement devices were re-arranged to collect data on added features while changing from bare frames to infilled-strengthened frames. Loading was achieved by pushing the central "foundation" beam against the reinforced concrete reaction beams and providing support on the opposite side of the specimen with the beam extrusions resting against another reaction beam. The two reinforced concrete reaction beams were connected via two pairs of tie beams, which would balance the reaction forces, should the friction forces between the reaction beams and the laboratory floor be exceeded. In order to limit biased deformations in such a slip condition, the central points of these tie beams were further anchored to the floor using steel cantilever post.

Axial loads on the columns were introduced using loading platens and chords designed for 300kN maximum load, which allowed each column to be loaded individually. Four 30-diameter tie rods were used to connect the loading platens at either end of the columns. The loading platens were placed into a railed-bedding that would allow limited rotations and practically full freedom for the deformations along the column height.

4.1.2. Measurements and Data Acquisition

Measurements of deformations and forces were done using:

- Four load cells of 200, 300, 700, & 1000kN capacity where the first two were used to control the axial load introduction to the columns, and the other two to measure the lateral load,
- During specimen construction, eighteen strain gauges were installed on one side of each specimen to measure strains at one of the beam-ends, and both ends of the two columns on one side. Each location had three gauges installed; one for the tie strain and two for the longitudinal reinforcement under flexural-axial loads,

- Four dial gauges were used to measure the overall translations and rotations of the specimen for the rigid body motion degrees of freedom,
- Eight dial gauges were used to measure the sway deformations of the columns or infill deformations on a line tilted 45 degrees from the beams/columns.
- Two LVDT's were used to measure the sway of the story with reference to the ground.

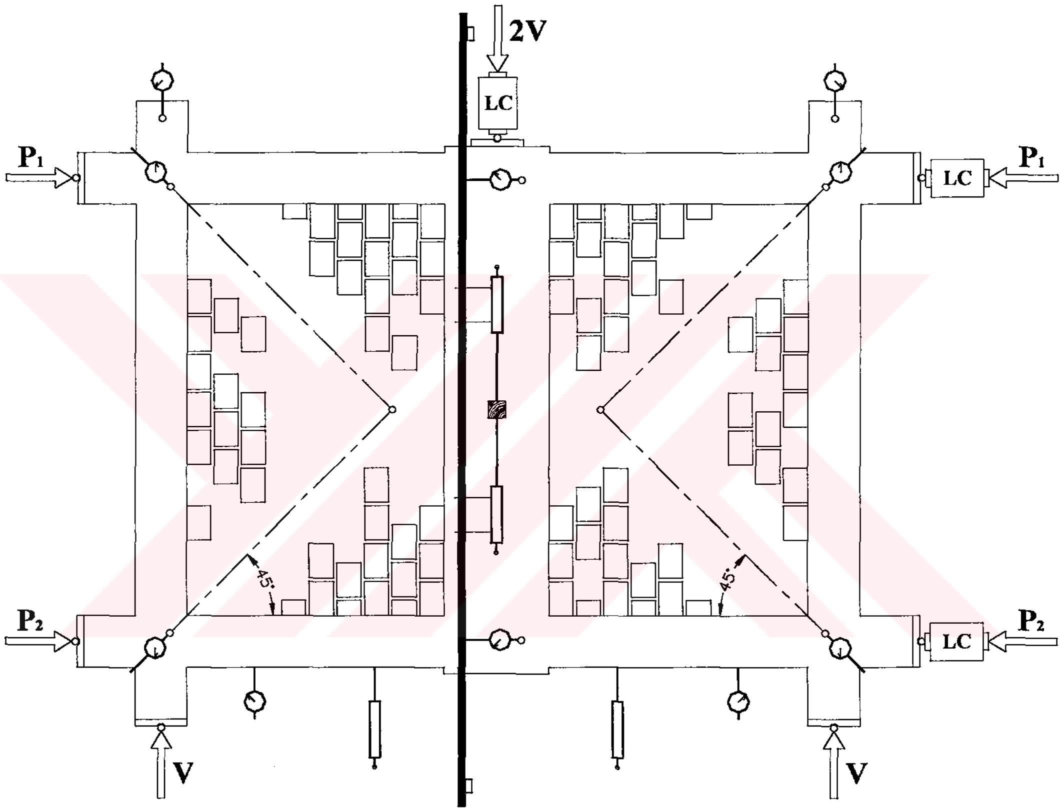

Figure 4.3. Load Introduction and Measurement Devices

During the tests, the overall translations of the specimens were monitored using the dial gauges at the supports of the specimen. Some lack of fit was necessary for the proper roller support movement. Under low lateral loads and small deformation, amplitudes of the overall rigid body movements were larger than the actual deformations and the error involved in their measurement. This resulted in the insensitivity of the setup to small deformations.

4.1.3. Loading History

Loading history applied to specimens was altered as additional specimens were tested depending on their increasing/decreasing capacities and deformation abilities. In general, the specimens were loaded using a force-controlled regime until the estimated peak load was reached or the deformations indicated relative increases within the same load cycle ranges. After this turning point, the loading was continued doubling the displacements reached from earlier cycles. Smallest displacement cycles stared from 5 or 10mm depending on the displacement reached at peak load.

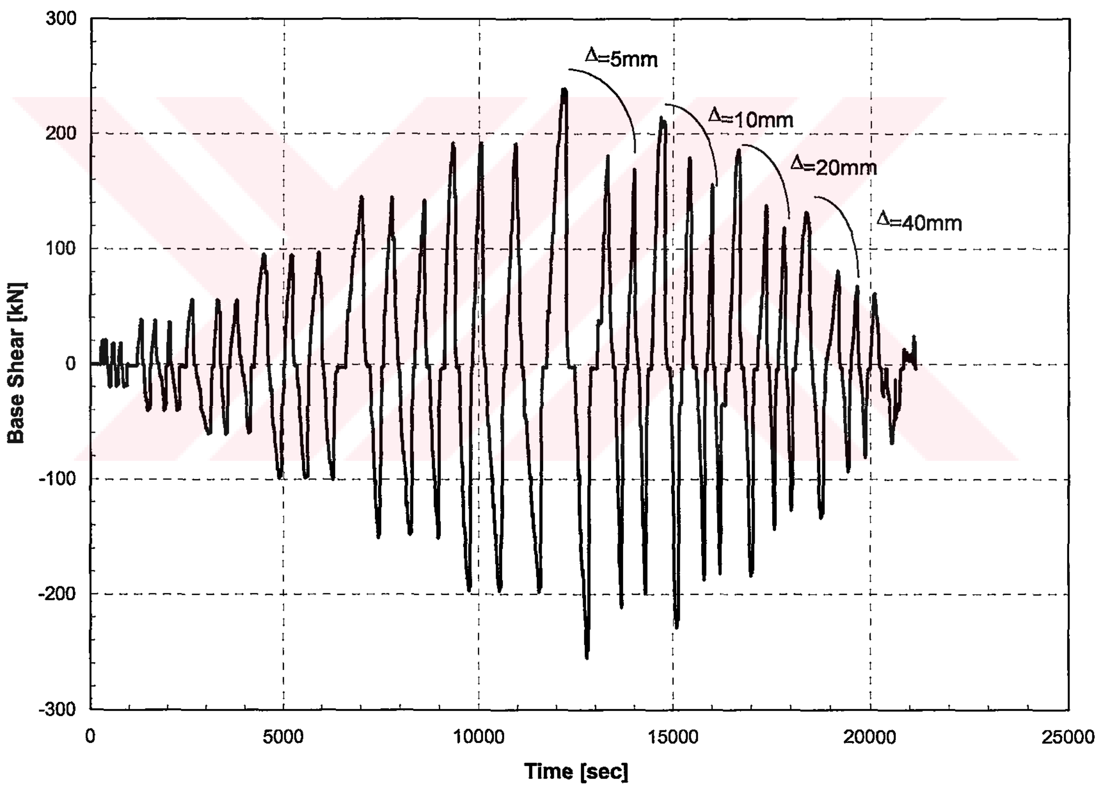

Figure 4.4. Lateral loading time-history of 01NC-IN

For bare frames the axial loads were maintained at an average of 100kN where the measured fluctuations during testing were due to the specimen geometry, support conditions, and lateral loading.

For infilled frames, the axial loads were kept at the same level until the lateral load cycles reached to a magnitude close to bare frame values and then started to be increased and decreased to represent the axial load fluctuations due to the overturning moments of a hypothetical upper structural configuration. Although, a proportional increase of the column axial loads was maintained by manual control of the lateral load and the axial loads jacks, no specific rules were specified, since, in general, the interaction of the maximum shear and overturning moment cannot be specified unless a lateral load distribution for the prototype structure is assigned.

Due to the physical restraint provided by the axial load application setup, a residual rebound load developed on the windward column, which prevented the tensile force development under large lateral displacements. This was already expected and accommodated during the loading assignments to individual columns. Therefore, at the highest lateral displacements, the leeward column received a maximum of 250kN and the windward column load fluctuated between 20-80kN.

4.1.4. Expected Failure Load

Expected failure loads were calculated using the procedure given by Paulay and Priestly (1992), Figure 4.5. In this procedure, a conservative estimate as a quarter of diagonal strut width is used. Strut force is derived as the load on the pin jointed truss elements and decomposed to check for strength of the infill material.

Possible failure states were defined as the bed joint sliding of the infill, tensile or compressive failure of the columns, shear failure of the columns and the corner crushing of the infill. Shear contribution of the masonry was regarded as bounded by the triplet shear strength for bed joint sliding checks.

Expected failure loads, for the tandem specimen configuration, were at lateral loads of 212 and 237kN before and after the overlay application, respectively. Failure mode identified was corner crushing under diagonal compression for both of the cases.

Material Parameters

L	=	1350	mm			
l_m	=	1200	mm			
H	=	900	mm			
h_m	=	750	mm			
d_m	=	1415	mm			
w	=	354	mm			
f_{ck}	=	14.3	MPa			
f_{ctk}	=	0.87	MPa			
E_c	=	14948	MPa			
f_{yk}	=	367	MPa			
f_{ykw}	=	367	MPa	ϕ4/100		
θ	=	0.5586	rad	32		deg

Tension Failure of the Column

b	=	150	mm
h	=	150	mm
A_s	=	314	mm^2
ρ_c	=	0.0140	
T_t	=	-115	kN

Compression Failure of the RC Column

b	=	150	mm
h	=	150	mm
A_s	=	314	mm^2
ρ_c	=	0.0140	
T_c	=	389	kN
θ	=	0.5586	rad

Before Retrofit

f'_m	=	3.4	MPa
E_m	=	2239	MPa
τ_0	=	2.00	MPa
t	=	94	mm

Sliding Shear Failure

Panel Shear

R_s	=	333	kN
V_b	=	282	kN
V_f	=	226	kN

Columns in Shear

$V_{cr,c}$	=	27	kN
$V_{cr,t}$	=	30	kN

ignore 50% V_c of the columns

V_c	=	21	kN
V_w	=	62	kN
V_r	=	73	kN
V_p	=	199	kN

Diagonal Compression Failure of the Infill

z	=	497	mm
R_c	=	125	kN
V_i	=	106	kN

Axial Load Couple

P_{couple}	=	71	kN	
P_{DL}	=	107	kN	
P_{max}	=	178	kN	**OK**
P_{min}	=	37	kN	**OK**

Failure due to **Diagonal Compression Failure of the Infill**

V_{max} = 106 kN (x2 212 kN)

After Retrofit

f'_m	=	3.8	MPa
E_m	=	2239	MPa
τ_0	=	3.00	MPa
t	=	94	mm

Sliding Shear Failure

Panel Shear

R_s	=	499	kN
V_b	=	423	kN
V_f	=	418	kN

Columns in Shear

$V_{cr,c}$	=	27	kN
$V_{cr,t}$	=	30	kN

ignore 50% Vc of the columns

V_c	=	21	kN
V_w	=	62	kN
V_r	=	73	kN
V_p	=	225	kN

Diagonal Compression Failure of the Infill

z	=	497	mm
R_c	=	139	kN
V_i	=	118	kN

Axial Load Couple

P_{couple}	=	79	kN	
P_{DL}	=	107	kN	
P_{max}	=	186	kN	**OK**
P_{min}	=	28	kN	**OK**

Failure due to **Diagonal Compression Failure of the Infill**

V_{max} = 118 kN (x2 237 kN)

Figure 4.5. Capacity calculation sheet for infilled frames

4.2. Test Results

Observations made during testing of the specimens were noted associating with the apparent damage level, measured deformations and applied lateral load. This qualitative information was summarized and provided below to illustrate the overall specimen behavior with characteristic events encountered under lateral loading. The load levels and the displacements of the eight one-third scale specimens were reported as noted. However, due to the tandem configuration, actual loads carried by the half model specimen correspond to the half of the reported or graphed. On the other hand, the displacement quoted need not be altered due to the same reason.

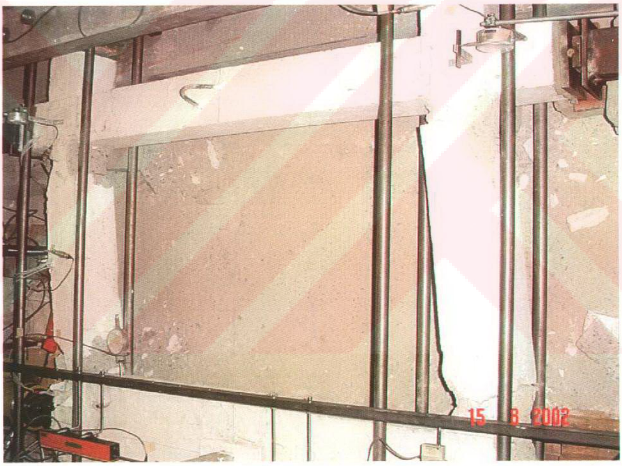

Figure 4.6. Failure of ductile bare frame 05CC-BR

4.2.1. Bare Frames

Lateral loading of the code-compliant (05CC-BR) and non-compliant (02NC-BR) frames started with loads as low as 5kN, and increased until 80kN with increments of 5-20kN. After the 80kN cycles the loading is continued in a displacement-controlled manner starting with 10mm displacement cycles.

Both of the bare frames developed initial flexural cracking at 20kN cycles and these cracks remained as the only ones until the lateral displacements were increased up to 20mm. Such local cracking was the result of slip and bond failure of the plain reinforcing bars and one of the reasons of pinched hysteresis behavior.

A shear crack formed on one of the columns of 02NC-BR at a lateral load level of 89kN during the first displacement cycle of 20mm magnitude at the reverse loading branch of the sequence. After the formation of this crack, the NC specimen started to drop load for displacements of equal magnitude.

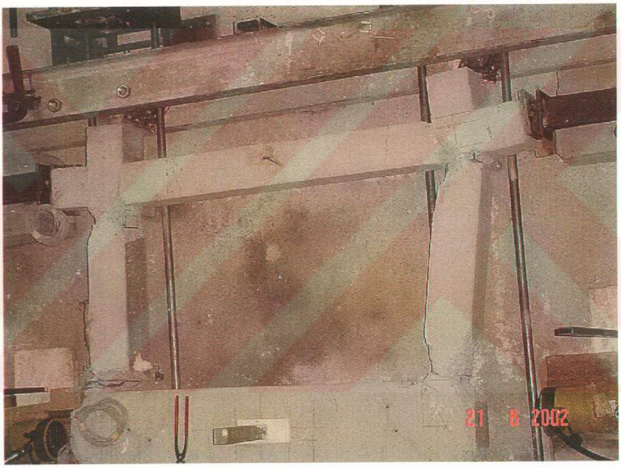

Figure 4.7. Failure of non-ductile bare frame 02NC-BR

Failures of the bare frames were due to the plastification of the column ends and the shear failure of the non-compliant frame (02NC-BR) under combined action of axial and lateral loads. The failure of the code compliant bare frame (05CC-BR) was judged due to its excessive lateral deformation. However, for this specimen the core concrete which was properly confined was still properly confined. Thus, any failure not simulated by the testing arrangement would be due to excessive lateral sway and the reduced column capacities unable to sustain the additional P-Δ forces.

Non-compliant detailing was observed to cause the loss of the core concrete and the buckling of the longitudinal reinforcement. Such a failure mode implied sudden loss of the gravity load carrying capacity. The extreme case of loss of unconfined core concrete is apparent in Figure 4.7, where one of the columns can be seen to have shortened by as much as half the cross-section depth.

4.2.2. Infilled Frames with Bare Infill Walls

Behavior of the infilled frames was dominated by the failure pattern of the infilled masonry, where the frame with symmetric infill cracking pattern (01NC-IN) failed under a combined mode formed by the shear-moment-axial force interaction at the frame column ends. However, for the infilled frame with asymmetric cracking pattern (08CC-IN), the failure was due to the pivoting of the infill at the column one-third height.

Figure 4.8. Failure of ductile HCT infilled frame 08CC-IN

Infilled frame with the code compliant detailing, 08CC-IN, showed no cracks until the second cycle of the 200kN lateral loading. However, a cracking sound was heard at the 140kN level. Diagonal tensile cracking developed at the first introduction of the 170kN lateral load. Additional cracking continued on the following 200kN cycles. However, the cracking was largely confined to only one of the infill panels due to the non-uniformity of the HCT material. During the 250kN lateral load cycle, a shear crack opened on one of the columns at 220kN lateral load. Failure was due to the gravity collapse of the frame after full crushing of the infill, and at a column hinge pivoted immediately above the confined end zone of the column.

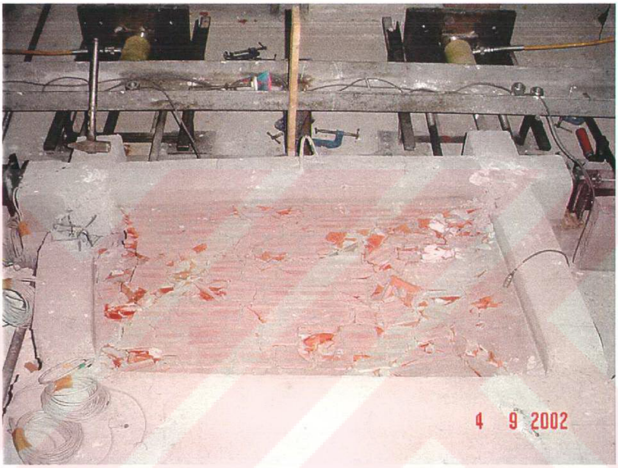

Figure 4.9. Failure of non-ductile HCT infilled frame 01NC-IN

Non-compliant infilled frame, 01NC-IN, had the first cracks at 40kN lateral load level at the interior corners of the beam-to-column joints. First cracking sound was heard again at 140kN lateral load but within the 150kN lateral load cycle in contrast to 08CC-IN, and the associated diagonal cracking immediately followed. After the first diagonal cracks, no additional cracks formed until a lateral load level of 200kN was reached, previously formed cracks re-opened visibly at 170kN and an additional crack formed at 190kN. While cycling at 200kN level, the boundary separation between the frame and the infill walls started.

Within the 5mm displacement cycles, additional diagonal cracking progressed at 230-240kN lateral loads and the angle of the cracks narrowed as cracking progressed. During this additional cracking, the lateral load started to drop rapidly for any given displacement level. At 20mm displacement cycles, the heavily cracked infill parts adjacent to columns and at the mid height of the infill crushed totally and spalled. Cracks that formed due to the compression of the infill near the column ends widened at this displacement, and the high axial loads combined with such cracking caused the crushing of the column end zone that was not properly confined due to poor detailing represented by this code non-compliant specimen.

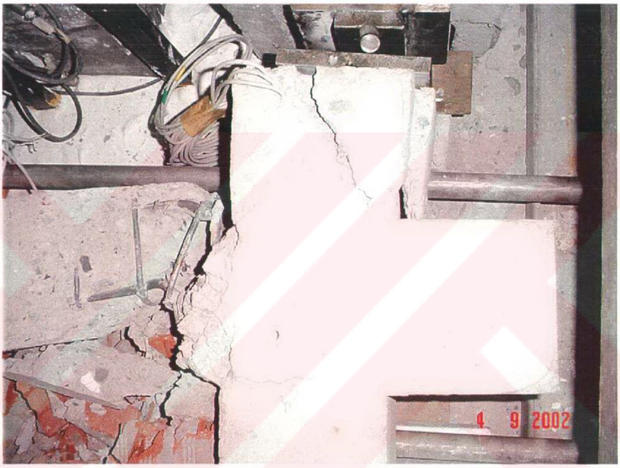

Figure 4.10. Crushed column end zone of 01NC-IN

Observed failures were dominated by the capacity exceedance of the columns under large overturning forces that forced a gravity collapse when combined with overall large sway, stiffness and strength deterioration, and thus further amplified the P-Δ forces.

4.2.3. Glass Sheet Applied Infilled Frames

Glass sheet application to the infilled frames 06CC-GS and 07NC-GS, with and without code compliant detailing respectively, was limited to an overlay application confined into the infill boundaries. Therefore, the overall behavior was governed by the changing failure mode of the infills.

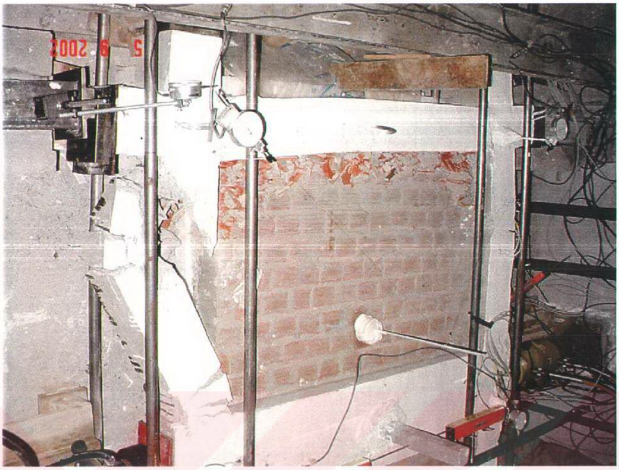

Figure 4.11. Failure of ductile HCT infilled frame 06CC-GS

Figure 4.12. Failure of non-ductile HCT infilled frame 07NC-GS

At 40kN lateral load, few cracks formed on the beams of the compliant specimen, 06CC-GS, which were followed by additional cracks on the framing at 100 and 150kN. Within the first loading cycle of 200kN, HCT cracking sound was heard at 170kN but no visible cracking was observed. Diagonal cracks only appeared at the first forward loading cycle of the 250kN level and developed in the following cycles. This was accompanied by the beam-infill interface separation.

Figure 4.13. Crushed column end zone and buckled reinforcement

During the 5mm displacement cycles the column-infill interface separation was observed and corner crushing of the infill initiated. With the corner crushing the specimen started to deform appreciably more for a given lateral load level and the loads resisted for a fixed displacement dropped significantly. Corner crushing ensued within 5, 10 and 20mm cycles, where in 20mm cycles one of the columns started to crack vertically. With the large displacement cycles, the contribution of the infill dropped rapidly, and the lower corner of the crushed infill section pivoted the column and forced a flexural deformation at the mid-height. Due to the increased ductility demand under shorter column length and crushing of the unconfined central region, gravity failure of the columns occurred.

Deformation and failure characteristics of the non-compliant infilled frame with glass-sheet overlay were essentially the same as the compliant frame. Failure was a corner crushing mode for both of the tested specimens' infills, first a diagonal tensile cracking mode developed at a load level close to three quarters of the plain infilled specimens, and continued to carry further load until the compression failure load of the infill corners was reached.

Due to the stiffening effect of the glass-sheet on the infill, the deformations at the same load level were smaller than those of the specimens with plain infill masonry. Moreover, the overall displacement capacity of the system was reduced, since the maximum sustainable deformation of 40mm of the plain infilled specimens was reduced by the glass-sheet application.

4.2.4. Glass Sheet and Laminate Brace Applied Infilled Frames

In this case, glass sheets were continued to cover one side of the surrounding frame and introduced a new load transfer mechanism from the infill wall to the columns. The laminates were added to increase both the stiffness and the strength, and as an alternative load path for the lateral loading during the degradation of the infill stiffness and strength.

For both of the specimens the cracking sound was heard at a far lower level (170kN for 04NC-GL and 195kN for 03CC-GL) than the actual diagonal crack formation at 300kN. An increase in the deformations for a given lateral load level was observed for most of the cycles below peak load but no load drop was observed. At 300kN lateral load several cracks appeared consecutively, however, a significant drop at load was still not observed. During the first 5mm displacement cycles of the non-compliant specimen and the 10mm cycle of the compliant specimen one of the laminates failed at the bond interfaces with the reinforced concrete and the load dropped suddenly forcing the glass-sheet rupture at the column-infill interface and accelerating the infill strength deterioration. For the non-compliant frame, this phase of the loading induced torsion cracks on the column due to the eccentric bond of the FRP to the frame. At the end of the 10mm displacement cycles the glass-sheet connection to frame was fully lost and the failure of the columns due to mid height hinging like the earlier glass-sheeted cases started.

Similar to the infills with the glass sheet application only, the lateral load capacity increased appreciably and the displacement capacity further reduced. Although, the overall deformation capacity of the system decreased from 80mm to a sustainable 20mm, the peak capacity increased five fold.

Figure 4.14. Failure of ductile HCT infilled frame 03CC-GL

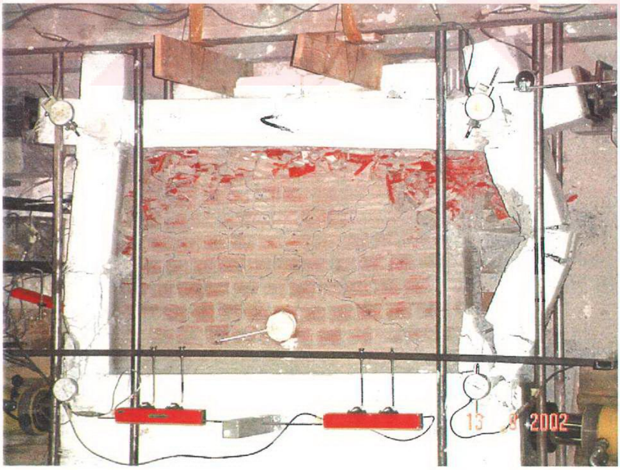

Figure 4.15. Failure of non-ductile HCT infilled frame 04CC-GL

During testing, corner crushing of the infills was accelerated due to the sudden loss of the laminate brace stiffness and strength contribution near the peak load, which resulted in abrupt loading of the infill and the surrounding frame, and caused simultaneous corner crushing and frame hinging.

Failures were due to the pivoting of the frame column on the crushed corner of the infill wall, and the increasing demand on ductility and shear strength to support this demand over a shorter column length. The portion of the column that failed was the first reinforcement cage opening after the termination of the confinement zone.

4.3. Discussion of the Test Results

Force deformation patterns of the strength and stiffness deteriorating structures in the nonlinear regime are strongly load history dependent. Starting from initial cracking in the early stages of lateral loading, and with any further cracking and material loss, the limits for the final failure mode, deformation and load are quenched into the structural systems behavior. In the pre-peak regime, the cracks or slip deformations influence the stiffness of the structure by governing the contact loss and gain. Within the post-peak region, the maximum deformations in the history of the loading and associated deterioration and section loss define the further pattern of load drop and stiffness loss.

Structural systems like hollow clay tile infilled non-ductile reinforced concrete frames are made up of components that are brittle and show major material loss due to the failure of the HCT. Non-ductile reinforced concrete element loose strength and stiffness due to the physical disintegration of the unconfined concrete, delay in crack closure and slip of reinforcement. Unless the load application is very abrupt, these failures are still a function of the imposed displacements but exhibit rapid deterioration in contrast to the ductile elements where the section loss is largely related to the unconfined concrete cover.

Unlike the non-ductile reinforced concrete elements, the major drops in load and stiffness for the HCT are related to the growth of cracks emanating from the original flaws of the tiles, instability of face shells / webs after failure of their connections, and shear controlled face shell / web tensile cracking. Although initiated by the displacements of the surrounding frame, the failures of the HCT units are generally stability related. When regarded in this context, it is obvious that any error in loads or displacements imposed to the system will alter the deformation capacity and the peak loads to be yet reached.

4.3.1. Overview of Observed Failure Patterns

Common to all infilled frame tests were the formation of diagonal tensile cracks and imminent corner crushing failure after the increase of crack density at infill corners. As expected, the application of the glass-sheet and laminates increased the lateral load levels of first crack formation, corner crushing and ultimate load. Accompanying the increase in these force levels, the displacements at which these loads were reached dropped substantially. Moreover, the maximum displacement capacity of the frames reduced for any increase in infill stiffness and strength.

Initial cracking sound indicating internal cracking not visible on the surface was heard at increasingly higher loads for glass-sheeted and laminated infilled walls as compared to the bare infill wall case. Infill face shell cracking load increased in parallel to the internal cracking and peak load capacity. Notable was that the detailing of the framing did not pose any difference to the pre-peak regime.

Frames with bare infill demonstrated a higher maximum displacement capacity and had modes of failure similar to one another. The strength and stiffness deteriorations observed were due to the following failure pattern,

- Diagonal and X cracking with consecutive crack paths lying at a narrower angle to the center beam
- Formation of a temporary diagonal strut and limited corner crushing
- Crushing of the mid-height row of HCT and tiles in contact with the column
- Bending of the beams due to arching action of the infill during dilation
- Infill panel separation from beam and/or column faces
- Cracking at column end zones
- Formation of column sway mechanism
- Failure of columns at plastic hinge zones under axial-shear-moment interaction

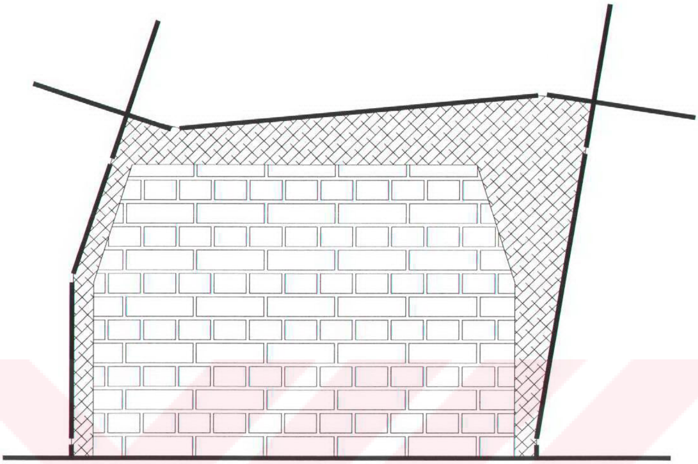

Figure 4.16. Sway mechanism with column mid-height pivoting

Frames with glass-sheeted infill with or without bracing carbon fiber laminates showed the following failure patterns,

- Diagonal and X cracking at high loads and low deformations with an even crack distribution
- Sudden release of the bracing force onto the infill and acceleration in infill and frame cracking
- Crushing of the infill corners
- Near mid-height pivoting of the column and forced flexural deformations and concrete cover crushing at this pivot, Figure 4.16.
- Hinge formation at column ends
- Large residual deformations at the pivot of the column an development of a geometric imperfection
- Gravity failure of the column due to large eccentricity and strength / stiffness deterioration due to mid-height hinge

4.3.2. Force – Deformation Response

In the following, plots of the force-deformation response recorded during testing for infilled frames are compared to the reference bare frame and bare infilled frame cases. Points of reference for such a comparison are the behavior of the non-compliant bare frame (02NC-BR) due to its performance benchmarking the past seismic design practices as designed, and the non-compliant bare infilled frame representing the properties of the existing building stock (01NC-IN) as constructed. Therefore, all force-deformation plots have the envelopes of 02NC-BR and 01NC-IN superimposed to simplify the discussions.

For 08CC-IN, the delay in the load drop within the third quadrant of the plot for the 5mm displacement cycle (backward loading) triggered the progressive and accelerated crack growth for the following 10mm cycle and resulted in major load drop in contrast to 01NC-IN envelope. It is also clear that this regime influenced the loading in the other direction (forward loading) as well, however, to a lesser extent. Worth noting is that the maximum loads reached in the following cycles remained bounded by the second cycle envelope which coincided with the maximum load at the 5mm cycle.

Envelope of the non-compliant bare frame in Figure 4.17 points that after the 20mm cycles the strength and deformation characteristics were governed by those of the framing system.

Infilled specimen 01NC-IN demonstrated similar force-deformation behavior for both of the forward and backward loading and deformation cycles. Since there was only limited deformation or peak load overshooting during loading, the load drops after the peak load followed a similar trend and the maximum deformation capacity was higher than the ductile reinforced infilled frame. Since the hinging of the column occurred without pivoting of the infill panel and immediately at the end zones of the columns, the bare frame deformation response of 02NC-BR closely represented the stiffness and the strength of this specimen after the first cycle of the 40mm displacement cycle.

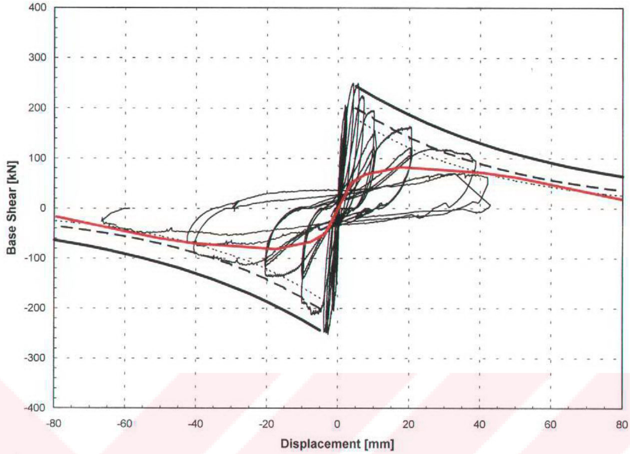

Envelope of first (—), second (▪ ▪), and third (- -) cycles of 01NC-IN &
Envelope of 02NC-BR (—)

Figure 4.17. Force-displacement trace of 08CC-IN

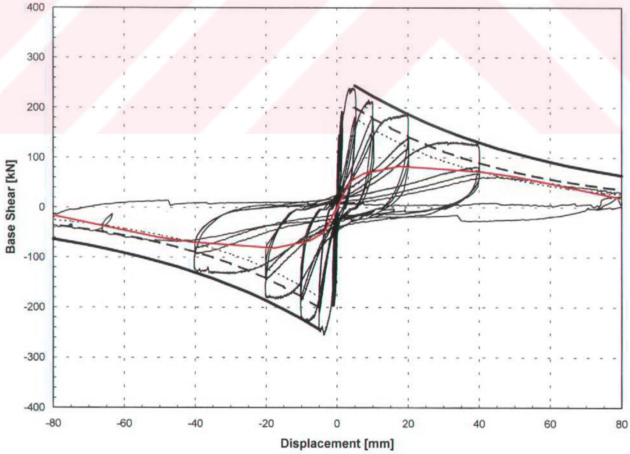

Envelope of first (—), second (▪ ▪), and third (- -) cycles of 01NC-IN &
Envelope of 02NC-BR (—)

Figure 4.18. Force-displacement trace of 01NC-IN

Peak loads reached in both of the infilled frame tests were close to the values found from expected load calculations made after the materials testing.

Infilled frames with glass-sheet applied panels developed slightly higher peak loads and exhibited significantly reduced maximum deformation capacity. The load dropping near the peak loads of the 5 and 10mm displacement cycles (with reverse slope) indicate that the crack propagation continued after the peak load until the aimed displacement was reached. Since the initial peak loads were not attained at the same displacement levels for forward and backward cycles, the rest of the force-displacement trace was not symmetric. This effect was more pronounced for the 07NC-GS specimen, where a major overstrength of the infill delayed the forward cycle strength deterioration for the 5 and 10mm cycles and accelerated the strength and stiffness decay for the following regime. At the final failure stage both of the glass-sheeted infilled frames experienced mid height column hinging, and therefore, the force-deformation pattern was governed by the bare frame failure mode for displacements higher than 20mm. The curve associated with this mode was derived using the 02CC-BR as a backbone and scaling up by the ratio between the collapse load calculated assuming full height panel sway mechanism and the observed hinging locations of the actual failure mode. For a mechanism with one of the plastic hinges at mid height of one of the columns this ratio is defined as $6M_p / 4M_p$, where the plastic moments, M_p, are functions of the nominal axial loads acting on the columns.

Peak loads of the glass-sheeted and laminate braced infilled frames were higher than the other infilled frames and the load drop was more sudden. Due to the major confinement effect of the glass-sheet and the laminate, the HCT units had cracked extensively and uniformly prior to the loss of the laminate connection to the RC frame. After the initial abrupt load drop, the strength deterioration accelerated because of the already largely cracked infill being exposed to large deformation cycles where no reserve resistance was left. Therefore, the force-deformation trace approached to the bare frame failure envelope rapidly and the gravity collapse of the frame is reached within 40mm displacement cycles. It is important to note that the extensions of the glass-sheet to the faces of the columns reduced the impact of the laminate bond loss and the trace between the peak load and the peak displacement aimed for that cycle (10mm) included additional points because of this contribution.

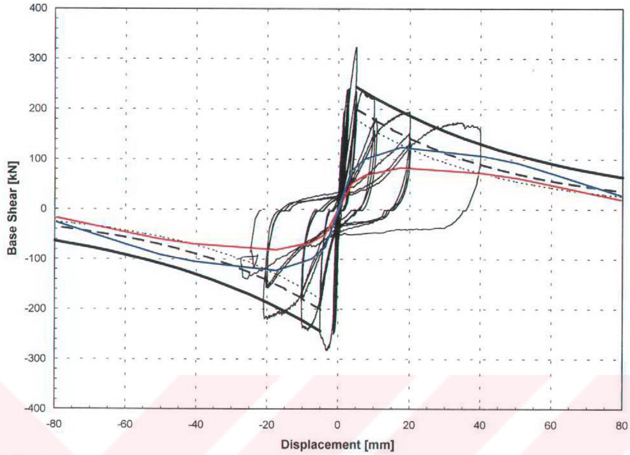

Envelope of first (—), second (▪ ▪), and third (- -) cycles of 01NC-IN &
Envelope of 02NC-BR (—) and plastic collapse mode (—)

Figure 4.19. Force-displacement trace of 06CC-GS

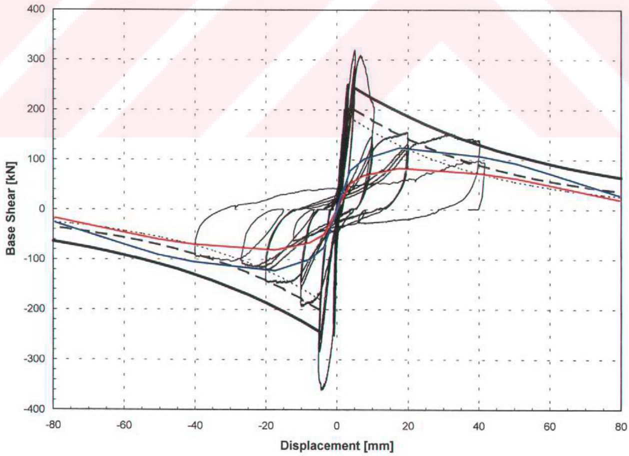

Envelope of first (—), second (▪ ▪), and third (- -) cycles of 01NC-IN &
Envelope of 02NC-BR (—) and plastic collapse mode (—)

Figure 4.20. Force-displacement trace of 07NC-GS

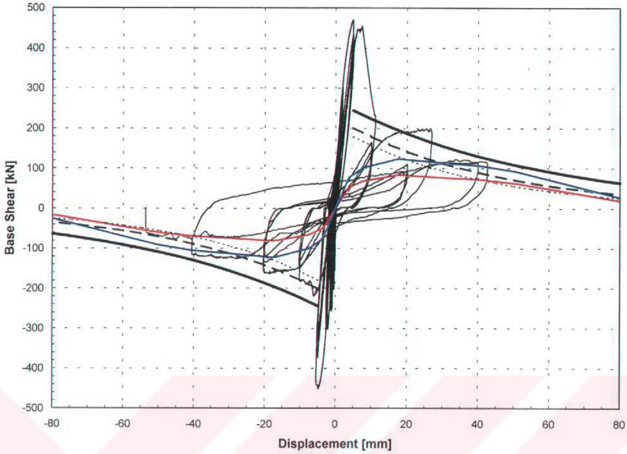

Envelope of first (—), second (▪ ▪), and third (- -) cycles of 01NC-IN &
Envelope of 02NC-BR (—) and plastic collapse mode (—)

Figure 4.21. Force-displacement trace of 03CC-GL

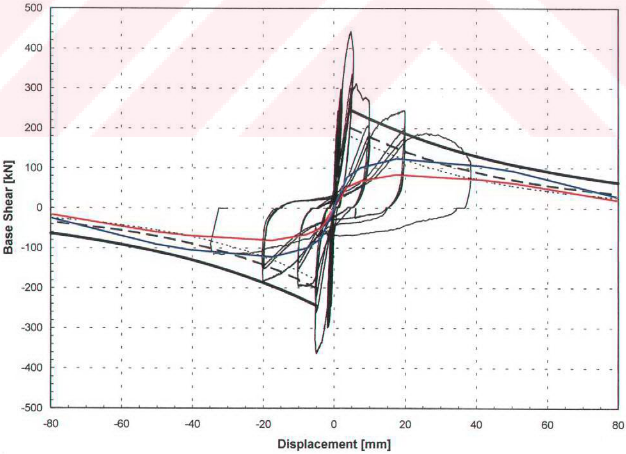

Envelope of first (—), second (▪ ▪), and third (- -) cycles of 01NC-IN &
Envelope of 02NC-BR (—) and plastic collapse mode (—)

Figure 4.22. Force-displacement trace of 04NC-GL

From the framing ductility point of view, the tested frames showed that the ductility of the bare frame was masked by the presence of the infills and only defined the points of unconfined concrete crushing under heavy alternating axial loads. Therefore, unless the full heights of the columns are properly confined the contribution of proper or deficient detailing should be expected as minimal.

5. FINITE ELEMENT MODELING OF HOLLOW CLAY TILE INFILLED FRAME BEHAVIOR

After several years of research in modeling of the infilled frames, methods that are based on braced frame analogy with diagonal struts of constant or varying section or material properties are still favored due to their simplicity in implementation from the engineering practice point of view (Stafford Smith, 1966; Hakam, 2000). When calibrated (Mainstone, 1971) or allowed to have non-linear material properties (Hakam, 2000) equivalent struts may encompass the critical force-deformation pattern of the composite system. On the other hand, methods based on calibrated analytical models relying on large scale or model test results as reference require re-calibration for every new structural system because of their inherent empirical format.

Fully nonlinear finite element analysis of the infilled frame systems employing, material, geometric, and contact non-linear elements may be an alternative to element or formula level calibration. In this case, the number of the parameters to be specified grows disproportionately as compared to empirical or analytical methods, and the data required may not be provided by the standard testing procedures. Even if the data for correct modeling of the fully nonlinear finite element models can be collected, the time to be allotted to such an undertaking cannot be justified from the engineering practice point of view.

To date, a method that is different than the fully nonlinear finite element analysis and that can encompass all the simple behavioral aspects to be evaluated by a practicing structural engineer does not exist. Equivalent strut methods are of closest proximity to such a method, however, cannot qualify due to the violation of contact surface assumptions under the gravity load effects (King and Pandey, 1978). Moreover, diagonal strut models cannot capture the failures observed in HCT infilled frame testing, because of the hinges and failures were located within the column and beam length.

A method suitable for engineering use should be able to model the gravity load share of the infill panels, capture failures within the physical element length of the beams and columns, accommodate irregular and discontinuous panel configurations, and be based on simple material and geometrical properties of infill and frame materials.

5.1. Modeling Parameters

Nonlinear analysis of infilled frames using finite element method has already been undertaken by several researchers as reviewed in the earlier sections. Some of the basic features common to these modeling approaches are summarized below.

- There is a nonlinear contact formation phase at the beginning of tests and also their FEM analysis models, which requires explicit address of the elastic stiffness and post elastic strength and stiffness deterioration
- The contact surface/length between the frame and the infill cannot be assigned a priori and needs to be established within the analysis procedure and be compatible to the directional changes of the imposed actions.
- Equivalent strut concepts developed analytically can only define a small region of the overall force-displacement behavior, and do not represent the changes invoked by the variation of the panel aspect ratio successfully.
- Friction on the contact surfaces may be an important parameter while starting the FEM analyses but the stabilized contact area does not depend on the exact magnitude of the friction coefficients used.
- Material nonlinearity of the infill panel may be considered unidirectional because of the highly directional stress pattern enforced by the separation of the interface, which induces no-tension boundary conditions.
- Observed failure patterns of the infills hint that the material properties of modeling interest are the tensile strength and strain limits for the interfaces and mortar beds. The exact magnitude of the compressive strength or crushing strain is of secondary importance.

Laboratory testing of the hollow clay tile infilled frames brought additional insight for the modeling of this type of structures. Following points were regarded of relevance for modeling

- For small lateral loads, the infilled frame system behaves like a monolithic shearwall.
- Separation of the infill from the bounding frame is not as immediate as suggested in the literature and occurs past the diagonal cracking load.
- Deformability of the infill is a function of the deterioration of material strength, stiffness and contact.
- Failure of the infill starts in the form of diagonal tensile cracking. Cracks follow both through the units and along the bed and head joints.
- After major cracking, infill dilates across the large cracks and forms a double arching mechanism, which applies an outward thrust against columns and beams.
- Double arching ceases once there is some corner crushing.
- Under large displacements, the infill zones in contact with the frame columns deteriorate and the mid-height HCT courses crush and split the infill into two parts.
- After major deterioration of the infill, the surrounding frame fails under a soft story mechanism with or without pivoting within the column net length.

Characteristics of infilled frame behavior outlined above show that the close resemblance of the modeled behavior to the tested requires two major points to be addressed in detail; tensile strength of the material forming the HCT and nonlinear contact at the frame-infill panel interface. Following sections outline the development of a simplified nonlinear analysis scheme developed for the HCT infilled frames which accounts for these points. The discussions are only for plane stress models since only the in-plane behavior of the infilled frames are of interest.

Modeling aims set forward in the paragraphs above were intended to be met using plane truss configurations that can be formed using the frame, infill geometries and simple compression and tension test parameters of the constituting materials. Recent developments in structural modeling rendered the structural analysis programs capable of simulating point-wise nonlinearity available to the standard engineering office use. Moreover, the pushover methods supported by the performance-based codes promote the use of these programs and allow a practice ground for engineers. Therefore, point-wise nonlinear pushover analysis has been chosen as the modeling framework for the foregoing development.

5.2. Modeling Contact Behavior

Contact behavior at the frame-infill interface may be modeled using nonlinear plane stress elements or more simply by link elements that transfer only the interface axial and shear forces. For simplicity in modeling, bar elements with non-linear hinges were used in the FE models developed in what follows.

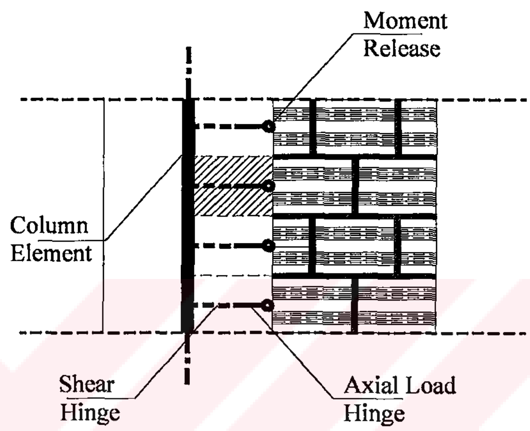

Figure 5.1. Interface modeling

5.2.1. Rigid Link Elements

Frame-infill interface properties were modeled using bar elements with the same overall dimensions as the grid spacing used for the infill modeling and a thickness equal to the infill panel. These elements were assigned moment release conditions at their ends, which were connected to the infill panel. Thus, only the transfer of the axial and shear forces acting on the contact surface was allowed. Each link from the frame to the infill was formed using two bar elements in series. First element connected to the surrounding frame had a shear hinge that was active for shear loads above a nominal value representing the cohesion at the interface. This element had no capability of reproducing a dry friction condition because of the assigned constant shear yield level. The second element had an axial force hinge that can model the compressive load transfer and loss of contact under tension by the specified a high compressive but low tensile strength, Figure 5.1.

5.2.2. Stafford Smith's Tests

Ability of such link elements to model actual contact conditions was demonstrated using mortar infilled frame test results of Stafford Smith (1966). Four of the test sets, with three identical samples each, were chosen as the reference case. These specimens had fully welded steel frames of same section height and varying width surrounding 152.4x152.4mm (6x6in) mortar plates. The mortar compressive strength, 28.1MPa (2t/in^2), and modulus of elasticity, 1.9GPa (140t/in^2), were given in the reference, and the steel modulus of elasticity was assumed as 210GPa. To achieve the best approximation for the mortar stiffness, the mortar was modeled with a dense mesh of plane stress membrane elements. Steel sections and rigid links were modeled as frame elements. The rigid links were assigned the same material properties as the infill mortar and a tensile strength of one-tenth of the compressive. Table 5.1 presents the contact length results obtained from the original reference and compares with the described finite element model.

Table 5.1. Contact length modeling using rigid link elements

Section Width*	***4.8mm***	***6.4mm***	***9.5mm***	***19.1mm***
(a) Test Results (in mm)				
200 series	22.2	31.8	47.6	60.3
210 series	31.8	31.8	50.8	57.2
220 series	31.8	44.5	50.8	63.5
Test Average	*28.6*	*36.0*	*49.7*	*60.3*
(b) Finite Element Modeling Results (in mm)				
Coarse Mesh	*28.6*	*38.1*	*47.6*	*60.3*
Fine Mesh	*28.6*	*38.1*	*49.2*	*61.9*
**Section height is 19.1mm in all tests*				

5.2.3. Discretization of HCT Units

To simplify the modeling of the infill panels, the plane framework approach for plane stress analysis was adopted for modeling of the web and face shells of the HCT units. The plane framework analysis approach was widely used within a period between 1960-1980 where the finite element methods were in early development phase, computational power of the common computers were not adequate for analysis of large models with several shell elements, and the analysis methods for plane truss, frame and grillage systems were widespread and more efficient.

First proposed by Hrennikoff (1941), and later developed by McCormick (1963) and Yettram and Husain (1966), plane framework methods for plane stress analysis were based on the stiffness equivalence of a truss or trussed frame system to an idealized plane stress element. Initially, the pin jointed truss systems proposed by Hrennikoff were specific to a Poisson's ratio of 1:3 or locally unstable if generalized for all possible Poisson's ratios. With the introduction of the trussed plane frame models of McCormick (1963) and Yettram and Husain (1966), this problem was overcome. An alternative approach was developed by Jai (1998), where the section sizes of the assumed truss elements were calibrated using plane stress finite element models.

In early patch tests for the analyses to follow, the framed truss models were assessed to be successful under uniform boundary conditions and distributed loading, however, performed poorly under combined loading cases and local load input in contrast to the original truss system proposed. Therefore, for the approximate plane stress analysis Hrennikoff's original truss system for rectangular configuration was adopted, Figure 5.2.

Using the 19.1mm thick (3/4in) 152.4x152.4mm (6x6in) square panel of Stafford Smith's tests for the accuracy check of the deformations, two models one with membrane elements and one with Hrennikoff truss elements were developed, Figure 5.3. The accuracy of the plane framework analysis along the loaded direction is good even for different Poisson's ratios of 0.2 for membrane and 0.33 for the plane framework models, Table 5.2.

For the HCT units the areas describing the vertical side, A_{S1}, horizontal extreme flanges, A_{S2}, diagonals representing the vertical face and web shells, A_D, boom for the central flange of the unit, A_M, and the vertical section of the face and web shells, A_V, were defined as the superposition of the equivalent truss element areas from the plane framework method with the actual flange and mortar bed and head joint material cross-sections. No scaling other than that implied for the modeling of the plane framework method for the analysis of the vertical shell sections was involved and the rest of the area computations were mere tributary area calculations. Defining the aspect ratio of sides as k, the equivalent areas for the Hrennikoff model were defined as $A_1=3/8[(3k^2-1)/k]at$, $A_2=3/8[3 - k^2]at$, $A_D=3/16[(1+k^2)^{3/2}/k]at$, where the thickness of the planes stress element, t, and the size of the height of the considered element height, a, were taken for one core height, Hrennikoff (1941).

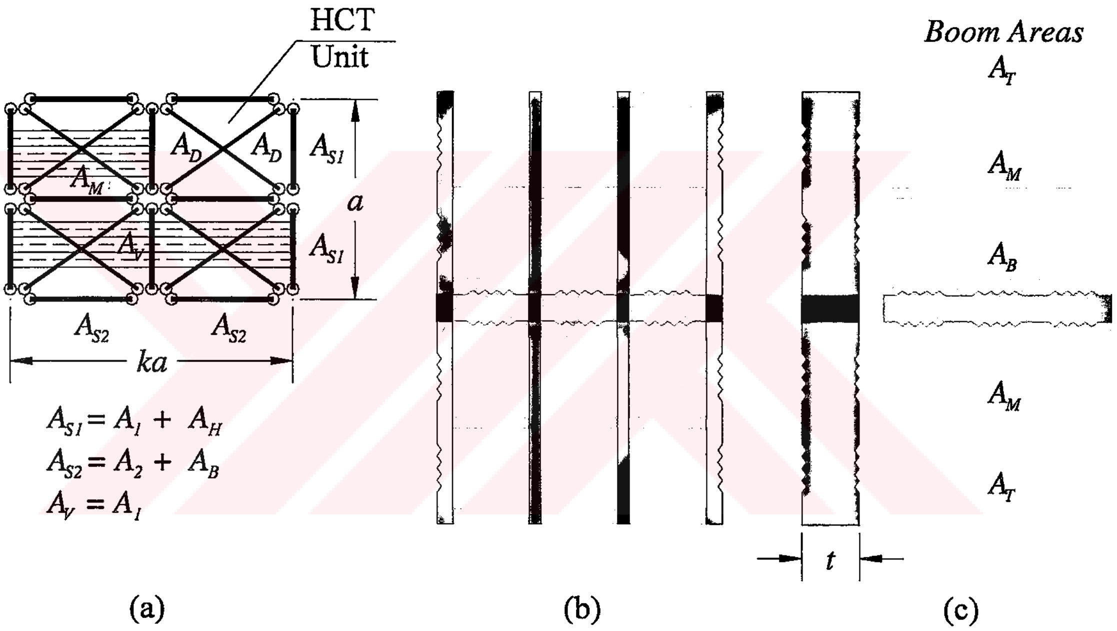

Figure 5.2. Hrennikoff truss equivalent of plane stress element

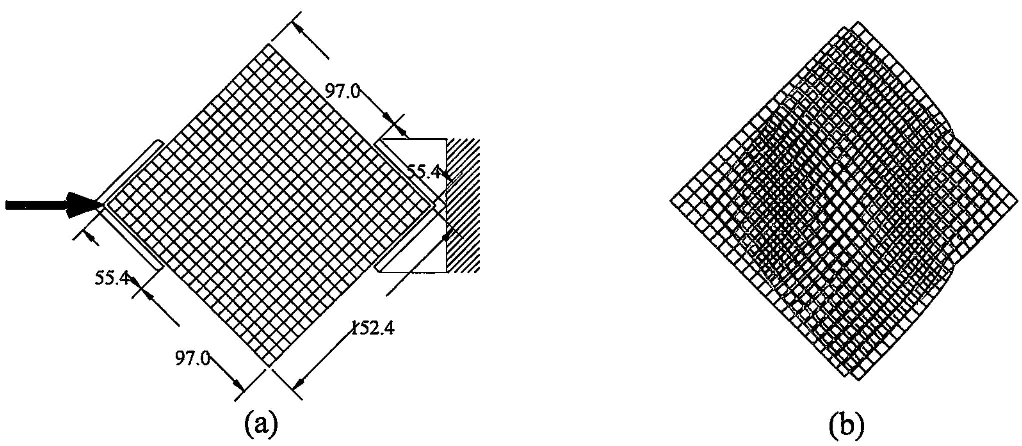

Figure 5.3. Plane stress analysis for accuracy check under 1.9kN

Table 5.2. Accuracy comparison for plane framework analysis

Location	**Deformations in mm**				**Error in per cent**	
	Membrane Elements		**Hrennikoff Elements**			
	UX	***UZ***	***UX***	***UZ***	***UX***	***UZ***
Top Corner	0.04074	0.00979	0.04023	0.01320	-1	35
Center Point	0.04057	0.00000	0.04013	0.00000	-1	-
Loaded Corner	0.09589	0.00000	0.09539	0.00000	-1	-
Middle Left Edge	0.05276	0.00162	0.05245	0.00512	-1	216

5.3. Pushover Analysis of Infilled Frames

Assumptions referred above define the overall geometry of the plane framework model proposed for the analysis of the HCT infilled frame behavior. To introduce the material nonlinearity, the definition of the hinges was based on the characteristic properties obtained from material testing, model test observations and index values derived from the FE analyses. Nonlinear properties were input using hinges on each element to represent the relevant behavior such as axial force - moment interaction hinges for beam and columns elements defining the surrounding frame, axial and/or shear force hinges for the contact elements, and axial force hinges for the infill truss model. Using the performance based analysis backbone definition format, Figure 5.4, the structural properties of the hinge elements used in the analysis are given in Table 5.3. Axial force - moment interaction hinges were generated automatically by the program.

Two separate modeling levels were assumed and named after the relative size of the elements used in the model versus the size of the HCT unit. The detailed model involved eight diagonal braces to model the vertical webs of the HCT units and six vertical and horizontal truss bars define the boundaries and median axes in the orthogonal directions for a given HCT. This model was named as meso-scale model since the structure of the HCT was modeled by an approximation involving assumptions on the interaction of the assigned individual elements, Figure 5.5. The rough or engineering model of the infill panel involved an order of magnitude less number of elements and therefore named as macro model considering that each section involved in the model could model a wall piece, an opening or a different structural element with average properties assigned to each cell, Figure 5.6.

Backbone peak force and displacement capacities were assumed based on the redundancy of the elements acting in parallel or in series. Therefore, the axial load hinges of the meso-scale models were assigned the overstrength parameter 1.28 to make-up the compressive strength value specified as 17.9MPa to maximum recorded as 22.9MPa, and the displacement limit for this level was assigned twice the maximum standalone crushing strength of the prism deformation to simulate the confined case. Contrary to this case, a load drop was specified for the macro-scale model to model the non-uniform strain and stress distribution across the specified diagonal element width.

Definition of the backbone curve point coordinates were regarded as equivalent to the definition of the stress-strain curves of the individual materials. Therefore, no member specific changes were made and a given backbone for a given material and hinge type was kept the same throughout.

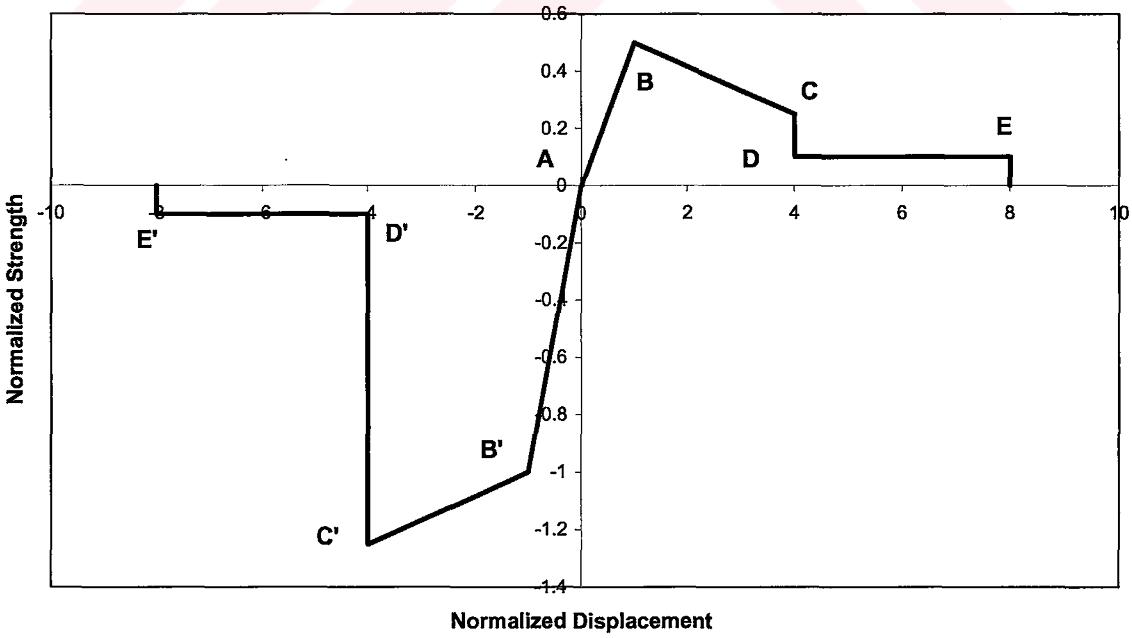

Figure 5.4. Sample curve for backbone point definition

Table 5.3. Backbone curve parameters for pushover analysis

Backbone Point	Infill Axial Hinges		Boundary Shear Hinges		Boundary Axial Hinges	
	Force	*Displacement*	*Force*	*Displacement*	*Force*	*Displacement*
E'	0.000	-40.0	0.025	-100.0	-0.100	-50.0
D'	-0.250	-4.0	0.050	-50.0	-0.100	-6.0
Meso - C'	-1.280	-2.0	0.100	-25.0	-1.000	-6.0
Macro - C'	-0.750	-2.0	0.100	-25.0	-1.000	-6.0
B'	-1.000	-1.0	0.100	-1.0	-1.000	-1.0
A	0.000	0.0	0.000	0.0	0.000	0
B	0.500	0.5	0.100	1.0	0.100	1.0
C	0.250	2	0.100	25.0	0.050	6.0
D	0.050	4	0.050	50.0	0.010	6.0
E	0.000	80	0.025	100.0	0.010	50.0

For the pushover analysis the SAP2000 Finite Element Program Version 7 was used as a calculator. The results were provided in the graphical format in Figure 5.7, 5.8, 5.9, 5.10, 5.11, and 5.12. For all of the cases the initial stiffness, cracking load and the peak load were approximated within a reasonable margin. The macro-scale model represented the similar pre-peak behavior as the meso-scale model in the beginning of the elastic region up to forces close to the cracking load, for larger loads the deviations grew but the pattern remained similar. Moreover, the failure pattern demonstrated in the deformation plots of the models indicated that all models defined the failure modes correctly and simulated the cracking and deterioration patterns closely.

Initial part of the pushover load force-displacement response is governed by the material properties of the HCT infill under tensile stresses. In this region, the stiffness is defined fully by the elastic properties assigned to the infill and frame materials up to cracking. After cracking the slope and evolution of damage is dictated by the tensile strength, until a balance point is reached at the peak load where the compressive failure of the HCT starts. After the peak load, the shape of the curve depends on the post peak compressive force-deformation specified for the HCT.

Even though a gross simplification is involved in the macro-scale model, the results are still within close proximity to the test and meso-scale model curve. Improvement of this modeling approach can be based on a proper averaging scheme using the meso-scale model as a starting point. However, in the absence of reliable standardized testing procedures for the tensile strength of the HCT units the intuitive and geometrical concepts behind the models are regarded as their major qualities and no further elaboration attempted.

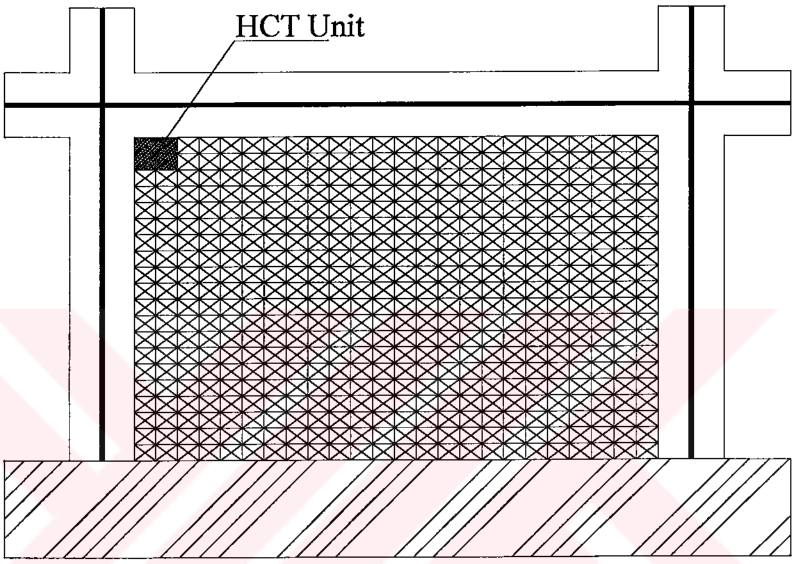

Figure 5.5. Meso-scale model detail for the HCT infill

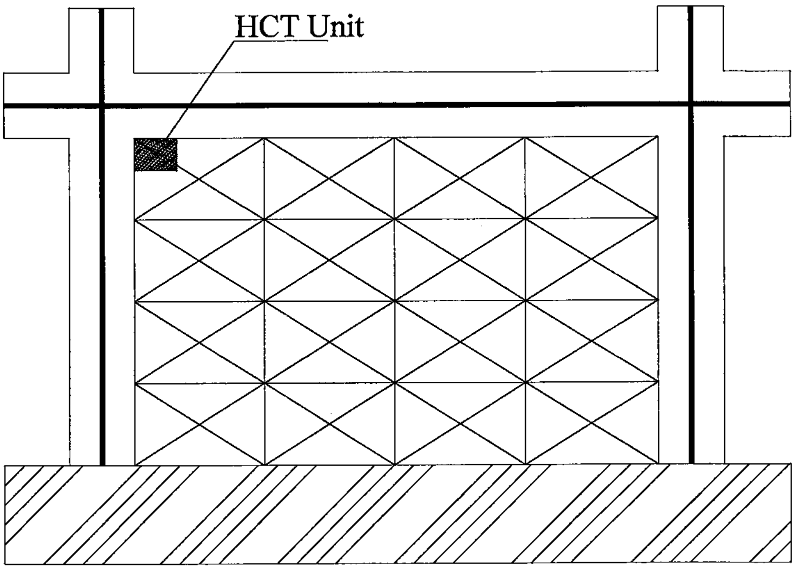

Figure 5.6. Macro-scale model detail for the HCT infill

6. CONCLUSIONS

In this dissertation, the studies undertaken on some probable means of strengthening of existing hollow clay tile masonry walls of ordinary construction using glass-sheet and carbon fiber laminates were documented. Investigations were based on testing of infilled frames and materials used in frame and infill construction, and numerical modeling of the specimen behavior. Laboratory tests were done in two separate phases where first the properties of the strengthened / modified standalone wall panels were investigated by testing of bare, rendered and glass sheet applied wall specimens. Masonry wall and prism tests were done on two types of hollow clay tiles where the difference was in amount of voids per masonry gross area. Within the scope defined, strength tests on individual brick units, masonry prisms, and small wall sections (wallette) were conducted. Wallette tests were done under diagonal compression. The tests were executed in increasing order of complexity and results of earlier tests were incorporated to the failure load prediction calculations of the tests to follow. Twenty-four wallette, forty wall coupon and prism, nine triplet shear, three masonry elastic modulus tests were undertaken. Several material tests on steel tensile strength, concrete compressive and split tensile strength, and mortar compressive strength followed the corresponding specimen tests.

After investigating the behavior of the infill walls as separate elements, infilled frames with and without strengthening measures were tested. Infilled frame testing was done on specimens that represent the field-encountered malpractices and the reference cases that represented the intended good design of today's engineering knowledge. In this second phase of the testing program, eight reinforced concrete infilled frames were tested under quasi-static cyclic reversing lateral loading. Properties of the frame specimens were derived from a prototype structure by scaling, and characterized the merits and flaws of existing reinforced concrete construction of past few decades. These specimens were grouped into two categories with respect to their reinforcement detailing for ductile frame response as code-compliant and non-compliant, where types of bare, masonry infilled, infilled with glass sheet overlay, and infilled overlaid and laminate braced frames were tested of either detailing group.

Data collected upon completion of the first and second phases of laboratory works, provided valuable information on the behavior of the hollow clay tile infilled reinforced concrete frames. Existing structural configurations were demonstrated to have the lateral stiffness and strength already acknowledged in the seismic reconnaissance works and shown that these properties unaccounted in original design or ordinary assessment works would violate the standard analysis assumptions. This observation further justified the attempt to utilize the infills as source for rehabilitation, and the motivation to control the failure pattern of the existing structures using fiber reinforced plastics.

Investigated retrofit schemes were shown to enhance the properties of the HCT infilled frames. The most important aspect of the retrofits using glass-sheet overlays was observed as to provide uniformity and predictability in infill behavior. These improvements can qualify the infills as structural elements and enable their use in seismic resistance calculations.

In current local engineering practice, the presence of the infill walls is still ignored and the assessments are done for the bare-frame capacity level. This approach assigns major seismic risks to most of the existing structures. As demonstrated with the tests undertaken, the available capacity may be vastly more than that is assumed, and can be further increased and its variations controlled using glass-sheet overlays. Moreover, the failure patterns of the infilled specimens, with or without strengthening, indicate that the neglect of infill walls need not be conservative and may lead to gravity collapse modes not foreseen in the conventional design or assessment procedures.

Presence of infills was observed to mask the detailing faults of the frame elements largely. Distinctly frame dominant behavior and failure pattern could only be observed contrasting the non-compliant and compliant bare frames. Although, both of the bare frames failed due to a sway mechanism, the failure of the code-compliant specimen could only be judged due to major strength drop and large drift, whereas the failure of the non-compliant bare specimen was due to the complete loss of gravity load carrying capacity. On the other hand, all infilled specimens failed in gravity load collapse modes and under decreasing overall deformation levels. The specimens with most extensive stiffening/strengthening had the least deformation ability and highest peak strength.

Strengthening applications were observed to rule out infill failure modes other than the corner crushing, and forced failures dominated by axial force-moment-shear force interaction on the surrounding frame elements.

Application of the glass-sheet overlays and carbon fiber laminates to the infill walls are observed to:

- Increase the peak load appreciably,
- Convert the infill failure modes to corner crushing for all cases,
- Reduce the overall displacement capacity,
- Mask the difference between the code compliant and non-compliant detailing,
- Increase the likelihood of sudden and brittle failures, which would subject the framing to abrupt load increases.

Except the comments on the failure mode modification, the points listed above also hold for the ordinary HCT infilled frames.

Ductility enhancement initially expected due to the reported test results on solid brick masonry found in the literature could not be reproduced for the parameters investigated, and regarded as a consequence of the large void ratio of the hollow clay tile masonry and its highly brittle nature. Brittleness inherent to the hollow clay tiles could not be masked by the glass-sheet due to major volumetric changes at every instant of web or face shell crushing of the masonry. Therefore, it is expected that a wall replacement strategy using bricks with less voids may provide improvements in this aspect, as well.

Extending the glass-sheet over to the sides of the columns and addition of carbon fiber laminates resulted in an integral-infill application, which increased the lateral load capacity further but resulted in abrupt loss of peak strength. This rapidly triggered the infill and frame failures, and the total displacement capacity of the system reduced significantly. To use the achieved additional capacity reliably, further research on alternative grouting and pasting agents may be required with the aim of replacing the epoxy to provide a more gradual / controlled loss of strength and bond, and thereby providing further ductility. On the other hand, similar enhancements could also be achieved if the carbon fiber laminate were to be replaced by a steel laminate providing additional material hysteresis and ductility.

During the course of the research work, the primary aim was to modify an infill hollow clay tile wall to achieve the capacity and ductility of a replacement reinforced concrete retrofit shearwall. The significant improvements achieved were only in the strength increase due to the high tensile strength of the materials used and the rapidly degrading compressive strength of the hollow clay tiles of the infill. As discussed above some further attempts to improve the proposed system ductility may require additional testing for following cases:

- Replacement of the pasting agents for glass-sheet and laminates,
- Maintaining the existing render or application of new fiber reinforced render before glass-sheet application to provide additional cross section and redundancy to the exterior shell,
- Replacement of the carbon fiber laminates with steel laminates to make use of the inherent material ductility,
- Replacement of the hollow clay tile walls with perforated or solid load bearing masonry walls,

Current new design codes are based on overall system ductility, which cannot be defined explicitly for an existing infilled structure. Therefore, coding procedure of the design for the tested or above discussed strengthening measures needs to be in performance-based format to cover the complete set of checks required for a structure with low ductility. At the current stage of the development of fiber based infill wall strengthening approaches, the tested or above stated retrofit alternatives should be considered force-controlled structural elements with no ductility or dissipativeness. For the retrofit design, modified infill panels may be used at several locations on the building plan to provide extensive overstrength to avoid the strength and stiffness deterioration of the infills. The uniformity of the retrofitted infill wall arrangement throughout the structure both on plan elevation must be achieved to limit irregular panel strength deterioration.

Developments in the testing procedures for the hollow clay tile masonry units and elements are required to provide reliable material property estimates for correct modeling of infilled frames. During the current study, finite element modeling of the tested specimens was used to cover the pitfalls of the testing procedures developed for solid masonry. The tension strength of the HCT units could only be assigned using a double shear setup newly developed within the laboratory research reported herein. Observed scatter in the test results was interpreted using the stress distribution results of the finite element models. A simple beam analysis to replace the finite element modeling was demonstrated to produce quick and conservative results.

A finite element modeling approach based on extending the use of the plane-framework methods of plane stress analysis was developed and used for the nonlinear modeling of HCT infills. Two models of different level of sophistication were proposed and were demonstrated to capture the pre-peak and post-peak load behavior of the infilled frame behavior for all tested cases. Material models assumed for the plane-framework elements were taken form the masonry prism test results, and only the actual physical geometry of the HCT and its mortar joints were used to build the model. Cracking pattern, cracking load, initial stiffness, peak load and failure mechanism given by the proposed modeling method was demonstrated to provide reasonable estimates for the tested behavior. The detailed, meso-scale, model was shown to trace the initial load path of the pushover curves successfully, and the crude model, macro-scale, provided comparable estimates. The accuracy of both of the models could be greatly enhanced if the post peak behavior of the HCT in the confined configuration could be better known. In the absence of such data, engineering estimates derived from concrete stress-strain relationships were modified to reflect the redundancy inherent to the system due to its cellular structure. A strict calibration of the models with the test data was not attempted due to the small number of tests and the lack of accurate material models for hollow clay tile masonry.

REFERENCES

Achyutha H., R. Jagadish, P. S. Rao, and S. S. Rahman, 1986, "Finite Element Simulation of the Elastic Behavior of Infilled Frames with Openings", *Computers and Structures*, Vol. 23, No 5, pp. 685-696.

Al-Chaar G., 1998, *Non-ductile Behavior of Reinforced Concrete Frames with Masonry Infill Panels Subjected to In-plane Loading*, Ph.D. Dissertation, University of Illinois at Chicago.

Al-Chaar G., M. Issa, and S. Sweeney, 2002, "Behavior of Masonry-Infilled Nonductile Reinforced Concrete Frames", *Journal of Structural Engineering*, Vol. 128, No.8, pp. 1055-1069.

American Society for Testing Materials (ASTM), 1981a, *C109 – Standard Test Methods for Compressive Strength of Hydraulic Cement Mortars (Using 2-in. or 50-mm Cube Specimens),* American Society for Testing Materials Philadelphia, Pennsylvania.

American Society for Testing Materials (ASTM), 1981b, *E447 – Standard Test Methods for Compressive Strength of Masonry Prisms,* American Society for Testing Materials Philadelphia, Pennsylvania.

American Society for Testing Materials (ASTM), 1981c, *E519 – Standard Test Methods for Diagonal Tension (Shear) in Masonry Assemblages*, American Society for Testing Materials Philadelphia, Pennsylvania.

Applied Technology Council (ATC), 1997a, *NEHRP Guidelines for the Seismic Rehabilitation of Buildings*, prepared by the Applied Technology Council (ATC-33 project) for the Building Seismic Safety Council, published by the Federal Emergency Management Agency, Report No. FEMA 273, Washington, D.C.

Applied Technology Council (ATC), 1997b, NEHRP *Commentary on the Guidelines for the Seismic Rehabilitation of Buildings*, prepared by the Applied Technology Council (ATC-33 project) for the Building Seismic Safety Council, published by the Federal Emergency Management Agency, Report No. FEMA 274, Washington, D.C.

Balendra T., K-H. Tan and S-K. Kong, 1999, "Vulnerability of Reinforced Concrete Frames in Low Seismic Region, When Designed According to BS8110", *Earthquake Engineering and Structural Dynamics*, 28, 1361-1381.

Benjamin, J. R. and H. A. Williams, 1958, "The Behavior of One-story Brick Shear Walls." *Journal of Structural Division*, ASCE, 84 (5), 1-30.

Bennett R. M, K. A. Boyd, and R. D. Flanagan, 1997, "Compressive Properties of Structural Clay Tile Prisms", *Journal of Structural Engineering*, Vol. 123, No.7, pp. 920-926.

Bertero B. and S. Brokken, 1983, "Infills in Seismic Resistant Building", *Journal of Structural Engineering*, Vol. 109, No.6, pp. 1337-1361.

Bracci J. M., A. M. Reinhorn, and J. B. Mander, 1995, "Seismic Resistance of Reinforced Concrete Frame Structures Designed for Gravity Loads: Performance of Structural System", *ACI Structural Journal*, Vol. 92, No. 5, pp. 597-609.

Buonopane S. G. and R. N. White, 1999, "Pseudodynamic Testing of Masonry Infilled Reinforced Concrete Frame", *Journal of Structural Engineering*, Vol. 125, No.6, pp. 578-589.

Chaker A. A. and A. Cherifati, 1999, "Influence of Masonry Infill Panels on the Vibration and Stiffness Characteristics of R/C Frame Buildings", *Earthquake Engineering and Structural Dynamics*, 28, 1061-1065.

Chiou Y-J., J-C. Tzeng and Y-W. Liou, 1995, "Experimental and Analytical Study of Masonry Infilled Frames", *Journal of Structural Engineering*, Vol. 125, No.10, pp. 1109-1117.

Chrysostomou, C. Z., P. Gergely, and J. F. Abel, 1988, *Preliminary Studies of the Effects of Degrading Infill Walls on the Nonlinear Seismic Response of Steel Frames*, National Center for Earthquake Engineering Research, Technical Report NCEER-88-0046.

Dawe, J. L. and C. K. Seah, 1988, "Lateral Load Resistance of Masonry Panels in Flexible Steel Frames", *Proceedings of the Eighth International Brick and Block Masonry Conference*, Trinity College, Dublin, Republic of Ireland.

Dhanasekar, M., A. W. Page, and P. W. Kleeman, 1985, "Steel Frames with Brickwork and Concrete Infilling", *Proceedings of the Institute of Civil Engineers – Part 2*, 81: 593-605.

Dhanasekar, M. and A. W. Page, 1986, "The Influence of Brick Masonry Properties on the Behaviour of Infilled Frames", *Proceedings of the Institute of Civil Engineers – Part 2*, 79: 295-313.

Ehsani M. R., H. Saadatmanesh, and A. Al-Saidy, 1997, "Shear Behavior of URM Retrofitted with FRP Overlays", *Journal of Composites for Construction*, Vol. 1, No. 1, pp 17-25.

Ehsani M. R., H. Saadatmanesh, and J. I. Velazquez-Dimas, 1999, "Behavior of Retrofitted URM Walls under Simulated Earthquake Loading", *Journal of Composites for Construction*, Vol. 3, No. 3, pp 134-142.

El-Attar A. G., R. N. White and P. Gergely, 1997, "Behavior of Gravity Load Designed Concrete Buildings Subjected to Earthquakes", *ACI Structural Journal*, Vol. 94, No. 2, pp. 133-145.

El-Haddad M. H., 1991, "Finite Element Analysis of Infilled Frames Considering Cracking and Separation Phenomena", *Computers and Structures*, Vol. 41, No 3, pp. 439-447.

Flanagan R. D. and R. M. Bennett, 1999, "Bidirectional Behaviour of Structural Clay Tile Infilled Frames", *Journal of Structural Engineering*, Vol. 125, No.3, pp. 236-244.

Flanagan R. D. and R. M. Bennett, 1999, "In-plane Behaviour of Structural Clay Tile Infilled Frames", *Journal of Structural Engineering*, Vol. 125, No.6, pp. 590-599.

Govindan P., M. Lakshmipathy, and Santhakumar A. R., 1986, "Ductility of Infilled Frames", *ACI Journal*, July-August, pp. 567-576.

Gülkan P. and M. A. Sozen, 1999, "Procedure for Determining Seismic Vulnerability of Building Structures", *ACI Structural Journal*, V.96, No.3, pp. 336-342.

Ghosh A. K. and A. M. Made, 2002, "Finite Element Analysis of Infilled Frames", *Journal of Structural Engineering*, Vol. 128, No.7, pp. 881-889.

Hakam Z. H-R., 2000, *Retrofit of Hollow Concrete Masonry Infilled Steel Frames Using Glass Fiber Reinforced Plastic Laminates*, Ph.D. Dissertation, Drexel University.

Hassan A. F. and M. A. Sozen, 1997, "Seismic Vulnerability Assessment of Low-rise Buildings in Regions with Infrequent Earthquakes," *ACI Structural Journal*, V.94, No.1, pp. 31-39.

Holmes, M., 1961, "Steel Frames with Brickwork and Concrete Infilling", *Proceedings of the Institute of Civil Engineers*, 19: 473-478.

Holmes, M., 1963, "Combined Loading on Infilled Frames", *Proceedings of the Institute of Civil Engineers*, 25: 31-38.

Hrennikoff A., 1941, "*Solutions of Problems of Elasticity by the Framework Method*", *Proceedings of the American Society of Mechanical Engineers, Journal of Applied Mechanics* (63) A:169-175.

Illston J. M. (Ed.), 1998, *Construction Materials, Their Nature and Behavior*, 2nd Edition, E&F Spon, New York.

Irwin A. W. and A. B. Afshar, 1979, " Performance of Reinforced Concrete Frames with Various Infills Subject to Cyclic Loading", *Proceedings of the Institute of Civil Engineers*, (2) 67: 509-520.

Jai J., 1998, *Reinforcing Masonry Walls with Composite Materials*, Ph.D. Dissertation, Stanford University.

Jain S. K. and R. Navin, 1995, "Seismic Overstrength in Reinforced Concrete Frames", *Journal of Structural Engineering*, Vol. 121, No.3, pp. 580-585.

Johnson F. B. and J. H. Matthys, 1973, "*Structural Strength of Hollow Clay Tile Assemblages*", *Proceedings of the American Society of Civil Engineers, Journal of the Structural Division* (99) ST2: 259-275.

Kahn L. F. and Hanson R. D., 1979, "Infilled Walls for Earthquake Strengthening," *Journal of the Structural Division, Proceedings of the American Society of Civil Engineers,* (105) ST2, pp. 283-296.

King, G. J. W. and P. C. Pandey, 1978, "The Analysis of Infilled Frames Using Finite Elements", *Proceedings of the Institute of Civil Engineers*, (2) 65: 749-760.

Klingner, R. E. and V. V. Bertero, 1978, "Earthquake Resistance of Infilled Frames", *Journal of the Structural Division, Proceedings of the American Society of Civil Engineers,* (104) ST6, pp. 973-989.

Kunnath S. K., G. Hoffmann, A. M. Reinhorn and J. B. Mander, 1995, "Gravity-Load-Designed Reinforced Concrete Buildings – Part I: Seismic Evaluation of Existing Construction", *ACI Structural Journal*, Vol. 92, No.3, pp. 343-354.

Kwan K. H., C. Q. Lo, and T. C. Liauw, 1990, "Large-scale Model Tests and Plastic Analysis of Multibay Infilled Frames", *Proceedings of the Institute of Civil Engineers*, (2) 89: 261-277.

Liauw, T. C., 1970, "Elastic Behaviour of Infilled Frames", *Proceedings of the Institute of Civil Engineers*, (2) 46: 343-349.

Liauw, T. C. and K. H. Kwan, 1982, "Non-linear Analysis of Multistorey Infilled Frames", *Proceedings of the Institute of Civil Engineers*, (2) 73: 441-454.

Liauw, T. C. and K. H. Kwan, 1983a, "Plastic Theory of Infilled Frames with Finite Interface Shear Strength", *Proceedings of the Institute of Civil Engineers*, (2) 75: 707-723.

Liauw, T. C. and K. H. Kwan, 1983b, "Plastic Theory of Non-integral Infilled Frames", *Proceedings of the Institute of Civil Engineers*, (2) 75: 379-396.

Liauw, T. C. and K. H. Kwan, 1984, "Plastic Design of Infilled Frames", *Proceedings of the Institute of Civil Engineers*, (2) 77: 367-377.

Liauw, T. C. and K. H. Kwan, 1984, "Nonlinear Behaviour of Non-integral Infilled Frames", *Computers and Structures*, Vol. 18, No 3, pp. 551-560.

Liauw, T. C. and K. H. Kwan, 1985, "Unified Plastic Analysis for Infilled Frames", *Journal of Structural Engineering*, Vol. 111, No.7, pp. 1427-1448.

Liauw, T. C. and S. W. Lee, 1977, "On the Behavior and the Analysis of Multi-story Infilled Frames Subjected to Lateral Loading", *Proceedings of the Institute of Civil Engineers*, 63: 641-656.

Liauw, T. C. and C. Q. Lo, 1988, "On Multibay Infilled Frames", *Proceedings of the Institute of Civil Engineers*, (2) 85: 469-483.

Madan A., A. M. Reinhorn, J. B: Mander, and R. E. Valles, 1997, "Modeling of Masonry Infill Panels for Structural Analysis", *Journal of Structural Engineering*, Vol. 123, No.10, pp. 1295-1302.

Mainstone, R. J., 1971, "On the Stiffness and Strength of Infilled Frames", *Proceedings of the Institute of Civil Engineers* Sup., pp. 57-90.

Mallick, D. V. and R. P. Garg, 1971, "Effect of Openings on the Lateral Stiffness of Infilled Frames", *Proceedings of the Institute of Civil Engineers*, 49: 193-209.

Mallick, D. V. and R. T. Severn, 1967, "The Behavior of Infilled Frames under Static Loading", *Proceedings of the Institute of Civil Engineers*, 38: 639-656.

Mallick, D. V. and R. T. Severn, 1968, "Dynamic Characteristics of Infilled Frames", *Proceedings of the Institute of Civil Engineers*, 39: 261-289.

Mander, J.B., B. Nair, K. Wojtkowski, and J. Ma, 1993, *An Experimental Study on the Seismic Performance of Brick Infilled Steel Frames*, National Center for Earthquake Engineering Research, Technical Report NCEER-93-0001.

Mander J. B., L. E. Aycardi, and D-K Kim, 1994, "Physical and Analytical Modeling of Brick Infilled Steel Frames", *Proceedings of the NCEER Workshop on Seismic Response of Masonry Infills*, D.P. Abrams editor, National Center for Earthquake Engineering Research, Technical Report NCEER- 94-0004.

May I. M. and J. H. Naji, 1991, "Nonlinear Analysis of Infilled Frames under Monotonic and Cyclic Loading", *Computers and Structures*, Vol. 38, No. 2, pp. 149-160.

McCormick C. W., 1963, "*Plane Stress Analysis*", *Proceedings of the American Society of Civil Engineers, Journal of the Structural Division* (89) ST4: 37-54.

Mehrabi, A.B., P. B. Shing, M. P. Schuller, and J. L. Noland, 1996, "Experimental Evaluation of Masonry Infilled RC Frames", *Journal of Structural Engineering*, Vol. 122, No.3, pp. 228-237.

Mosalam K. M., R. N White and P. Gergely, 1997, "Static Response of Infilled Frames Using Quasi-static Experimentation", *Journal of Structural Engineering*, Vol. 123, No.11, pp. 1462-1469.

Otani, S., 1997, "Lessons Learned From Past Earthquakes", *Proceedings of, Fourth Turkish National Conference of Earthquake Engineering*, Ankara, Turkey, September 1997, pp. 631 - 646.

Otani, S., 1999, "RC Building Damage Statistics and SDF Response with Design Seismic Forces", *Earthquake Spectra*, Earthquake Engineering Research Institute, Vol. 15, No. 3, pp. 485 - 501.

Paulay T. and M. J. N. Priestley, 1992, *Seismic Design of Reinforced Concrete and Masonry Buildings*, 1st Edition, John Wiley & Sons, New York.

Polyakov, S. V., 1956, *Masonry in framed buildings*, pub. by Gosudarstvennoe Izdatelstvo po Stroitelstvu I Arkhitekture (Translation into English by G.L.Cairns).

Riddington, J. R., 1984, "The Influence of Initial Gaps on Infilled Frame Behavior", *Proceedings of the Institute of Civil Engineers*, (2) 77: 259-310.

Riddington, J. and B. Stafford-Smith, 1977, "Analysis of Infilled Frames Subject to Racking with Design Recommendations", *The Structural Engineer*, (52) 6: 263-268.

Saadatmanesh H., 1994, "Fiber Composites for New and Existing Structures", *ACI Structural Journal*, Vol. 91, No3, pp. 346-354.

Saneinejad, A and B. Hobbs, 1995, "Inelastic Design of Infilled Frames", *Journal of Structural Engineering*, (121) 4: 634-650.

Schwegler – Koller G., 1994, "Verstärken von Mauerwerk mit Faserverbundwerkstoffen", Ph.D. Dissertation, Eidgenössischen Technischen Hochschule Zürich.

Seah C. K., 1998, *A Universal Approach for the Analysis and Design of Masonry Infilled Frame Structures*, Ph.D. Dissertation, The University of New Brunswick.

Smolira, M, 1973, "Analysis of Infilled Shear Walls", *Proceedings of the Institute of Civil Engineers*, (2) 55: 895-912.

Stafford-Smith, B. S., 1962, "Lateral Stiffness of Infilled Frames", *American Society of Civil Engineers, Journal of the Structural Division* (88)6: 183-199.

Stafford-Smith, B. S., 1966, "Behavior of Square Infilled Frames", *American Society of Civil Engineers, Journal of the Structural Division* (92)1: 381-403.

Stafford-Smith, B. and C. Carter, 1969, "A Method of Analysis for Infilled Frames", *Proceedings of the Institute of Civil Engineers*, 44: 31-48.

Stafford-Smith B. and J. Riddington, 1978, "The Design of Masonry Infilled Steel Frames for Bracing Structures", *The Structural Engineer*, (56B) 1: 1-7.

Triantafillou, T. C., 1998, "Behavior of Retrofitted URM Walls under Simulated Earthquake Loading", *Journal of Composites for Construction*, Vol. 2, No. 2, pp 96-104.

Türk A. M., 1998, *Rehabilitation of Reinforced Concrete Frames by Reinforced Concrete Infill Walls,* Ph.D. Dissertation, Boğaziçi University.

Türk Standardları Enstitüsü (TSE), 1972, *TS 498 – Yapı Elemanlarının Boyutlandırılmasında Alınacak Yükler*, 1st Edition, Türk Standardları Enstitüsü, Ankara.

Türk Standardları Enstitüsü (TSE), 1984, *TS 500 – Betonarme Yapıların Hesap ve Yapım Kuralları*, 1st Edition, Türk Standardları Enstitüsü, Ankara.

Türk Standardları Enstitüsü (TSE), 1985, *TS 705 – Fabrika Tuğlaları – Duvarlar için Dolu ve Düşey Delikli*, 1st Edition, Türk Standardları Enstitüsü, Ankara.

Türkiye Cumhuriyeti Bayındırlık ve İskan Bakanlığı (TCBIB), 1944, *Zelzele Mıntıkaları Muvakkat Yapı Talimatnamesi*, T. C. Bayındırlık ve İskan Bakanlığı, Ankara.

Türkiye Cumhuriyeti Bayındırlık ve İskan Bakanlığı (TCBIB), 1949, *Türkiye Yersarsıntısı Bölgeleri Yapı Yönetmeliği*, T. C. Bayındırlık ve İskan Bakanlığı, Ankara.

Türkiye Cumhuriyeti Bayındırlık ve İskan Bakanlığı (TCBIB), 1953, *Yersarsıntısı Bölgelerinde Yapılacak Yapılar Hakkında Yönetmelik*, T. C. Bayındırlık ve İskan Bakanlığı, Ankara.

Türkiye Cumhuriyeti Bayındırlık ve İskan Bakanlığı (TCBIB), 1962, *Afet Bölgelerinde Yapılacak Yapılar Hakkında Yönetm*elik, T. C. Bayındırlık ve İskan Bakanlığı, Ankara.

Türkiye Cumhuriyeti Bayındırlık ve İskan Bakanlığı (TCBIB), 1968, *Afet Bölgelerinde Yapılacak Yapılar Hakkında Yönetm*elik, T. C. Bayındırlık ve İskan Bakanlığı, Ankara.

Türkiye Cumhuriyeti Bayındırlık ve İskan Bakanlığı (TCBIB), 1975, *Afet Bölgelerinde Yapılacak Yapılar Hakkında Yönetm*elik, T. C. Bayındırlık ve İskan Bakanlığı, Ankara.

Türkiye Cumhuriyeti Bayındırlık ve İskan Bakanlığı (TCBIB), 1998, *Afet Bölgelerinde Yapılacak Yapılar Hakkında Yönetm*elik, T. C. Bayındırlık ve İskan Bakanlığı, Ankara.

Wilson, E. L., *SAP2000 Integrated Finite Element Analysis and Design of Structures*, 1995, Computers and Structures Inc., California.

Wood, R.H., 1952, "Studies in Composite Construction – I. The Composite Action of Brick Panel Walls Supported on Concrete Beams", *National Building Studies Research Paper No.13.* H.M.S.O., London.

Wood, R.H., 1958, "The Stability of Tall Buildings", *Proceedings of the Institute of Civil Engineers*, Vol.11, 69-102.

Wood, R.H., 1978, "Plasticity, Composite Action and Collapse Design of Unreinforced Shear Wall Panels in Frames", *Proceedings of the Institute of Civil Engineers*, 2: 381-411.

Yettram A. L. and H. M. Husain, 1966, "*Plane-Framework Methods for Plates in Extension*", *Proceedings of the American Society of Civil Engineers, Journal of the Engineering Mechanics Division* (92) EM1: 157-168.

Zarnic R., S. Gostic, A. J. Crewe, and C. A. Taylor, 2001, "Shaking Table Tests of 1:4 Reduced-scale Models of Masonry Infilled Reinforced Concrete Frame Buildings", *Earthquake Engineering and Structural Dynamics*, 30:819-834.